BLOCK II SOLID ROCKET MOTOR (SRM) CONCEPTUAL DESIGN STUDY CONTRACT NAS 8-37295

FINAL REPORT - VOLUME I

Prepared for:

GEORGE C. MARSHALL SPACE FLIGHT CENTER
NATIONAL AERONAUTICS AND SPACE ADMINISTRATION
Marshall Space Flight Center, Alabama 35812

Attention: AS24D

Submitted by:

ATLANTIC RESEARCH CORPORATION
7511 WELLINGTON ROAD
GAINESVILLE, VIRGINIA · 22065-1699

TR-PL-12126

PROPULSION DIVISION

31 December 1986

BLOCK II SOLID ROCKET MOTOR (SRM)
CONCEPTUAL DESIGN STUDY
CONTRACT NAS 8-37295

FINAL REPORT - VOLUME I

Prepared for:

George C. Marshall Space Flight Center
National Aeronautics and Space Administration
Marshall Space Flight Center, Alabama 35812

Attention: AS24D

Submitted by:

Atlantic Research Corporation
Propulsion Division
7511 Wellington Road
Gainesville, Virginia 22065-1699

TR-PL-12126

31 December 1986

FOREWORD

This Final Report is structured in two volumes. Volume I includes Task I, Conceptual Design Studies, and Task II, Preliminary Development and Verification (D&V) Plan. Volume II consists of Task III, Capability Assessment, and Task IV, ROM Cost Estimate. Volume II contains proprietary data and shall not be disclosed outside the Government.

TABLE OF CONTENTS

VOLUME I - FINAL REPORT

1.0 INTRODUCTION

National Aeronautics and Space Administration's (NASA's) George C. Marshall Space Flight Center selected Atlantic Research Corporation's (ARC's) Propulsion Division to perform conceptual design studies of a Block II Space Shuttle Solid Rocket Motor (SRM). The ground rules for this conceptual motor design included the following:

- The existing performance, design, and verification requirements contained in Specification Number CPW1-3300, Part 1, for the Space Shuttle High Performance Solid Rocket Motor were used as the baseline requirements document for proposed design concepts except as changed and/or amplified by NASA. References to specific design characteristics such as segmented cases and other motor design characteristics and/or specification requirements unique to Morton Thiokol Incorporated's design were deleted; in those instances, ARC selected the specific design characteristics that best suited our overall motor design concept.

- Design concepts essentially duplicate the outside geometry of the current Space Shuttle SRM and its interfaces with other Space Shuttle elements so that impact to the aerodynamic and dynamic characteristics of the Space Shuttle vehicle is minimized.

- Design concepts do not use asbestos-filled insulation materials.

- Design concepts are not constrained to the current propellant formulation, but rather they provide the capability to successfully perform over an equivalent polybutadiene acrylonitrile acrylic acid terpolymer (PBAN) propellant formulation burn rate range of 0.360 to 0.400 inch/second. For information, the performance data contained in CPW1-3300 is based on a PBAN propellant formulation with a target burn rate of 0.368 inch/second at 60°F.

- Performance is in accordance with the requirements contained in CPW1-3300 from sea level to 200,000 feet over a propellant mean bulk temperature (PMBT) range of +40° to +90°F after being subjected to the natural and induced environments specified in paragraphs 3.2.7.1 and 3.2.7.2, respectively, of CPW1-3300 to the extent that the PMBT range of +40° to +90°F is not violated.

- Any Criticality I, IR, 2, and 2R pressure seal is fully redundant and verifiable (inspected and leak tested in the prescribed functional location). Further, no seal requires pressure actuation to perform its designed function.

- Verification methods prescribed in Section 4.0, Table V, of CPW1-3300 were not used; the method of verification is a product of this study contract.

- Appendix 10, deviations, and any references to approved deviations were deleted from CPW1-3300.

1.1 OBJECTIVE AND APPROACH

The objective of the Block II SRM Study Program was to define a conceptual design that offered

- Improved flight safety, reliability, and confidence,
- Equal or greater performance,
- Equal or lower cost,
- Compatibility, with the current Space Shuttle vehicle and launch facility.

The contract study flow diagram shown in Figure 1.1.1 schematically describes the approach chosen to satisfy the program objectives over the period of September 3, 1986 to December 30, 1986. The four interrelated work tasks were performed on schedule in the sequence shown.

The following design options and trade studies were defined at the beginning of the program:

- Segmented versus monolithic design,
- Case,
- Joint and seals,
- Insulation,
- Nozzle,
- Igniter.

The following evaluation criteria were also defined at program start: reliability, 65 percent; cost, 20 percent; and performance, 15 percent.

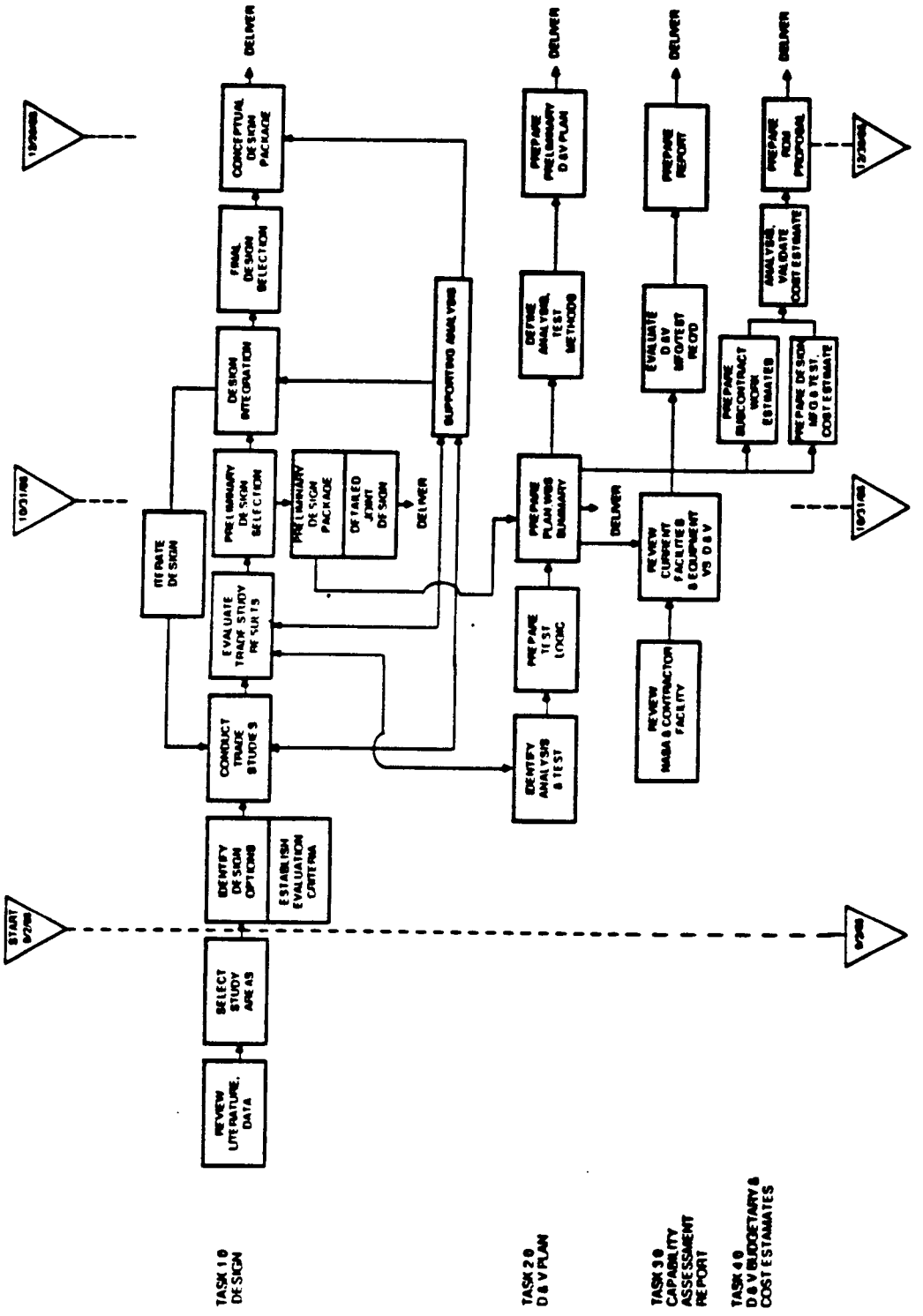

FIGURE 1.1.1. CONTRACT STUDY FLOW DIAGRAM.

1.2 SUMMARY AND CONCLUSIONS

ARC evaluated segmented and monolithic SRM design concepts with emphasis on joints and seals. Particular attention was directed to eliminating deficiencies in the SRM High Performance Motor (HPM) identified in the Report of the Presidential Commission on the Space Shuttle Challenger Accident, during the August 14, 1986 SRM Briefing to Industry, and through detailed review of SRM literature.

The selected conceptual design is described and discussed in Section 2.0. ARC's selection of this concept was driven by the following conclusions:

- An in-line bolted flange field joint is technically superior to either the original tang and clevis pinned case joint or the improved "capture feature" tang and clevis; however, the bolted flange field joint is heavier. The selected NASA Langley Research Center (LaRC) joint offers minimum joint sealing surface deflection.

- The heavier bolted joint weight penalty may be negated by extending the current case length to equal SRM casting segment length. ARC believes that case founding, forging, and heat treatment facility investments are cost effective.

2.0 CONCEPTUAL DESIGN STUDY

This section describes and documents Atlantic Research Corporation's recommended design concept for a Block II Space Shuttle SRM.

Trade studies were conducted to select specific SRM design features and materials in the following areas:

- Design approach (segmented vs. monolithic),
- Motor case,
- Joints and seals,
- Asbestos-free insulation,
- Propellant and liner,
- Igniter,
- Nozzle.

These trade studies were documented in the Mid-Term Study Report, which is included as Appendix A of this report. The detailed trade studies and analyses that led to the recommended design concept documented herein may, therefore, be found in Appendix A.

2.1 PRELIMINARY DESIGN CONCEPT

The recommended Block II SRM preliminary design concept is depicted in Figures 2.1.1 and 2.1.2 and is described below.

The SRM is a segmented design having casting segment lengths identical to those of the Space Shuttle Mission 51-L design. However, longer D6AC case segments are utilized, thereby eliminating all but two of the 51-L type factory joints. The three field joints connecting the four casting segments are of the inline bolted flange type, each fastened with high-strength steel studs with Inconel 718 nuts on each end. Each field joint incorporates redundant metallic O-ring face seals.

The nozzle-to-case joint also incorporates redundant metallic face-type seals. In addition, all internal insulation joints are of the unvented type with a labyrinth path that precludes direct exposure of the joint seals to hot combustion gases. Mating insulation joints are filled with low-strength, high-strain room temperature cure sealant. Stress relief features are incorporated in the insulation near the mating joints to permit relative motion of the insulation components without overstressing the insulation joint sealant.

The propellant formulation and grain configuration of each casting segment is identical to the High Performance SRM design.

The case insulation design is a hybrid system to optimize weight and performance. A Kevlar/silica/Hypalon material is used next to the case wall because its low thermal diffusivity provides the optimum thermal protection for the reusable case. To provide erosion protection near field joints and in areas that are exposed during propellant burn such as the aft case, the Hypalon insulation will transition to an NBR/phenolic with boric acid filler (USR-3800). The molded inhibitors will also be made from USR-3800. The castable liner will be a carboxyl-terminated polybutadiene (CTPB) material for compatibility similar to the current liner material with the asbestos fibers replaced with another filler material.

CASE

- FOUR LONGER D6AC CASE SEGMENTS REPLACE 9 ORIGINAL SEGMENTS

CASE FIELD JOINTS

- THREE MODIFIED NASA LARC IN-LINE BOLTED JOINTS

CASE SEALS

- REDUNDANT METAL O-RING FACE SEALS
- LABYRINTH UNVENTED INSULATION JOINTS

NOZZLE/CASE JOINT

- REDUNDANT METAL O-RING FACE SEALS
- LABYRINTH UNVENTED INSULATION JOINTS
- NO RADIAL BOLTS

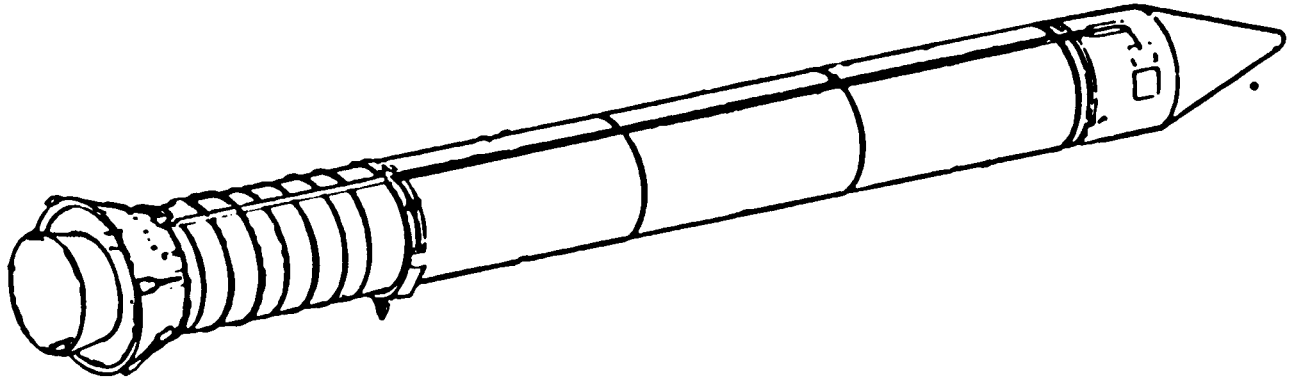

IGNITER

- REDUCED LEAK PATHS
- HTPB PROPELLANT
- MODIFIED GRAIN DESIGN

PROPELLANT

- TPH 1148

NON-ASBESTOS INSULATION

- LAYERED
  - -KEVLAR/HYPALON
  - - NBR/PHENOLIC

NOZZLE

- BASELINE MTC REDESIGN

FIGURE 2.1.1. PRELIMINARY BLOCK II SRM DESIGN FEATURES.

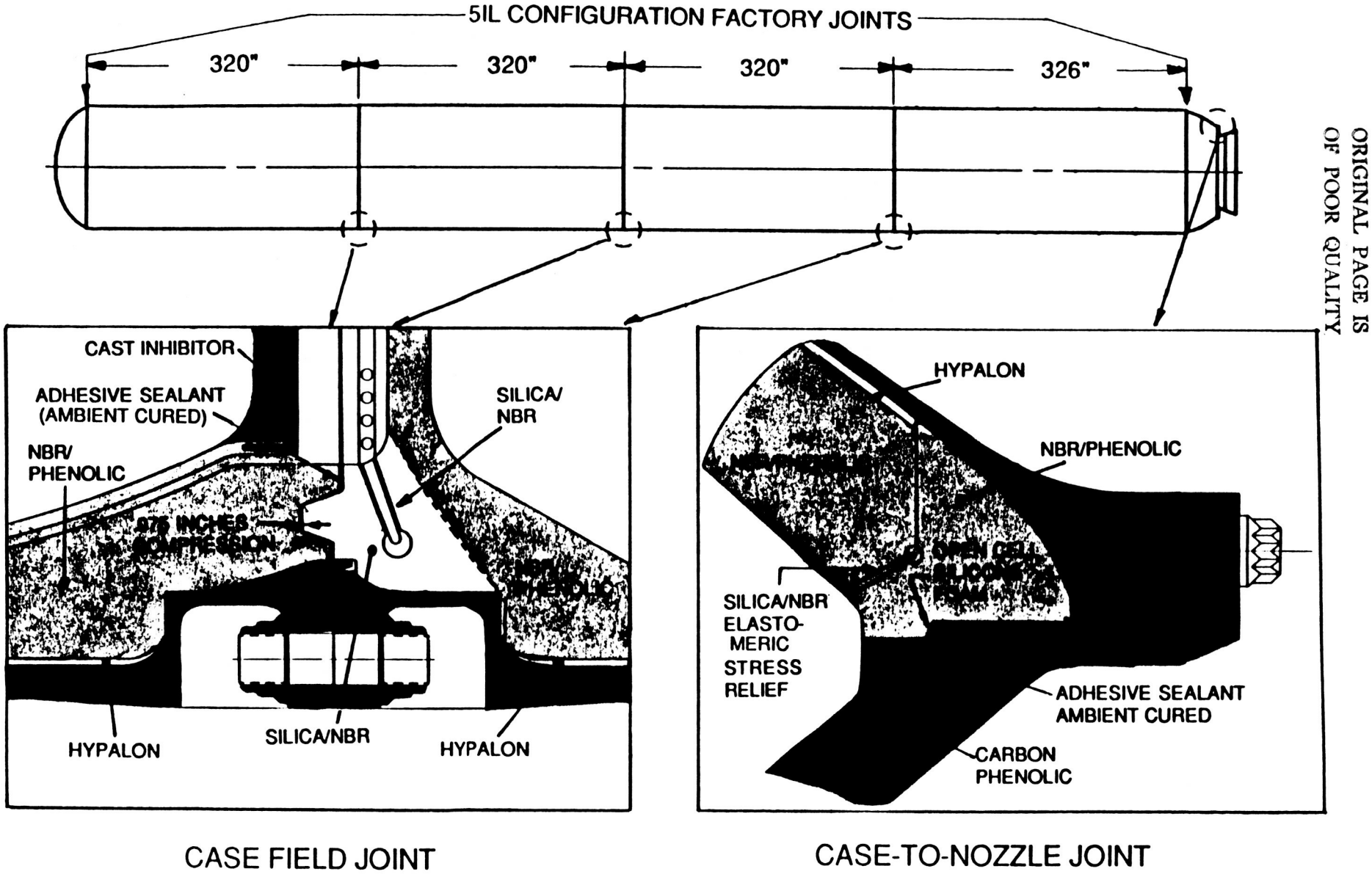

FIGURE 2.1.2. ARC BLOCK II SRM JOINTS.

The nozzle configuration is basically the same as the 51-L configuration except that certain materials have been changed to eliminate asbestos and/or to eliminate pocket erosion problems. Also, internal joints have been reconfigured as needed to provide redundant seals.

The preferred igniter design consists of an integral igniter adapter and case with a bolt-on aft closure formed from 200 maraging steel. The igniter assembly is insulated with Kevlar and silica-filled Hypalon and loaded with 18 percent aluminized HTPB propellant. All joints are sealed using T-ring variants and metal C-rings.

2.2 CASE

The motor case trade study, as shown in Appendix A, resulted in the selection of a double-length (casting segment) case fabricated from D6AC and using the roll forging method of metalworking. The selection of this configuration has been substantiated by a review of the concept with Ladish Co., Inc. to verify the technical capability to produce this configuration and to assess the cost impact of a double-length case segment. This assessment compares the technical challenge of a double-length case section with that of a single segment case. The newly selected joint configuration was included as a consideration in technical and cost evaluation. The motor case design for a typical center casting section is shown in Figure 2.2.1, which is included as Attachment 1 of this report.

Ladish has reviewed thoroughly the double-length motor case, which incorporates the bolted flange design. The configuration can be produced by using the following forge sequence, which incorporates the final heat treatment prior to final machining:

- Receive stock,
- Heat,
- Press upset,
- Edge roll,
- Clean pre-form,
- Reheat,
- Extrude and pierce,
- Clean donut,
- Condition donut,
- Reheat,
- First ring roll operation,
- Clean ring,
- Condition ring,
- Reheat,
- Second ring roll operation,
- Hot size,
- Heat treat and second size,
- Machine pre-form blank,

- Ultrasonic test,
- Roll reduce,
- Stress relieve,
- Cold size diameter,
- Rough machine clevis ends,
- Ultrasonic test,
- Final heat treat in a fixture,
- Ship in a fixture.

The following is a discussion of the above procedure and is intended to clarify the operations. Comments are provided on the forging units that will be required to complete the operation successfully. Section 2.3, Volume II, will address the cost of capital equipment required to produce the required length cylinder along with the increased thickness necessary to obtain the bolted clevis joint.

Ladish will purchase 50-inch-diameter, 49,500-pound billets (see Figure 2.2.2) of Ladish D6AC material from LTV for this requirement. This size is considerably larger than the present 40-inch-diameter, 31,000-pound billets used to make the single-length case. This increased size and weight is beyond LTV's present melt capabilities and will require new facilities for melting and handling. LTV is confident that it can maintain the present quality level in the larger stock size, but LTV will require a tryout heat to verify quality and refine its vacuum-arc remelting operation.

The next operation is designed to prepare the stock for making the forged donut (see Figure 2.2.3). This operation can be performed on equipment existing at Ladish. This operation represents low technical risk to motor case fabrication technology. The intermediate cleaning and conditioning operations are routine and will not require any additions or modifications to equipment.

The donut configuration, shown in Figure 2.2.4, is dictated by the roll reduced pre-form blank. Since the bolted flange design is thicker than the present clevis, the proportions between the cylinder section and the clevis becomes exaggerated in the donut. The tonnage of the present press is limited to finished flange thicknesses below 3.100 inches.

ORIGINAL PAGE IS
OF POOR QUALITY

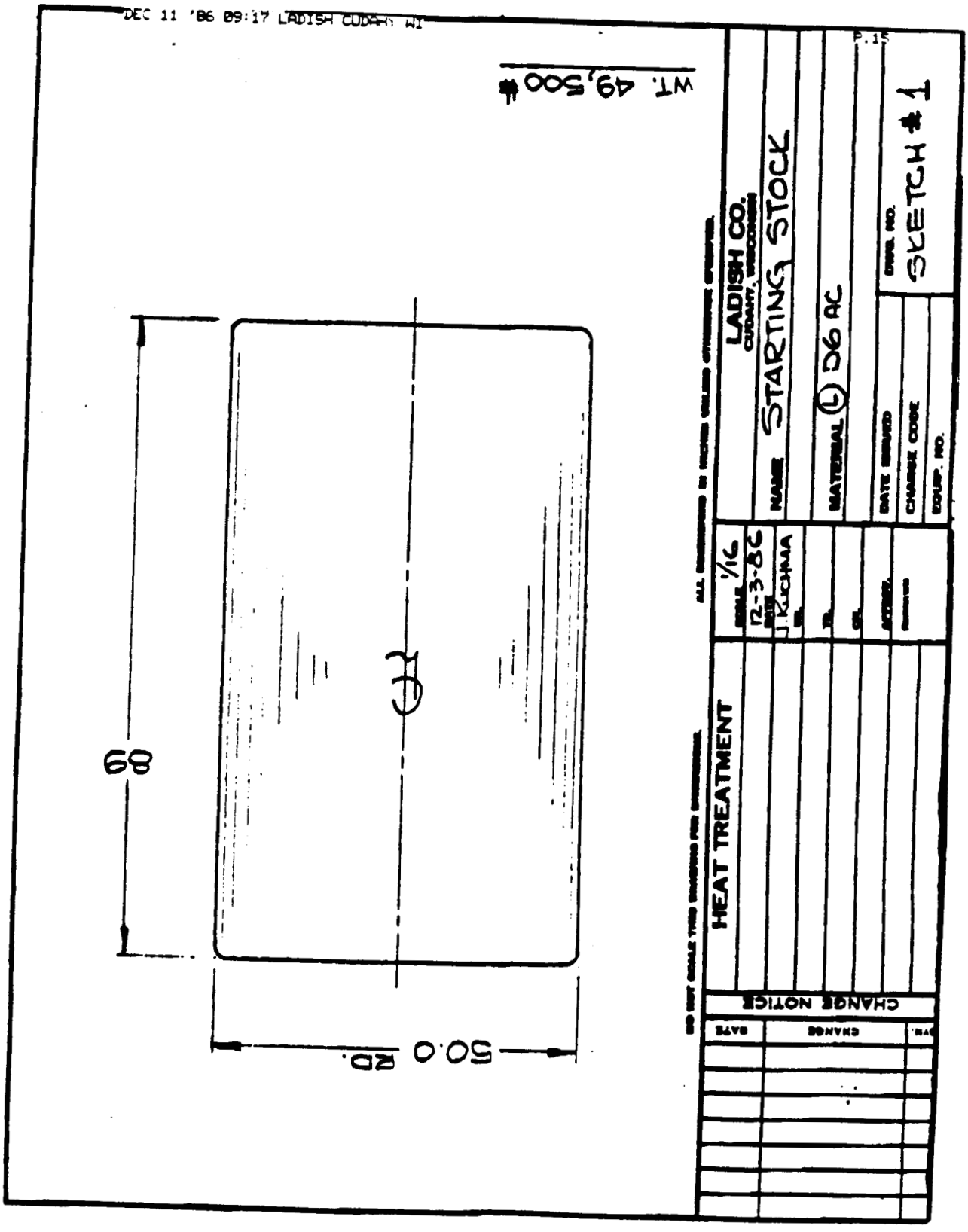

FIGURE 2.2.2. 50-INCH-DIAMETER BILLET.

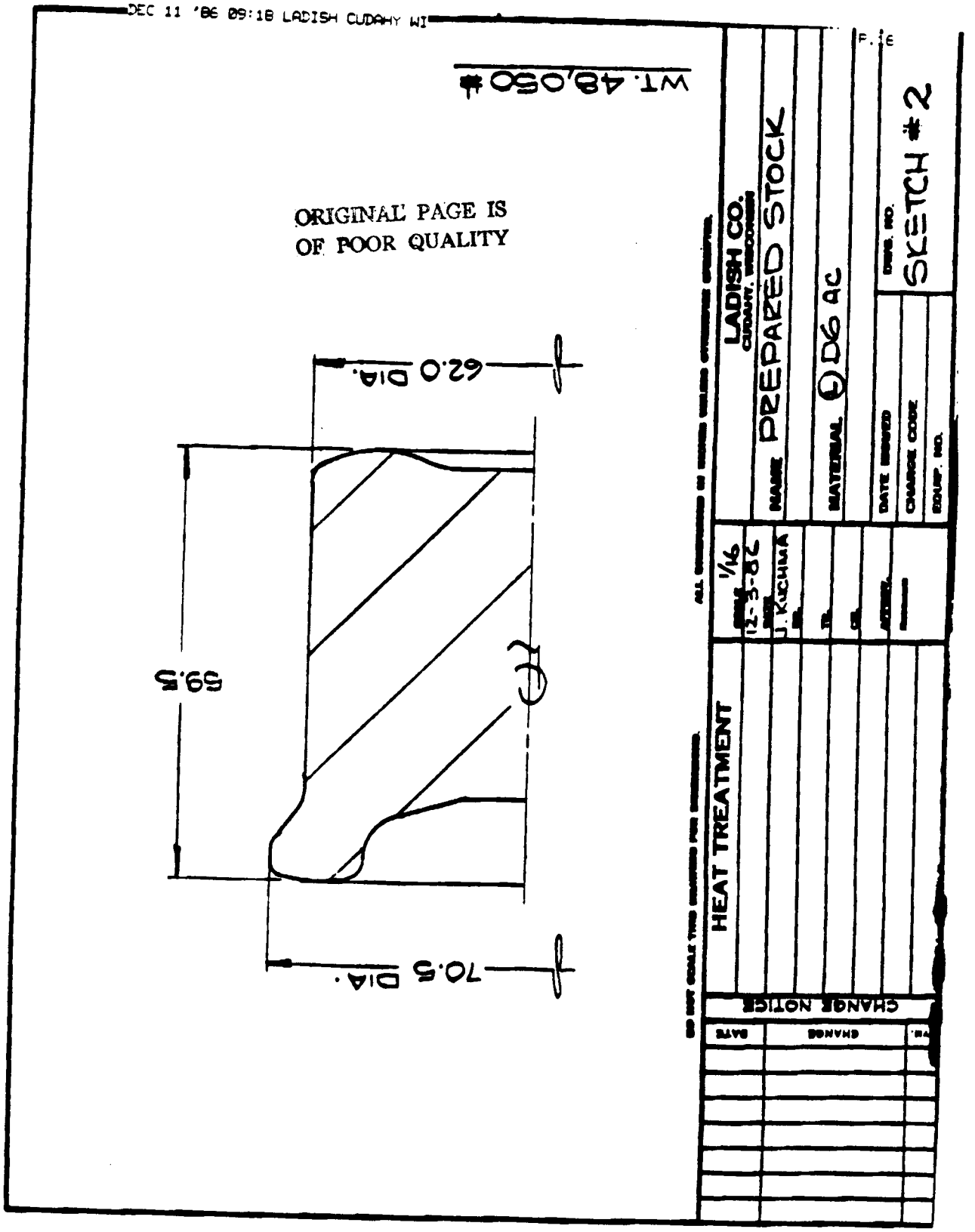

FIGURE 2.2.3. PREPARED STOCK.

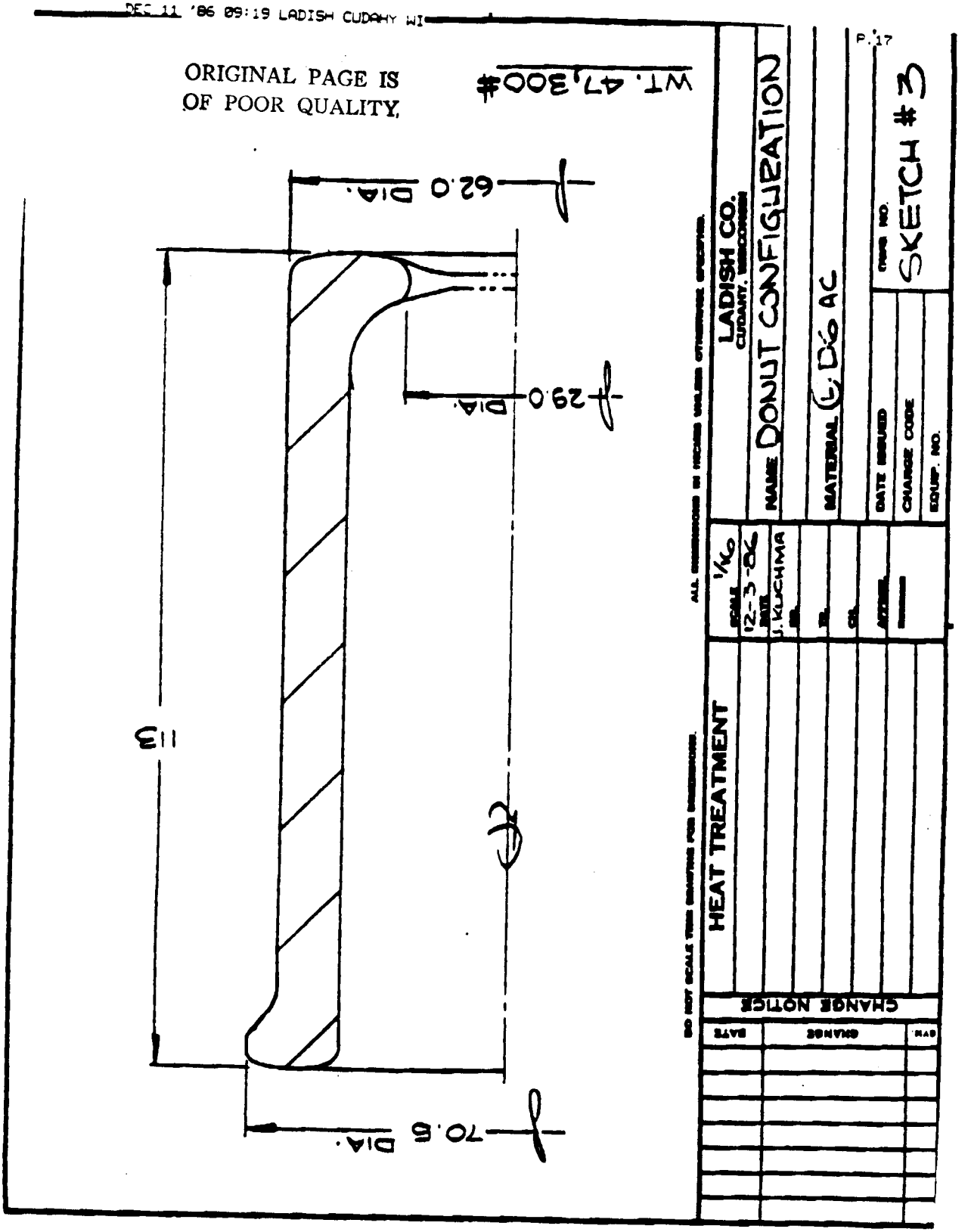

FIGURE 2.2.4. DONUT CONFIGURATION.

The hot roll operations (see Figures 2.2.5 and 2.2.6) can be produced using Ladish's current equipment; however, due to length and configuration, new ring roll tools will be needed. No major technical risks are expected with this change.

The hot size operation (see Sketch #6 in Appendix B of Volume II) is low risk and can be performed on equipment existing at Ladish. However, new sizing segments will be required due to the longer length pre-form size.

Machining of the pre-form blank (see Sketch #6 in Appendix B of Volume II) from the rolled ring should present no technical challenge. No new equipment will be needed for this operation.

Ladish has developed a method of using immersion sonic testing the large pre-forms that will be used. Slight modification of Ladish's equipment to accommodate the longer length is anticipated.

The next operation is the flow turning of the blank to its total length. A new machine will be required to manipulate the longer length and the starting pre-form blank's thicker wall section. The new machine will be patterned after Ladish's successful flow turn machine. No major problems in using this new piece of equipment are anticipated.

After flow turning, all handling is accomplished using fixtures to prevent damage to the ring due to its long length and thin wall section.

A new furnace will be required for the stress relieving operation. The case can be hung vertically in the furnace and fixtured to keep it round. This operation varies from present practice, since the 160-inch cylinders fit into existing furnaces and do not require the extensive fixturing necessary for the longer length. This operation is the first in this production sequence that varies to any great extent from the present practice.

The cold sizing operation will require a new press because of the added length. The press will be designed with added segment travel to accommodate the bolted flange joint, which has the added stock on the inside diameter. New sizing tools will be needed for the added length. This operation will be essentially the same as the current

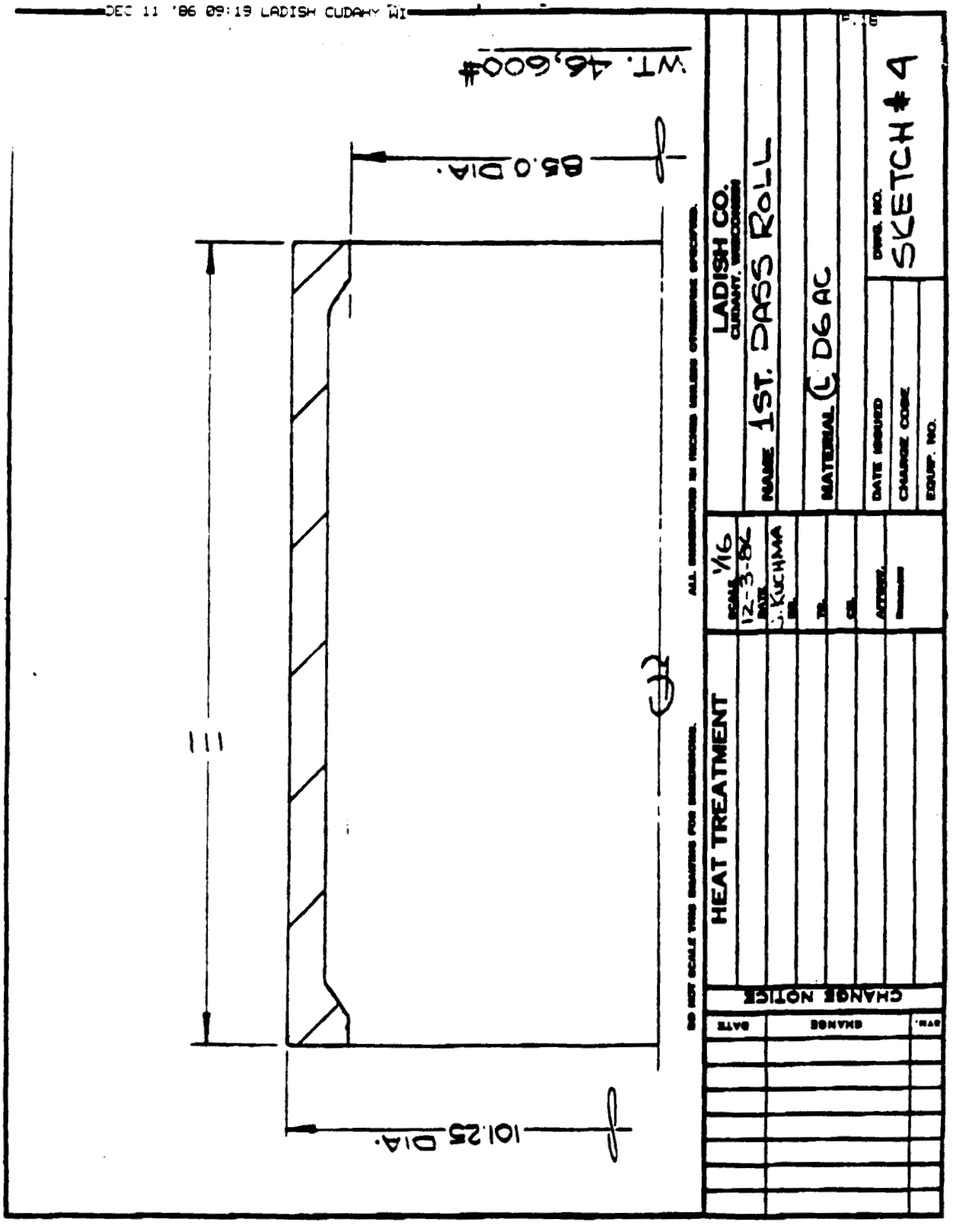

FIGURE 2.2.5. HOT ROLL OPERATION - FIRST PASS.

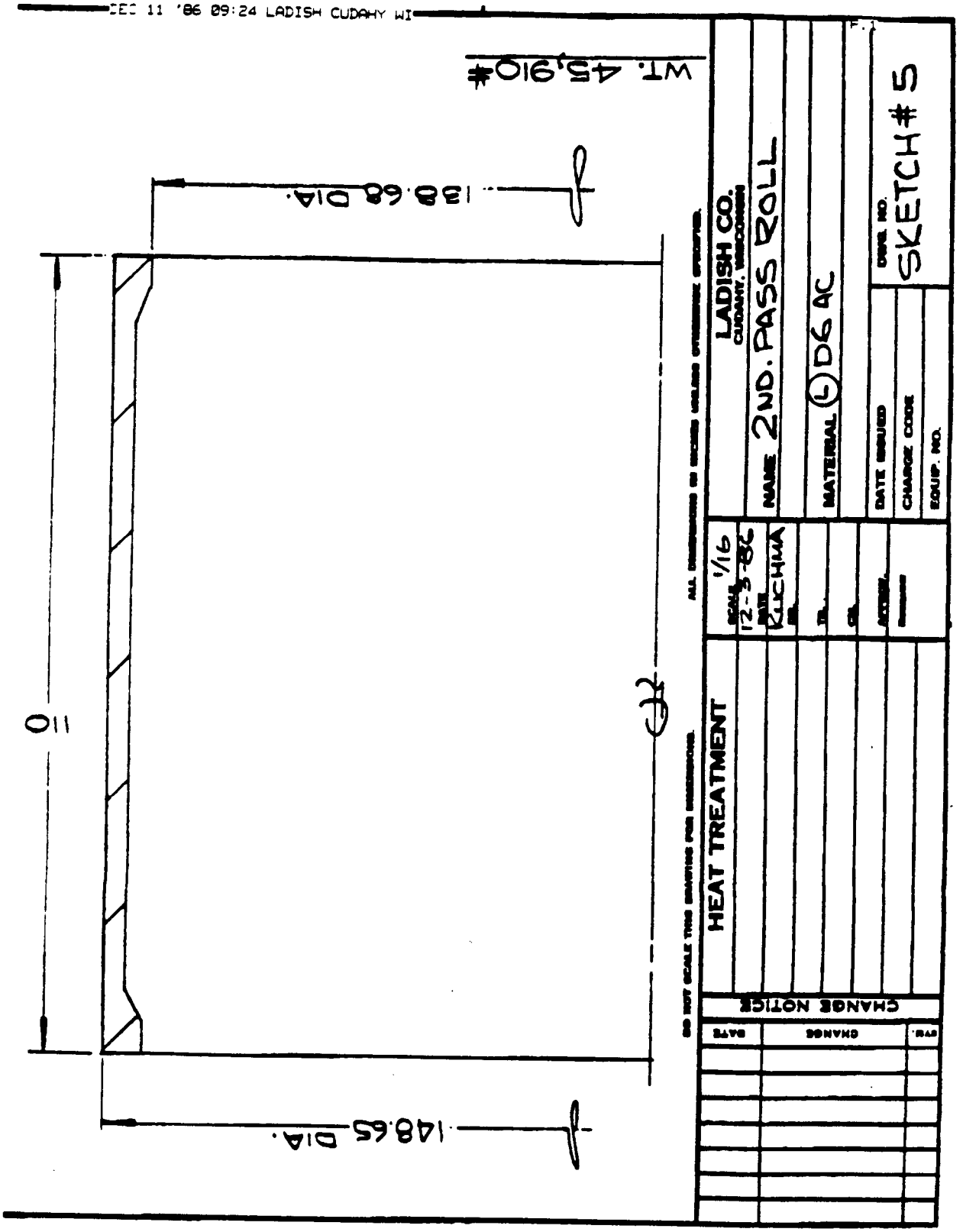

FIGURE 2.2.6. HOT ROLL OPERATION - SECOND PASS.

sizing practice. The machining of the bolted flange joint will be done on the current equipment modified for the increased length. Again, this operation is similar to existing practices with only the machine contour changing.

The final ultrasonic test of the roll formed cylinder will use the current inspection method but will require new facilities due to the increased length and the requirement to fixture the ring during sonic testing. This added weight will require stronger rollers and tank. Sonic testing these pieces in a fixture should not present any new technical challenges.

The final heat treatment (see Sketch #6 in Appendix B of Volume II) will take place in a new furnace. This operation is the only addition to the current process. A new furnace will be designed and installed for this operation. Again, fixturing will be required to maintain roundness. The heat treatment facility will include salt bath quench tanks.

Presently, components are shipped on flat cars blocked into the vertical position. The length of the double-length case will not allow this shipping configuration. The new motor cases will be shipped in the horizontal position with an internal fixture on rail cars that incorporate a shipping cradle. This method should provide sufficient transportation protection and maintain roundness during transportation.

The procedures that will be used to produce the double-length motor case incorporating the bolted flange are basically the same as those presently used for the 160-inch long motor case. The added length provides some problems that are not encountered with the present cylinder. The first is the new starting billet size and weight. Historically, the startup of new melt facilities requires debugging and introduces unknowns into the steel quality. Process characterization is, therefore, planned early in the Development Phase.

The second problem is handling of double-length motor cases. Ladish plans to develop new handling equipment and fixtures. Also, a learning process is planned during initial process development. Ladish is confident that after these two issues are understood, the process will be technically sound and cylinders can be made to the required quality and dimension requirements.

2.3 CASE JOINTS AND SEALS

This section discusses the structural analyses and the salient structural features of the metal case field joints and nozzle joint and of the case and nozzle insulation joints. Additionally, rationale for the selection of the seals is given and a discussion of their characteristics and background usage is presented.

2.3.1 METALLIC CASE JOINT

2.3.1.1 JOINT SELECTION

The selection process for the in-line bolted field joint is given in detail in the Mid-Term Report of Appendix A. In brief, the selection was driven by safety and reliability considerations, including the following:

- The in-line bolted joint allows a face seal arrangement. This arrangement, in turn, allows the use of metallic seals, which are known to be much more temperature resistant than rubber O-rings (2,500°F versus 500°F). They are also more resilient than rubber and will track instantaneously any flange opening. Furthermore, the metal is not sensitive to cold ambient temperatures.

- The bolted joint is amenable to analysis via three-dimensional finite element techniques, including the effect of pre-loading the bolts.

- Because of the above, the NASA Langley Research Center was able to optimize the bolt circle position relative to the membrane shell middle surface and, hence, minimize flange opening at the seal positions. These dimensions are incorporated into the current design.

2.3.1.2 CONFIGURATION AND STRUCTURAL FEATURES

Figure 2.3.1 shows the in-line joint that was analyzed and its critical dimensions. The design is identical to that of the November 23, 1986 LARC design with the following exceptions:

- The ARC design has an Inconel O-ring for both the primary seal and the secondary (redundant) seal. The seals are discussed in detail in Section 2.3.5.

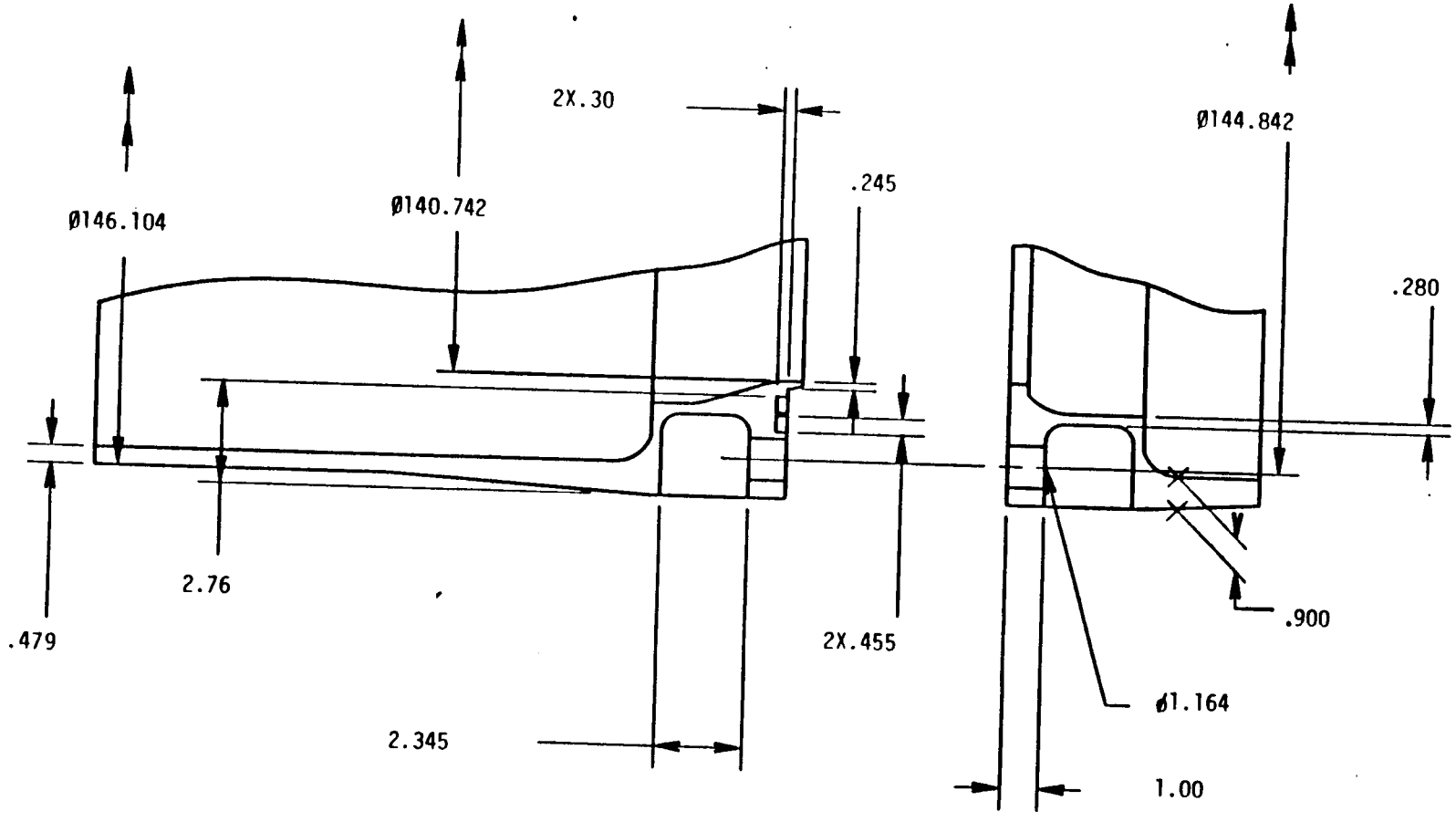

FIGURE 2.3.1. IN-LINE BOLTED JOINT CRITICAL DIMENSIONS (VALUES SHOWN ARE NOMINAL).

- The ARC design, as analyzed herein, utilizes a shear lip around the inboard circumference of the lower segment flange. This shear lip is used primarily to make rounding and fit-up easier during field assembly. This design has been modified slightly to thin the flange from 3.5 inches to 3.1 inches (inside to outside).

Bolting consists of 150 1.125-inch-diameter, high-strength studs from SPS, type MP 150. This scheme was found by LaRC to be reasonably efficient with respect to spacing, metal O-ring size, and flange thickness. Alcoves are large enough to allow the use of hydraulic tightening of the special nuts while employing an ultrasonic transducer for the LaRC pulsed phase locked loop system, which will be used to measure accurately stud pre-tension.(1) The transducer is affixed magnetically to the upper end of the stud. Four systems will be used simultaneously during field assembly.

Finally, we note that the case membrane shell is tapered for 7 inches from 0.479 inch nominal thickness to 0.90 inch nominal thickness at the alcove "roofs", thus minimizing the effects of the discontinuity.

2.3.1.3 DESIGN CONDITIONS

Table 2.3.1 outlines the major structural requirements for the SRM redesign. We note here that the ultimate safety factor of 1.4 was applied to both the equivalent axial load of 18.26×10^6 pounds and the internal MEOP of 1,004 psi in the stress analysis. This safety factor was applied to ensure that the flange gap opening would meet the required safety factor, as well as the stressed metal parts.

---

(1) Allison and Heyman, "Nondestructive Ultrasonic Measurement of Bolt Preload Using the Pulsed Phase Locked Loop Interferometer," The Second Symposium on Welding, Bonding, and Fastening, NASA Langley Research Center, October 23 - 25, 1984.

TABLE 2.3.1. JOINT AND SEAL DESIGN CONDITIONS.

1. MEOP = 1,004 PSIG.

2. ULTIMATE SAFETY FACTOR = 1.4.

3. YIELD SAFETY FACTOR = 1.2.

4. MAXIMUM MOMENT AT UPPER FIELD JOINT, M = 68 x 10^6 IN-LB.

5. EQUIVALENT LOAD:

$$W_{eq} = P \pi R^2 + \frac{2M}{R}$$

AT R = 72.0", P = 1,004 PSIG

$$W_{EQ} = 18.26 \times 10^{6} LB$$

6. MATERIAL:

D6AC CASE

CASE ULTIMATE = 200 KSI

CASE YIELD = 185 KSI

BOLT/STUD MULTIPHASE ALLOY (MP 150)

ULTIMATE = 260 KSI.

7. MAXIMUM ALLOWABLE FLANGE OPENING AT SEALS = 0.012 IN.

2.3.1.4 BOLT STRUCTURAL ANALYSIS

The ultimate bolt load is as follows:

$$F_u = 1.4\ (18.26\ no^6)/150$$
$$= 170{,}400 \text{ pounds/stud}$$

Pre-tensioning of the studs is held to 70 percent of their ultimate strength, or

$$F_p = 0.70\ (234{,}000)$$
$$= 164{,}000 \text{ pounds}$$

Thus, the pre-tension will be lost as the ultimate design load is approached; however, no problem will occur as long as the flange opening is kept to a safe level. The subsequent finite element analysis shows this to be the case. However, insofar as the studs are concerned, the ultimate safety factor (SF) becomes (with a listed strength of 234,000 pounds/bolt):

$$SF_u = \frac{234{,}000\ (1.4)}{170{,}400}$$
$$= 1.92.$$

This safety factor provides a margin over and above that which is required.

2.3.1.5 CASE WALL THICKNESS

Although the membrane wall portion of the motor case is presumably unchanged from the original lightweight HPM design, a few calculations are given regarding the membrane stress state and the safety factors to provide continuity with the overall joint analysis. The mean shell radius is taken as 72.8 inches and the minimum wall as 0.459 inch for these calculations.

BIAXIAL EFFECTS

It is important to account for the affect on ultimate strength that the two-to-one stress field found in a thin-walled pressure vessel might have. For the class of low alloy steels, similar to D6AC, the MIL-HDBK-5D suggests a factor of 0.90 to be used

to calculate strength enhancement in a two-to-one biaxial stress field. That is, the effective stress, σ_e, to be compared to the uniaxial tensile strength (σ_u = 200 ksi) is given by $\sigma_e = 0.9\ \sigma_\theta$, where σ_θ is the induced hoop stress.

SAFETY FACTOR

At the MEOP,

$$\sigma_\theta = \frac{1{,}004\ (72.8)}{0.459}$$

$$= 159{,}240 \text{ psi.}$$

Hence,

$$\sigma_e = 0.9\ \sigma_\theta$$

$$= 143{,}300 \text{ psi,}$$

and the ultimate safety factor is

$$SF = \frac{200{,}000}{143{,}300}$$

$$= 1.4.$$

Thus, the design requirement is met and case segments with the minimum wall at 0.459 inch can, in fact, be used as forward segments where the MEOP is taken as 1,004 psi.

We note that the enhancement factor for the classical von Mises stress is 0.866 for a two-to-one biaxial stress field, such that the von Mises failure criterion reasonably represents the D6AC material. For this reason, it was decided to present the NASTRAN stress contours (Section 3.2.1.7) in the form of von Mises effective stress.

MODEL SHELL STRESS

The NASTRAN shell von Mises stress away from the joint should be

$$\sigma^* = \frac{(0.866)(1.4)(1{,}004)(72.8)}{0.479}$$

$$= 185{,}000 \text{ psi.}$$

This value agrees very well with the finite element results (Figures 2.3.6 and 2.3.7).

2.3.1.6 FINITE ELEMENT ANALYSIS

A PATRAN/NASTRAN finite element model of the case, joint, and bolts was constructed as shown in Figure 2.3.2. As shown, the model is a 1/300 circumferentially repeating segment of the full-up motor. The axial length of the model is 56 inches, which is sufficient to capture the membrane behavior of the case away from the joint. The model consists of 1,724 solid elements. The stud and nuts are connected to the flanges only by linear contact elements, as are the mating flange surfaces.

The model is loaded according to Table 2.3.1 with the 1.4 ultimate factor included in the axial end load and in the internal pressure load. These "ultimate" loadings are reflected in all stress and displacement results. The applied pretension of the studs was induced into the NASTRAN solution as a cooling of the stud to an equivalent $\alpha \Delta T$ of -0.0090. The stud pre-tension was 58 percent of the ultimate strength, or 135,000 pounds. This value is lower than the intended value of 164 ksi, but it should have no significant effect on the calculated state of stress in the case or joint. Displacement values (flange opening) might be slightly greater than those with the full pre-tension.

2.3.1.7 FINITE ELEMENT RESULTS

DEFORMATIONS

Figure 2.3.3 shows the deformation pattern of the bolted joint in the vicinity of the flanges. The "heel-toe" action is clearly seen with contact indicated over most of the area of the seal grooves. Figure 2.3.4 shows the overall joint and shell deformation patterns. These patterns indicate that the model was, in fact, long enough (56 inches) to capture the membrane shell behavior away from the joint discontinuity. Figure 2.3.5 is a plot of the relative displacement between flanges (gap opening). The profile of the O-ring grooves is shown for reference. Only at the secondary seal under the alcove's gusset plate (halfway between bolts) is there a positive separation, and this value is a maximum of 0.0031 inch over the backup O-ring. With a 0.012-inch O-ring recovery capability, the ultimate safety factor on deflection (gap opening) is estimated to be

$$SF = \frac{0.012}{0.0031} (1.4) = 5.4$$

ORIGINAL PAGE IS
OF POOR QUALITY

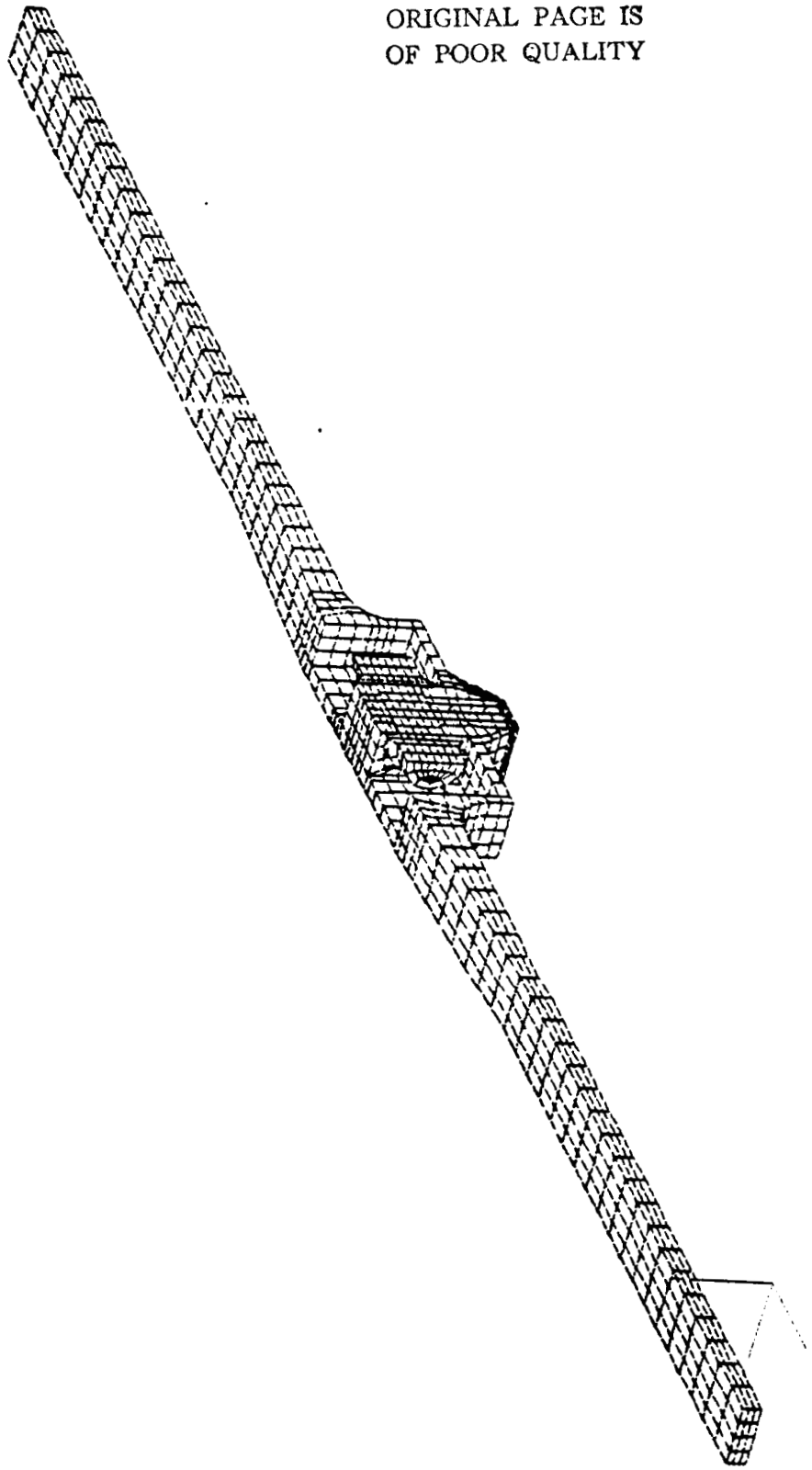

FIGURE 2.3.2. NASTRAN MODEL.

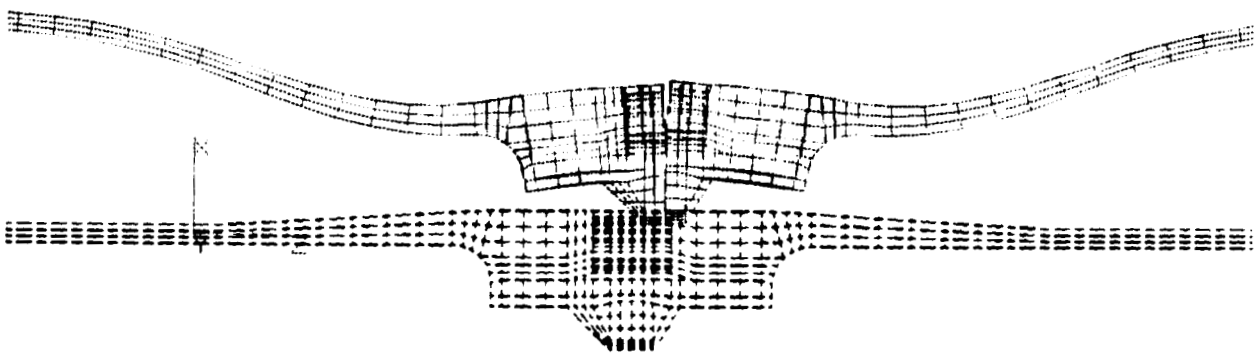

FIGURE 2.3.3. DEFORMED GRID AT FLANGES.

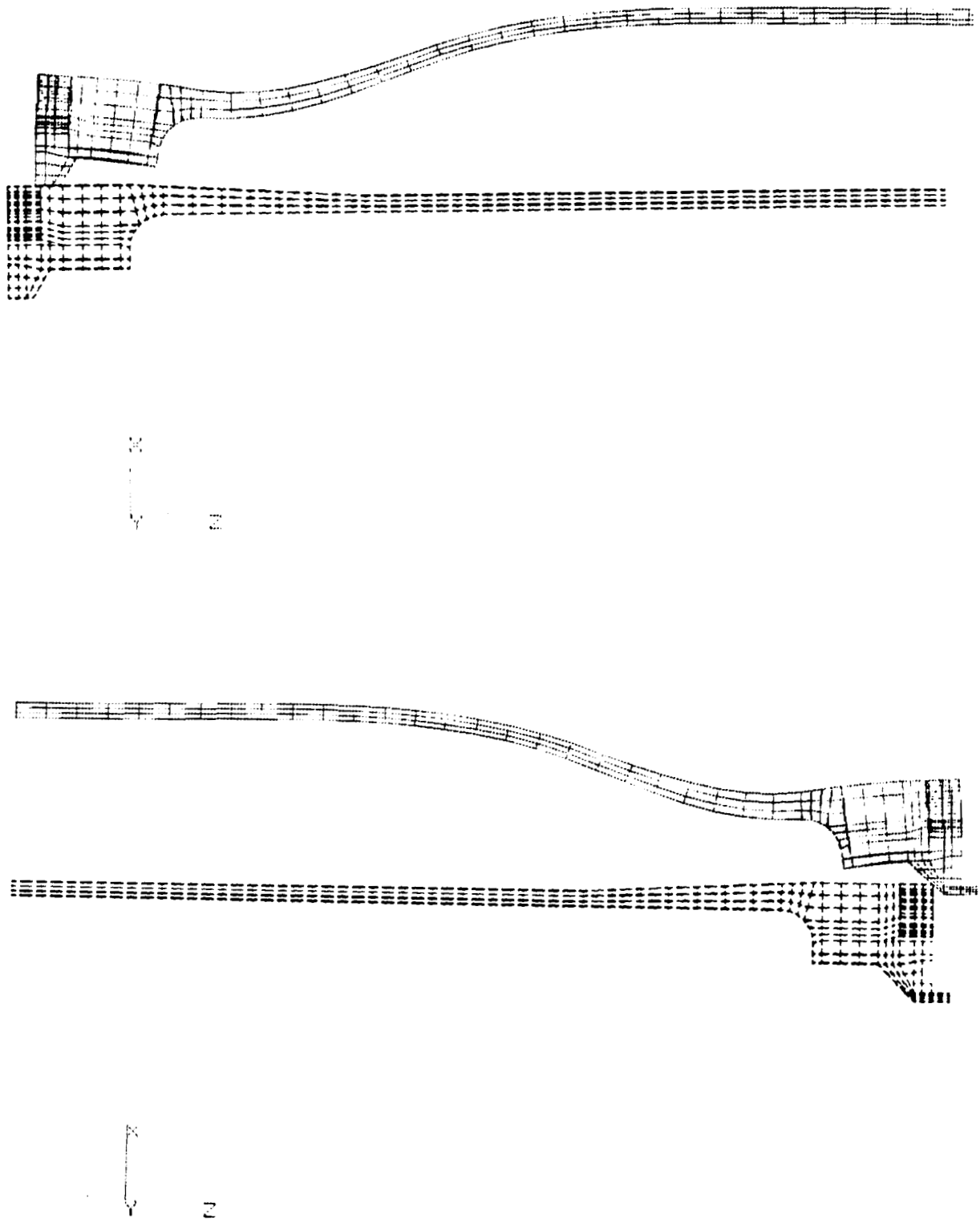

FIGURE 2.3.4. OVERALL CASE AND JOINT DEFORMATION.

ORIGINAL PAGE IS
OF POOR QUALITY

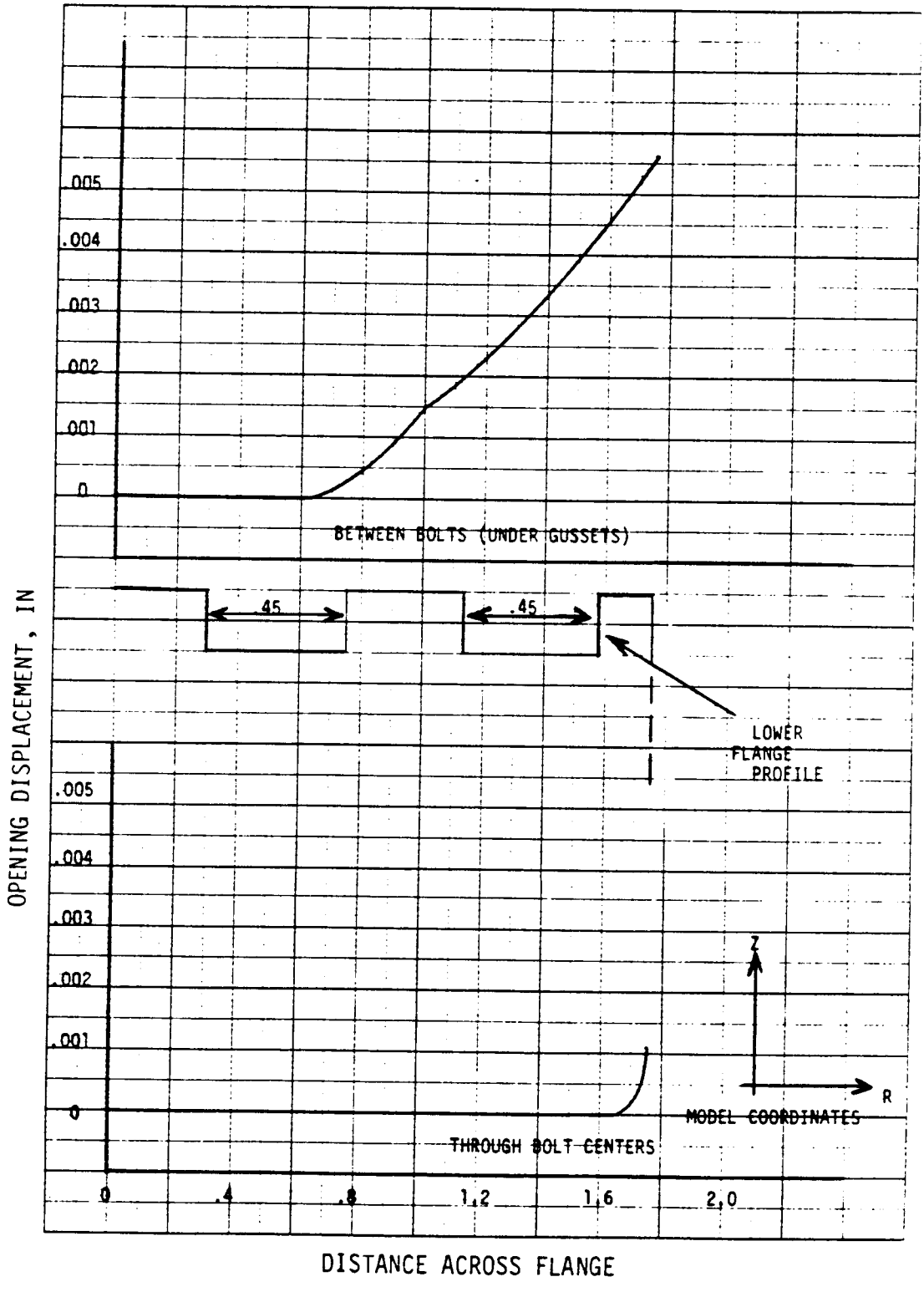

FIGURE 2.3.5. FLANGE FACE SEPARATION.

STRESS RESULTS

Figures 2.3.6 and 2.3.7 show stress contour plots on isometric views of the lower and upper segments. The color patches cover the indicated ranges of the values of the von Mises stress. These values agree well with the von Mises membrane stress in the shell (away from the joint) of 185 ksi as previously calculated in Section 2.3.1.5. Stresses throughout the tapered shell walls and the alcove gussets and roofs are satisfactorily low. However, stress concentration regions appear at the edges of the bolt holes on the respective mating surfaces of the upper and lower flanges. These areas of high stress are due to the presence of the holes in what would otherwise be a fairly uniform hoop tension field. Figures 2.3.8 through 2.3.11 show the von Mises stress contours. The very local nature of the stress concentrations is apparent in that the yield regions do not penetrate to the alcove sides of the flanges. The material that is stressed above about 185 ksi may, of course, yield, but it will not in any way threaten the ultimate strength of the joint structure. The maximum strain at the edge of the bolt holes can be estimated by

$$\varepsilon = \frac{261,500}{29 \times 10^6}$$

$$= 0.0090 \text{ inch/inch}$$

With a minimum elongation of 6 percent for the D6AC material, the ultimate safety factor would be

$$SF = \frac{0.060}{0.0090} (1.4)$$

$$= 9.3.$$

In a final Design Phase, this condition would be more rigorously analyzed via a nonlinear plasticity version of the NASTRAN code. We also note that the results shown herein are for an ultimate load condition. At the MEOP condition, the peak stress concentration reduces to

$$\sigma = \frac{261,500}{1.4}$$

$$= 186,800 \text{ psi.}$$

This pressure would cause, at worst, a tiny spot of yielded material.

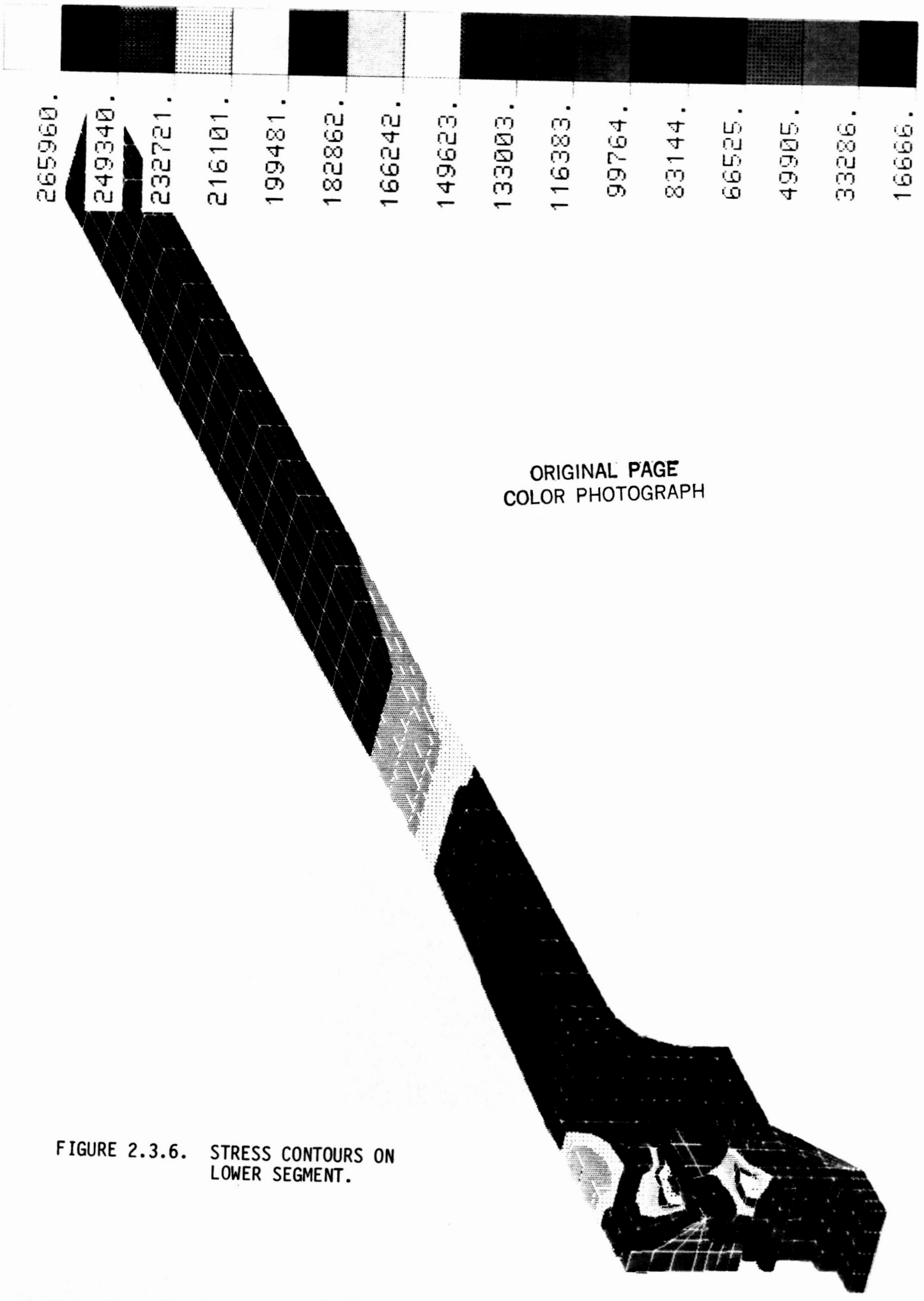

ORIGINAL PAGE
COLOR PHOTOGRAPH

FIGURE 2.3.6. STRESS CONTOURS ON LOWER SEGMENT.

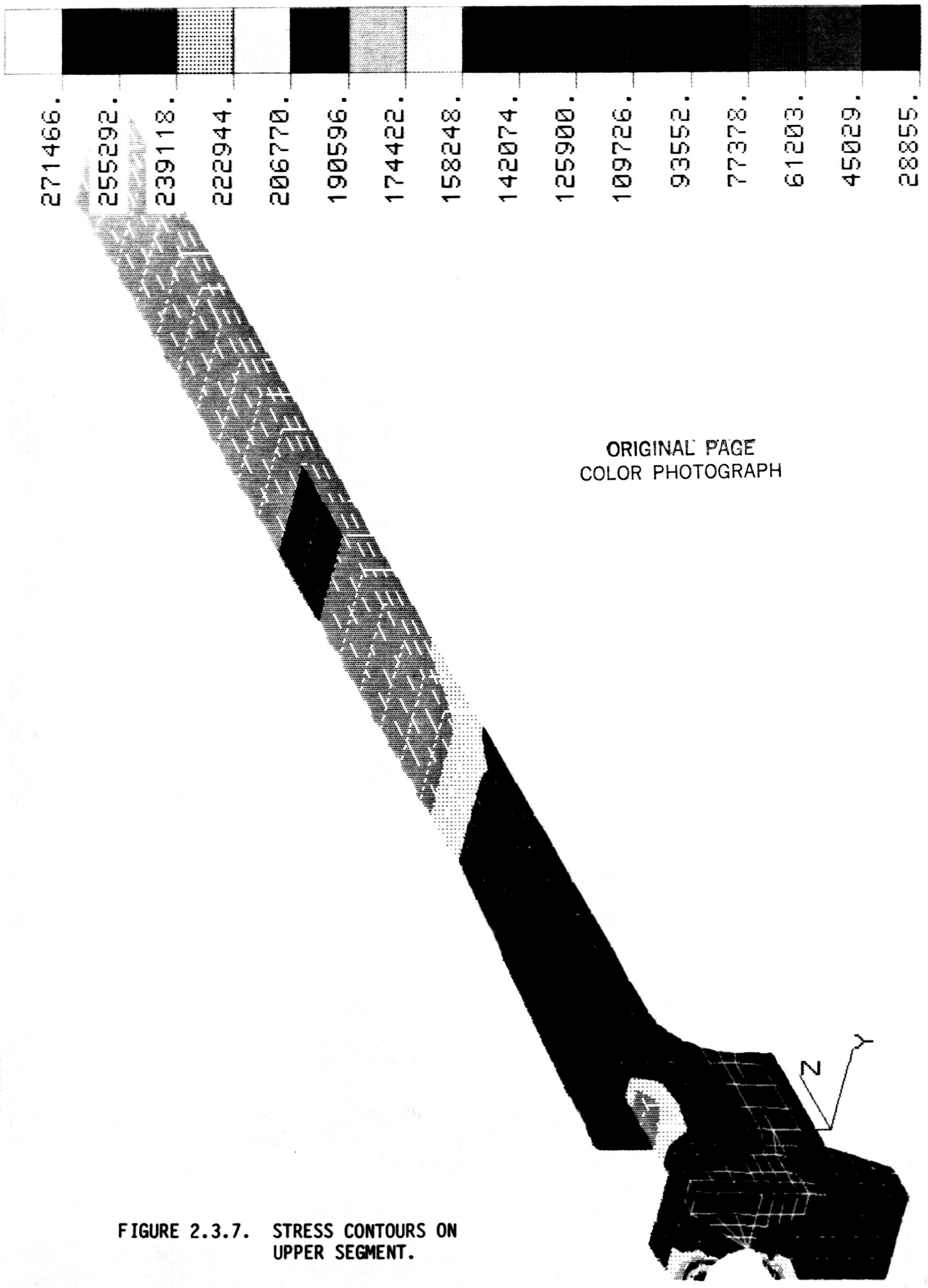

FIGURE 2.3.7. STRESS CONTOURS ON UPPER SEGMENT.

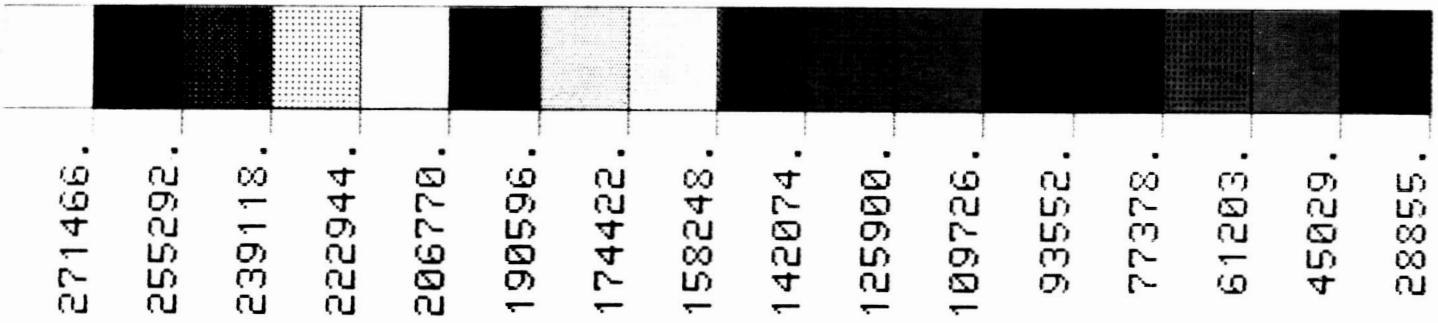

ORIGINAL PAGE
COLOR PHOTOGRAPH

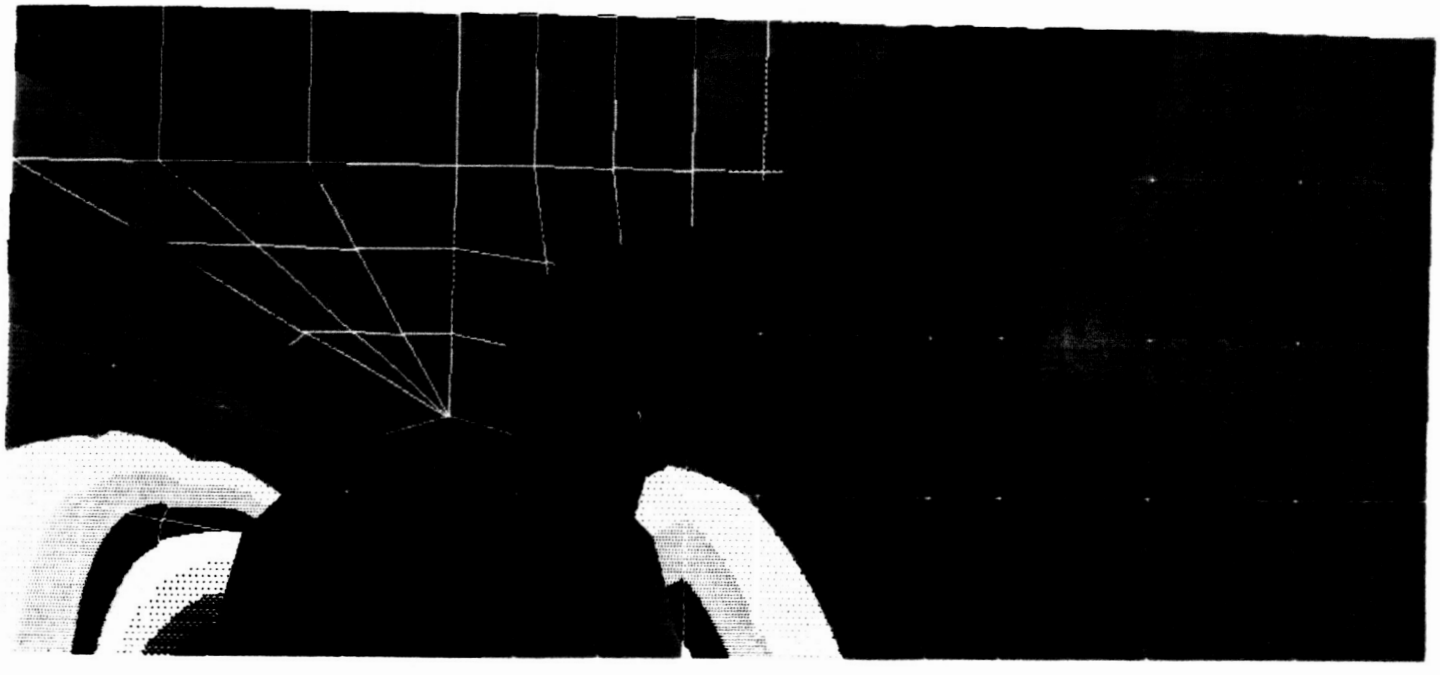

FIGURE 2.3.8. STRESS CONTOURS ON FLANGE - MATING SURFACE - UPPER SEGMENT.

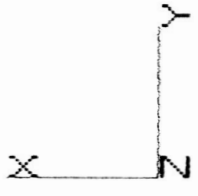

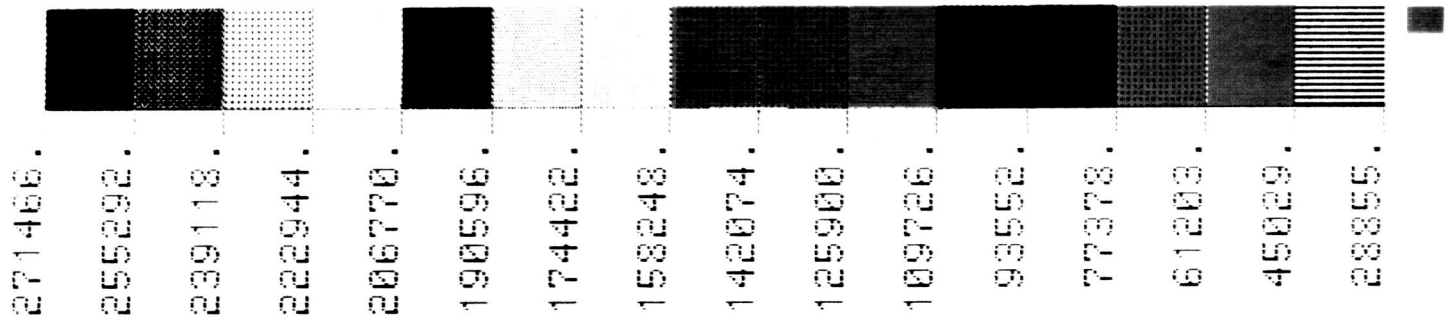

ORIGINAL PAGE
COLOR PHOTOGRAPH

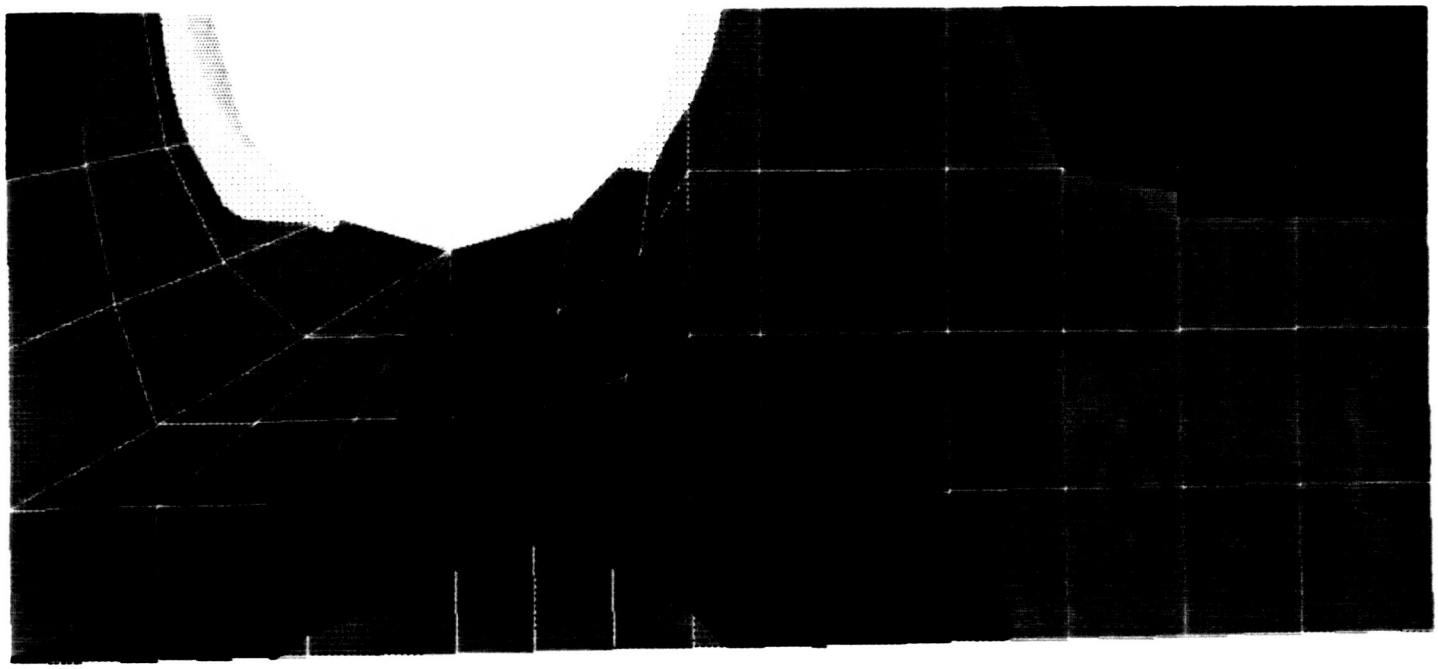

FIGURE 2.3.9. STRESS CONTOURS ON FLANGE - VIEWED FROM ALCOVE - UPPER SEGMENT.

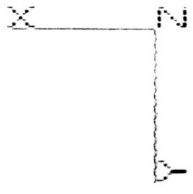

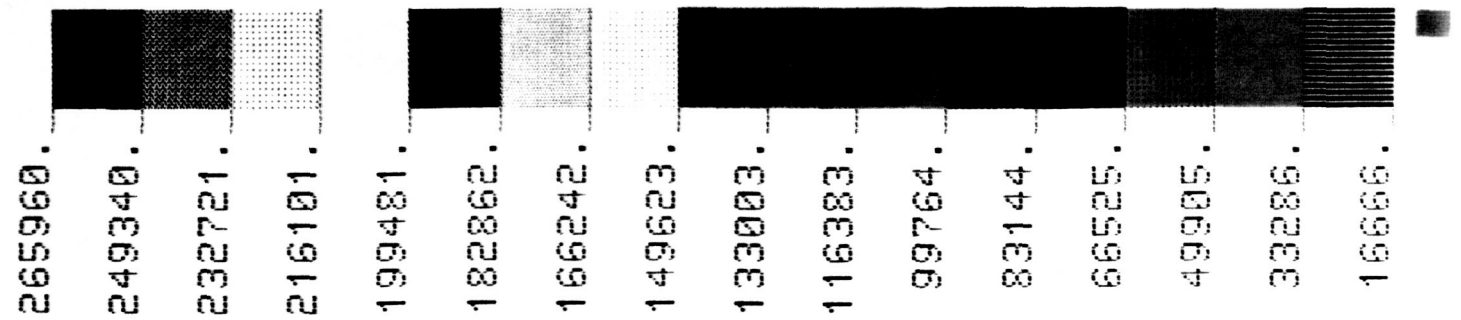

ORIGINAL PAGE
COLOR PHOTOGRAPH

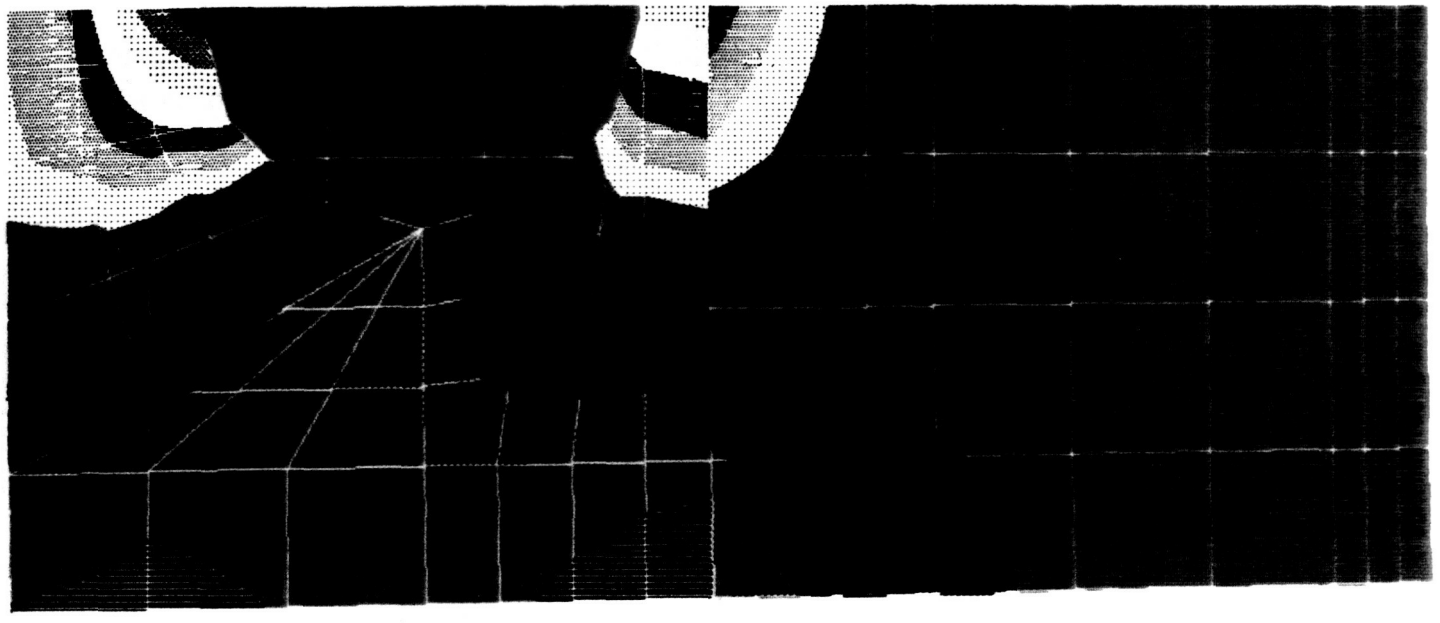

FIGURE 2.3.10. STRESS CONTOURS ON FLANGE - MATING SURFACE - LOWER SEGMENT.

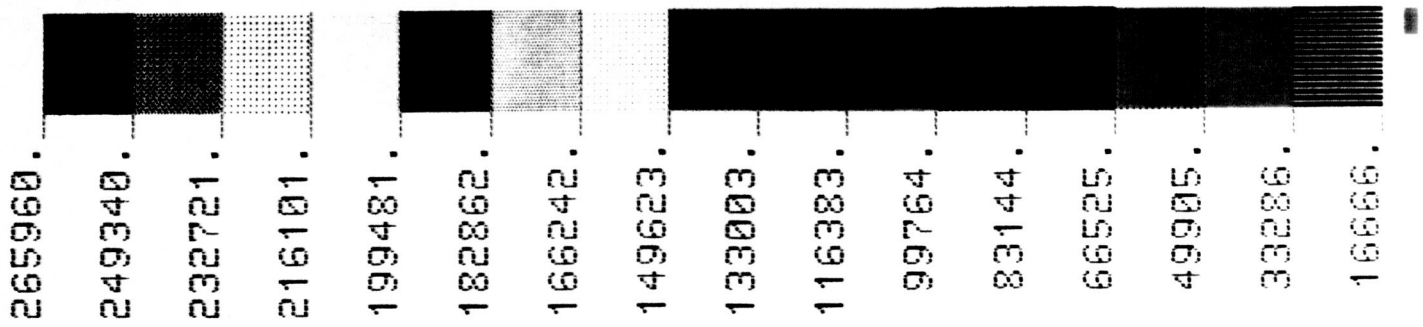

ORIGINAL PAGE
COLOR PHOTOGRAPH

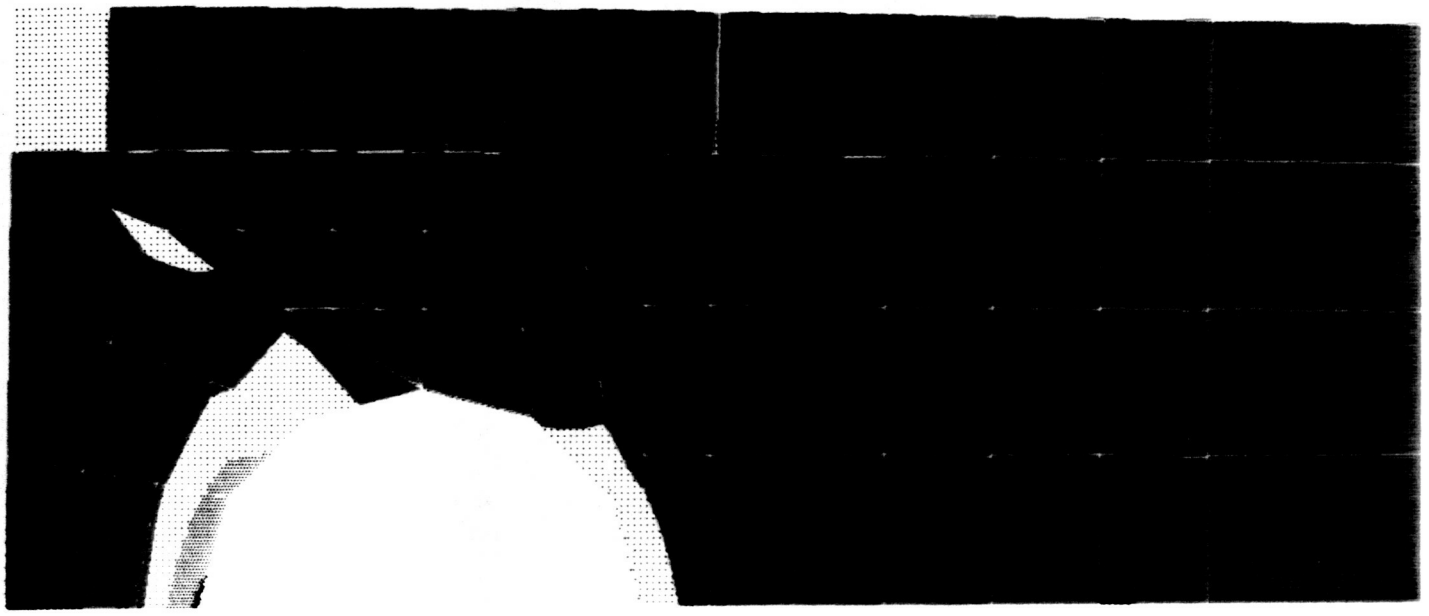

FIGURE 2.3.11. STRESS CONTOURS ON FLANGE - VIEWED FROM ALCOVE - LOWER SEGMENT.

2.3.1.8 SUMMARY AND CONCLUSIONS

Important results of the case joint structural analysis are listed below.

- The maximum flange opening (at the ultimate load) over the secondary metal O-ring is 3.1 mils. The ultimate factor of safety is 5.4.

- The membrane case safety factor is not affected by the joint design. For the "lightweight" case with a 0.459-inch minimum wall and 200,000-psi ultimate tensile strength, the ultimate safety factor is 1.4.

- The bolt ultimate safety factor is 1.92.

- Alcove gussets, backwalls, and roofs are relatively lowly stressed. The maximum gusset stress is about 170 ksi (at 1.4 x MEOP), and the maximum ultimate safety factor is in excess of 1.65.

- Stress concentrations appear at the edges of the bolt holes. The peak stress just reaches the yield strength at MEOP. The high stress regions are very localized, and the ultimate safety factor is estimated to be 9.3 based on plastic strain.

- The metal joint weight over that of an equivalent length membrane shell is 1,800 pounds.

The major conclusion is that the metallic components of the in-line bolted joint meet all of the design goals and safety requirements for the HPM baseline operating and reuse conditions. Further options were investigated that reduced the width of flange and, consequently, reduced the required forging thickness. The structural impact of narrowing the flange to 3.1 inches is estimated to be negligible.

2.3.2 CASE INSULATION FIELD JOINTS

In the first phase of this study, documented in the Mid-Term Report (Appendix A), trade studies and evaluations of various case and insulation joints were performed to select baseline joint and seal designs. An in-line bolted flange using two metallic O-ring seals were selected as the optimal case joint design. These seals are fixed in a compressed state and do not require gas pressurization to actuate sealing. For this type of sealing system, an unvented insulation joint was determined to provide the highest integrity and reliability.

The selected case insulation joint (Figure 2.3.12) is an unvented labyrinth-type that utilizes an elastomeric, open channel, stress relief component vulcanized within the case insulation. Radially oriented oval channels provide stress relief while preventing circumferential gas flow. A low modulus NBR/silica is used for the stress relief component to provide high elongation capability. NBR/silica is also used for the male portion of the overlap joint to provide a nominal 0.070 inch of compression at static conditions. A low-strength, high-strain, ambient-cured RTV adhesive/sealant fills the gap inboard of the compressed overlap. Detailed analyses of the insulation joint are presented below.

ARC performed a case insulation structural analysis. The objectives of this analysis were twofold: first, the nonvented configuration was analyzed to determine the effectiveness of the stress relief component, specifically, the normal and shear stress across the adhesive joint; and, second, the system was analyzed with an unbonded joint to determine the amount of opening at the unbonded interface. The latter result was necessary to proceed with the gas dynamic and heat transfer analysis of the metal case joint. Figure 2.3.13 shows the axisymmetric TEXGAP finite element approximation of the grain, insulation, and motor case. The model was extended for 28 inches forward and aft of the joint, and a condition of plane strain was assumed for the "cut" ends of the grain. An internal pressure of 1,004 psi was used in conjunction with a $\alpha \Delta T$ of 0.0024. The latter load assumes assembly at 80°F and a launch bulk temperature of 40°F.

Stress results are shown in Figure 2.3.14. These results are considered to be approximate since a complete laboratory tensile characterization of the viscoelastic grain and insulation materials would be required to better pinpoint their respective

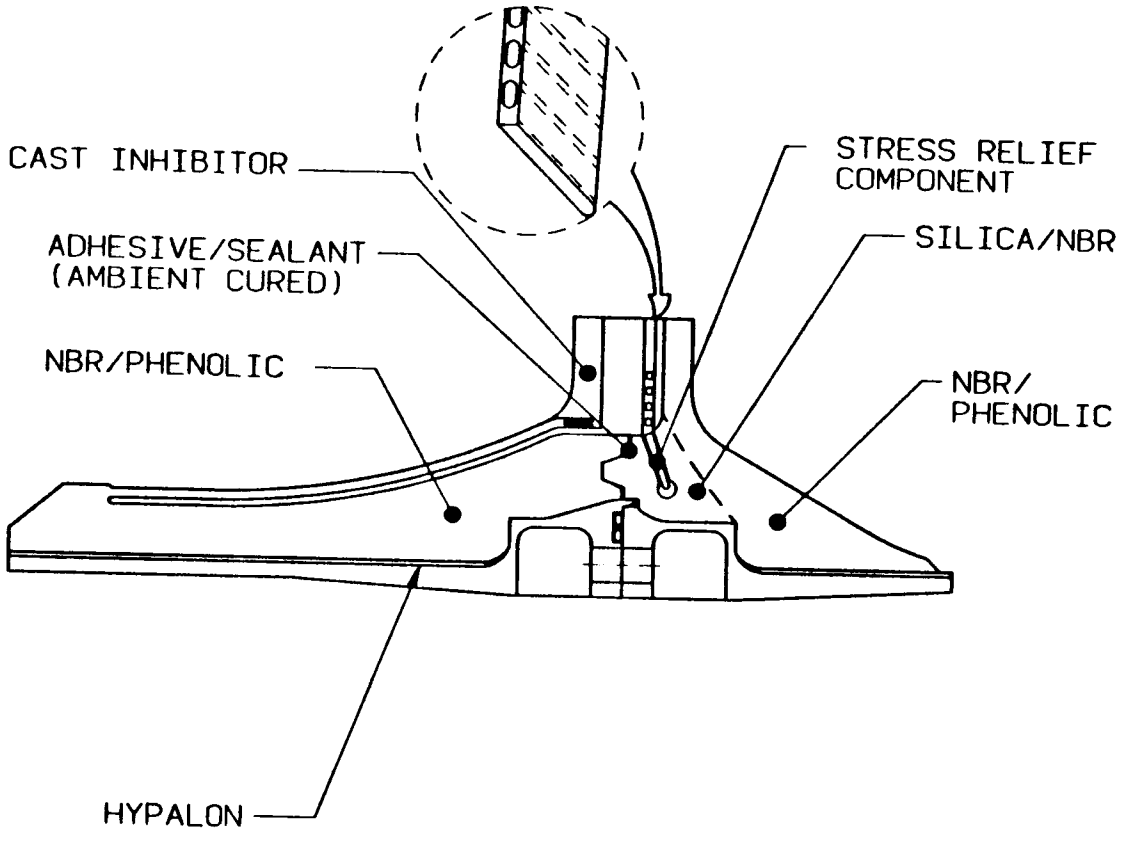

FIGURE 2.3.12. ARC BLOCK II SRM FIELD JOINT.

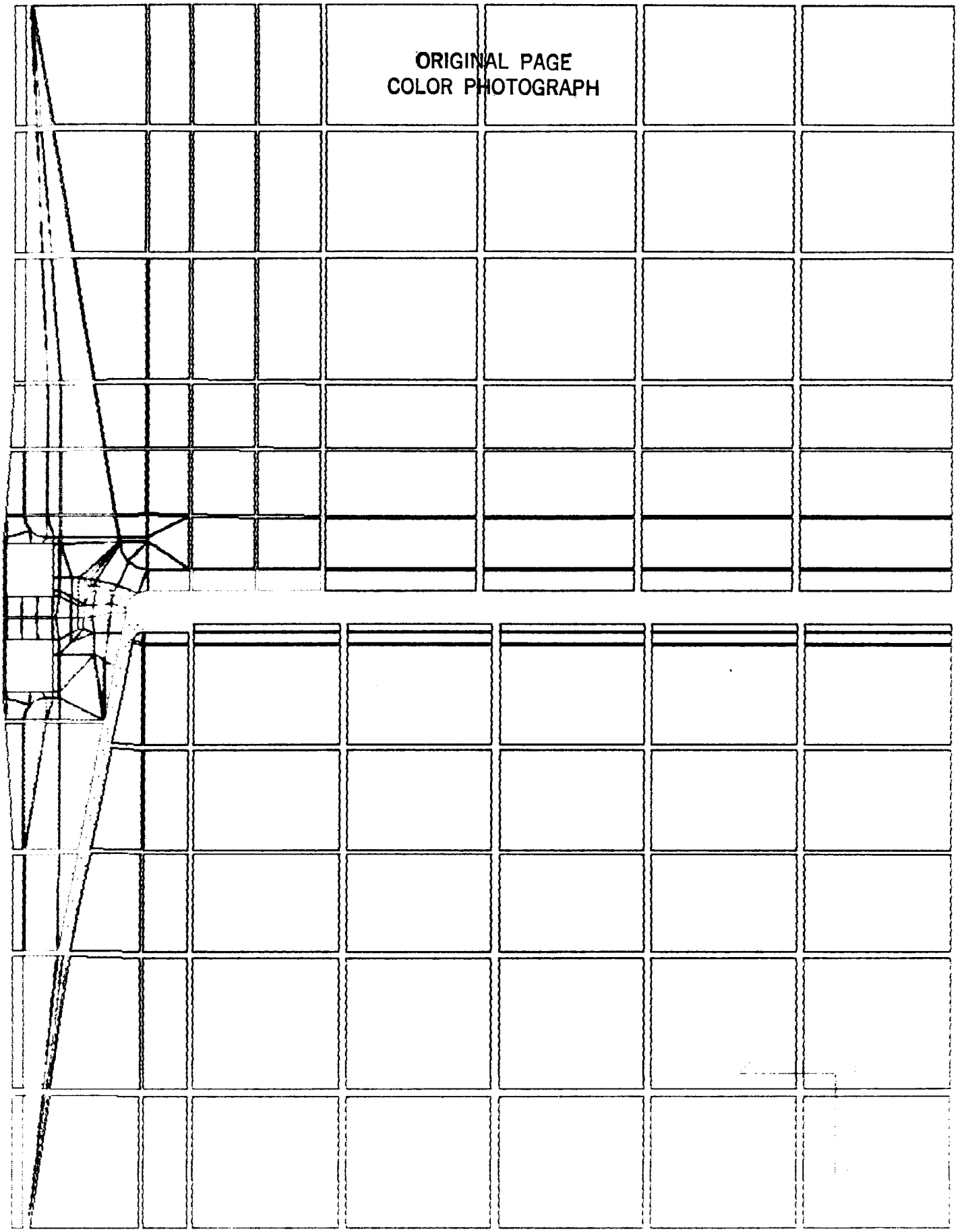

FIGURE 2.3.13. AXISYMMETRIC FINITE ELEMENT MODEL - CASE JOINT, INSULATION, AND GRAIN.

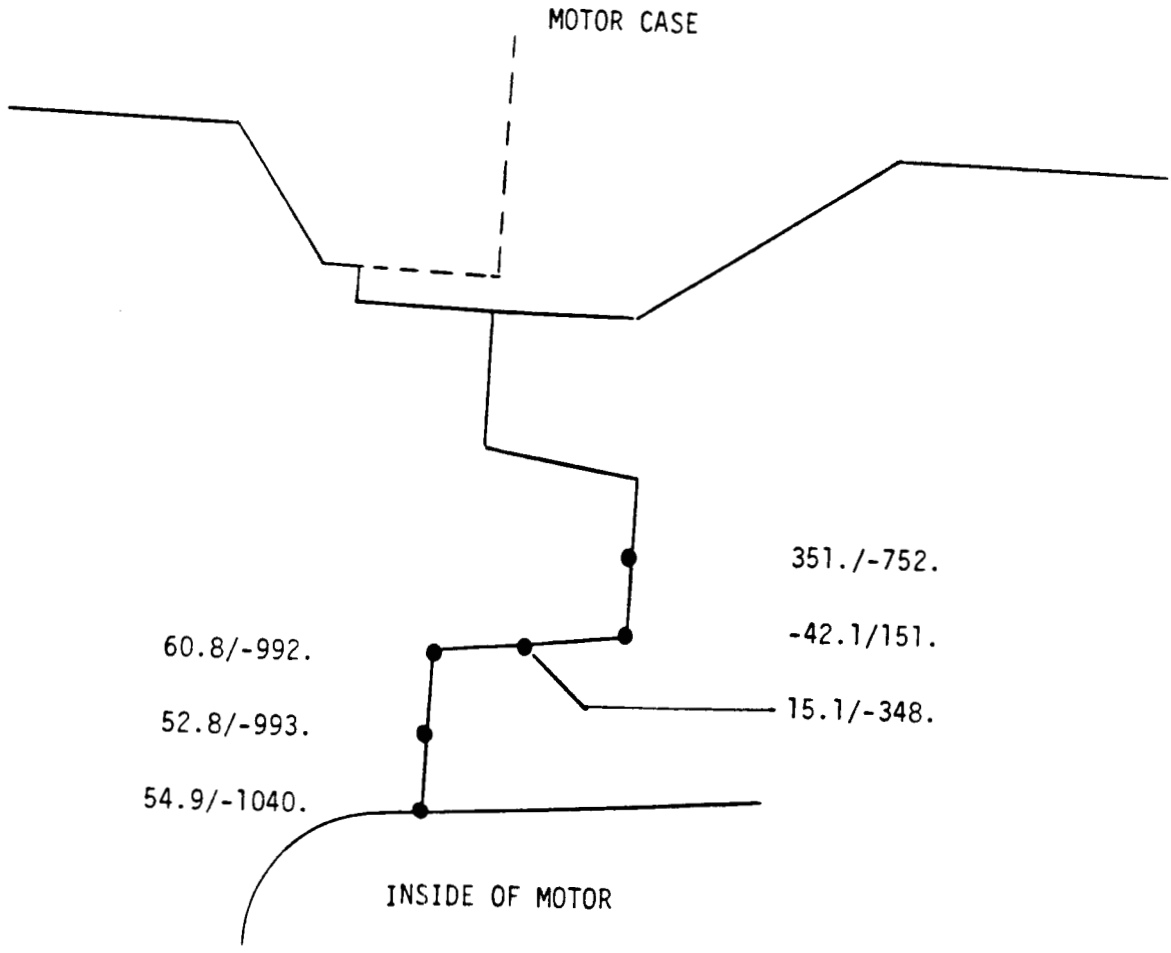

FIGURE 2.3.14. STRESSES ACROSS INSULATION BONDLINE.

moduli. The stress values presented are considered to be reasonably low and within the capability of adhesive systems. All stress normal to the bondline is compressive.

Deflection results are shown in Figure 2.3.15. These results were used in the thermal analysis below.

Thermal analyses of the case insulation joint were performed to evaluate the following three areas:

- Erosion and charring in the joint region,
- Heating in the stress relief channels,
- Heating in the insulation joint.

Details of the analytical techniques are contained in Section 2.4.

Heating rates are fairly benign in the joint region due to protection by the forward inhibitor. Convective film coefficients are approximately 30 percent of the values along the sidewall, and luminous thermal radiation from combustion gas is negligible due to the close proximity of the inhibitors. In-depth temperatures, erosion rates, and heat-affected rates are shown in Figure 2.3.16. The insulation joint is sized such that the compressed face of the overlap joint is not thermally degraded during motor operation.

Heating rates in the stress relief channels are solely dependent upon local gas flow rates in the channel. Thermal evaluation of gap heating rates requires coupling of a one-dimensional gas flow module to a two-dimensional conduction network module. Positive pressurization rates force hot gases into the channels; the gases transfer heat to the surrounding wall and contract, thereby decreasing pressure and causing a low level influx of additional hot gases. Conversely, a pressure decrease results in an efflux of gas from the channels. Circumferential flow is prevented by the insulation web between channels. The HPM pressure profile is fairly regressive, which tends to produce the majority of heating during the ignition phase. Oscillatory pressure fluctuations, such as those caused by vortex shedding from the inhibitors, and mass transfer effects from insulation decomposition were not included in the channel heating rate analyses summarized below.

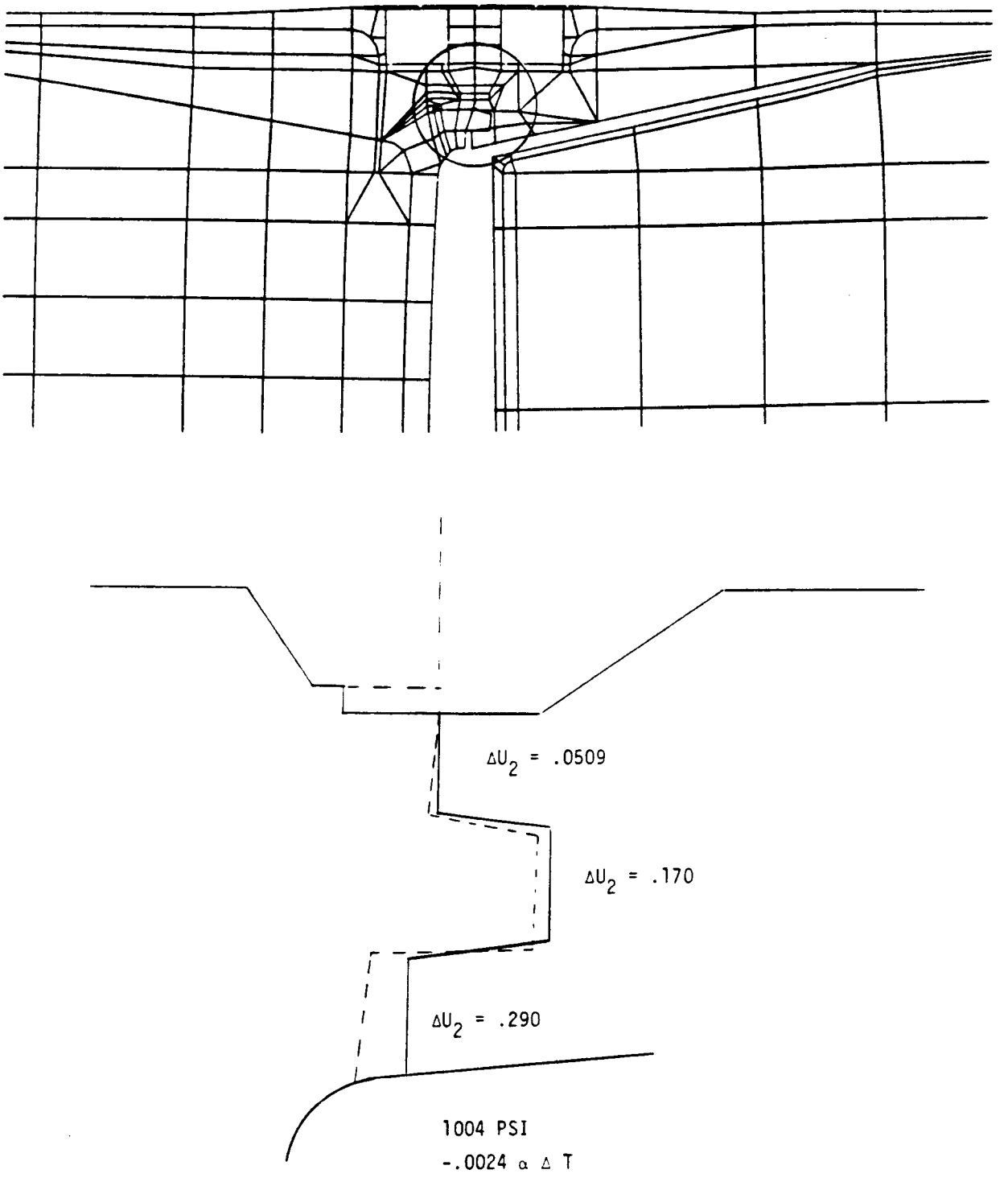

FIGURE 2.3.15. INSULATION SEAL JOINT OPENING CHARACTERISTICS - ADHESIVE ASSUMED TO BE FAILED.

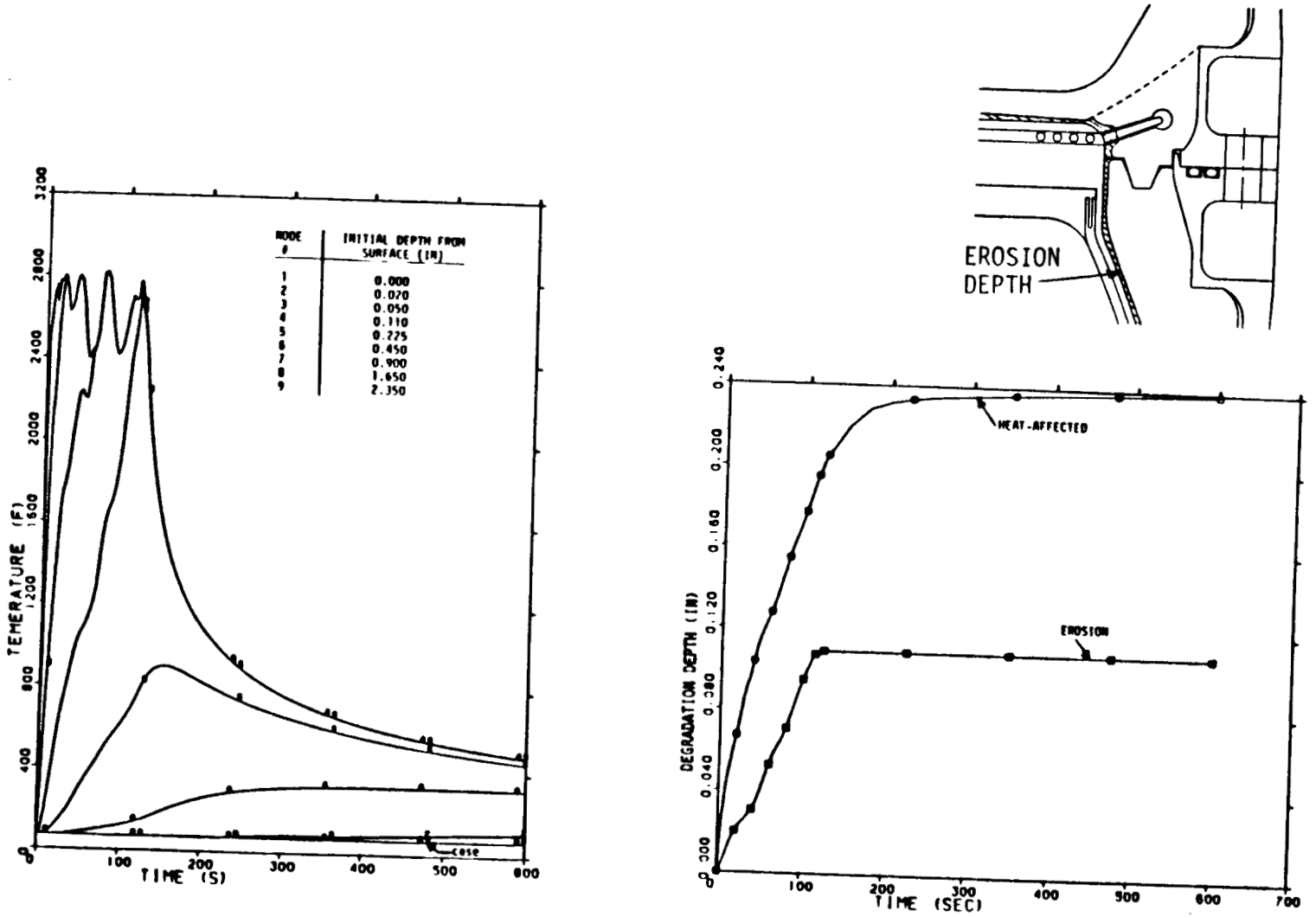

FIGURE 2.3.16. IN-DEPTH INSULATION TEMPERATURES AND DEGRADATION PROFILES FOR CENTER SEGMENT FIELD JOINT.

Figure 2.3.17 presents gas temperatures and heating rates along the length of the stress relief channel. Gas temperatures are shown to decay rapidly with time from ignition and with distance from the channel opening. These heating rates were used in heat and mass transfer analyses to determine erosion and degradation of the stress relief wall. Results shown in Figure 2.3.18 verify that the web between channels will not erode during motor operation, thereby preventing the occurrence of circumferential flow.

The stress relief component is configured to preclude opening of the unvented insulation joint during motor operation. Nevertheless, the joint must be capable of operating successfully in a vented mode to ensure that adequate reliability is achieved. In a vented mode, the primary heating is due to a combination of radial flow during the initial portion of burn and circumferential flow during the remainder of operation. A steady 0.5-psi pressure drop was used to determine mass flow rates in the joint. Erosion and heat-affected rates in the gap are presented in Figure 2.3.19. Erosion rates are sufficiently small to preclude failure of the compressed face of the joint.

The above analyses verify the thermal and structural integrity of the insulation joint design. Stress relief minimizes both joint stresses and deflections. Erosion is sufficiently small to preclude consumption of the web between stress relief channels and degradation of the compressed face of the joint overlap. Furthermore, the insulation joint is shown to be capable of withstanding circumferential flow if the joint becomes vented.

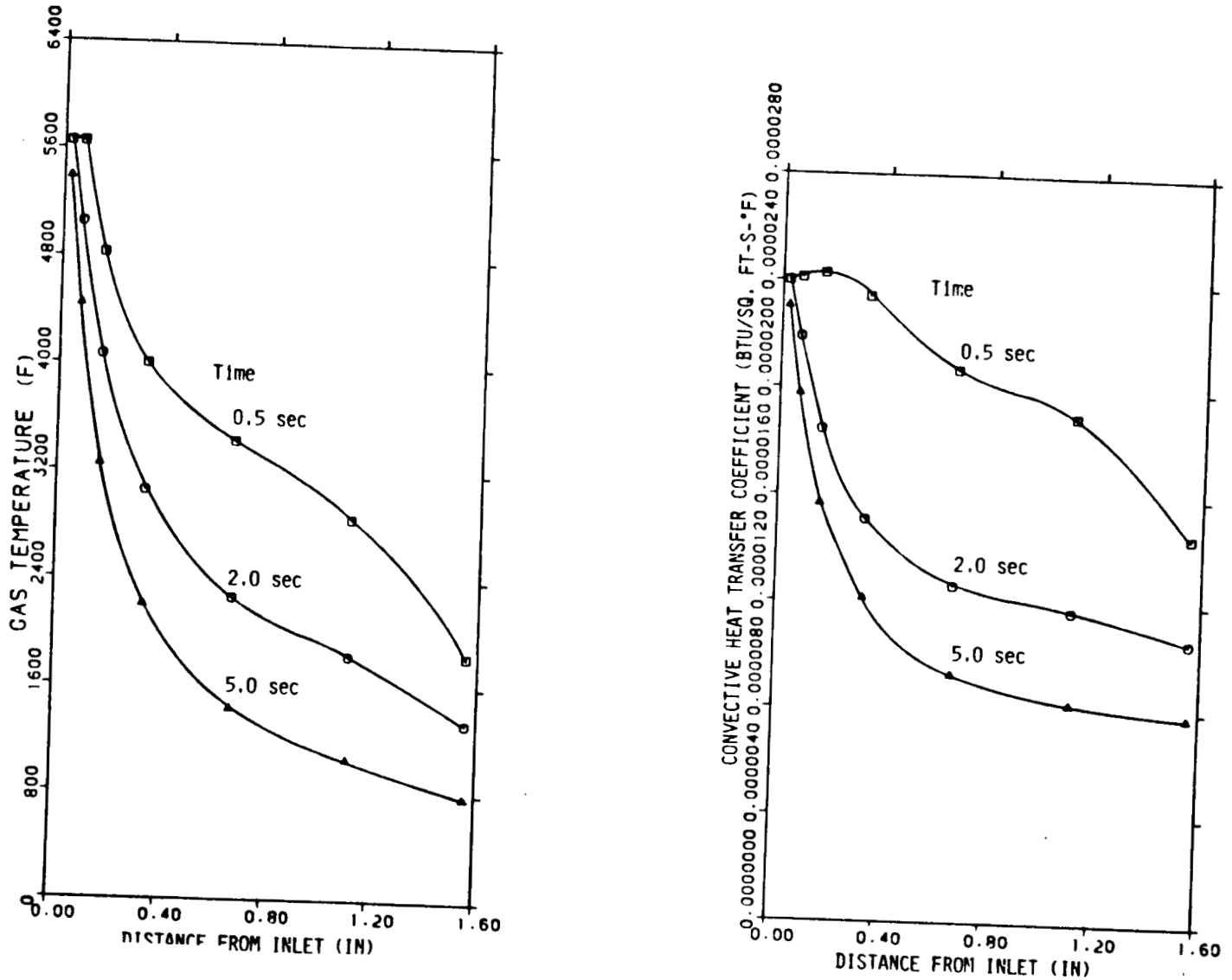

FIGURE 2.3.17. HEATING RATES IN CASE INSULATION STRESS RELIEF CHANNELS.

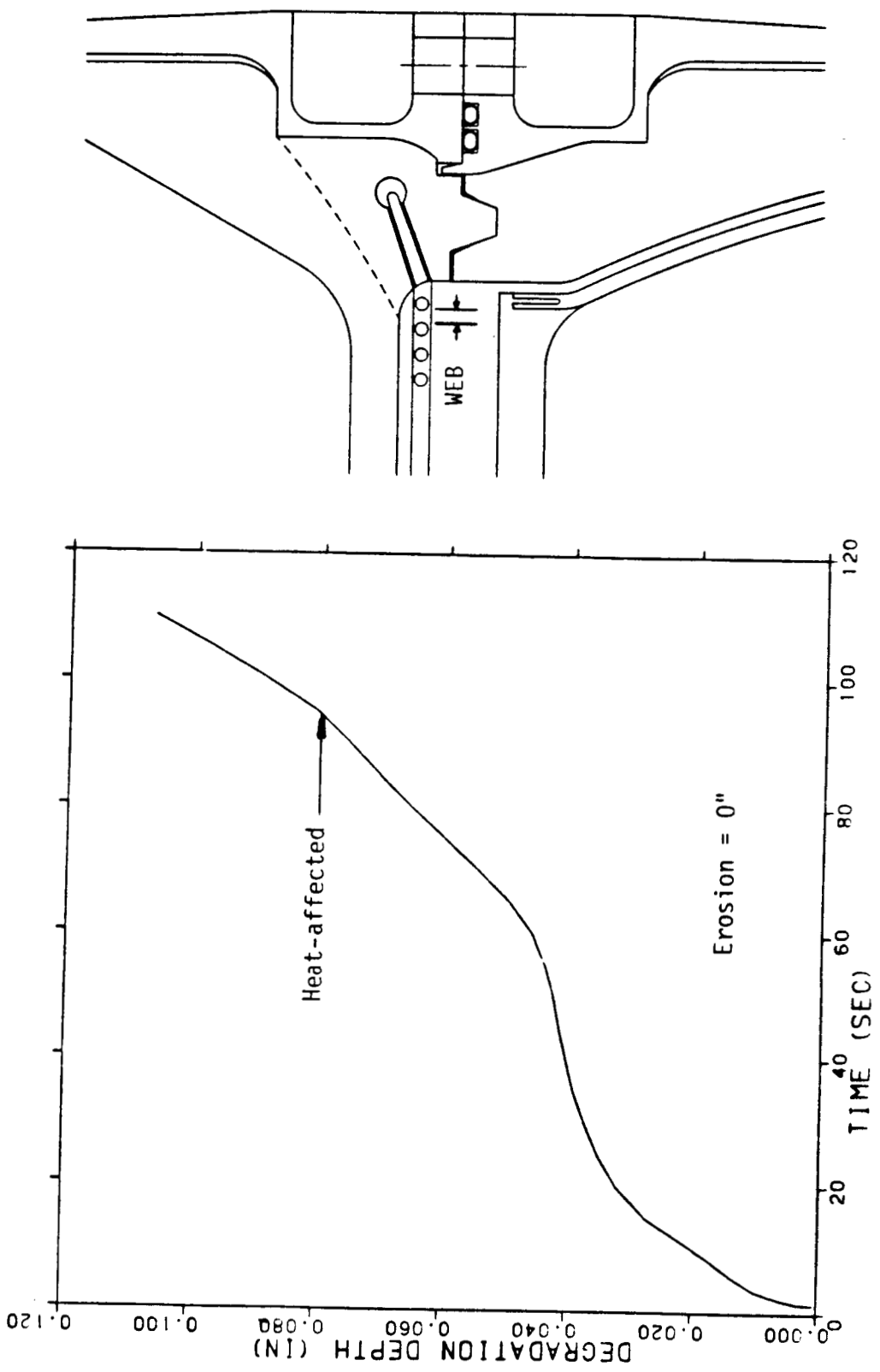

FIGURE 2.3.18. THERMAL DEGRADATION OF CASE INSULATION STRESS RELIEF CHANNEL WEB.

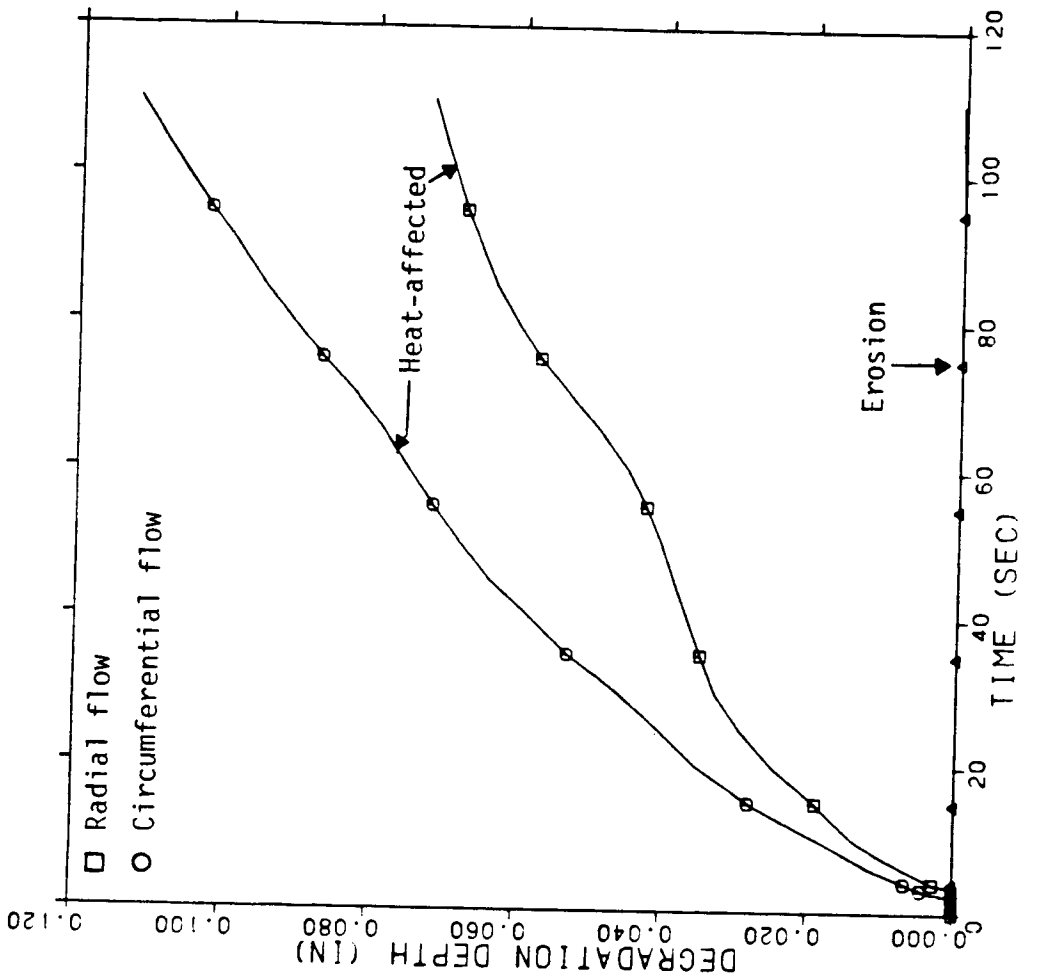

FIGURE 2.3.19. DEGRADATION PROFILES FOR THE CASE INSULATION JOINT.

2.3.3 NOZZLE-TO-CASE METAL JOINT

2.3.3.1 JOINT SELECTION

The selection process for the nozzle-to-case joint hardware configuration is described in Appendix A, the Mid-Term Report. The preliminary selection given in that report, the dual face seal approach, was confirmed by subsequent work. In brief, the selection was driven by safety and reliability considerations. Some of these considerations are

- The dual face seal joint allows the use of metallic seals, which are much more resistant to high temperatures than the rubber O-rings required by any design utilizing bore seals. The metallic seals will also track gap opening instantaneously, even at cold ambient temperatures, which significantly reduce the tracking capability of rubber O-rings.

- The dual face seal arrangement allows both the primary and secondary seals to be positively pre-loaded with the existing attachment bolts.

- In the event of leakage past the unvented insulation joint, the face seals are protected from direct impingement of a hot gas jet.

2.3.3.2 STRUCTURAL DESCRIPTION

The ARC Block II nozzle-to-case hardware joint design, which is shown in Figure 2.3.20, incorporates face seals as both the primary and secondary seals. Changes required from the 51-L design include increasing the width of the flange mating surfaces to accommodate the revised seals, increasing the nozzle flange thickness to reduce gap opening of the primary seal, and the addition of a shear lip on the nozzle flange with a radial interference fit. The shear lip eliminates relative radial sliding of the dome and nozzle flanges and reacts the resulting radial force in direct shear rather than by friction or shear in the bolt. Membrane thicknesses in the case dome and the nozzle fixed housing are unchanged from the 51-L design. Critical dimensions are shown in Figure 2.3.21. These revisions result in a 740-pound weight impact.

Also included in the Block II design are leak check ports, which allow verification of both the primary and secondary seals in the direction of operation. A rubber O-ring bore seal is retained to act as a leak check seal for the primary face seal.

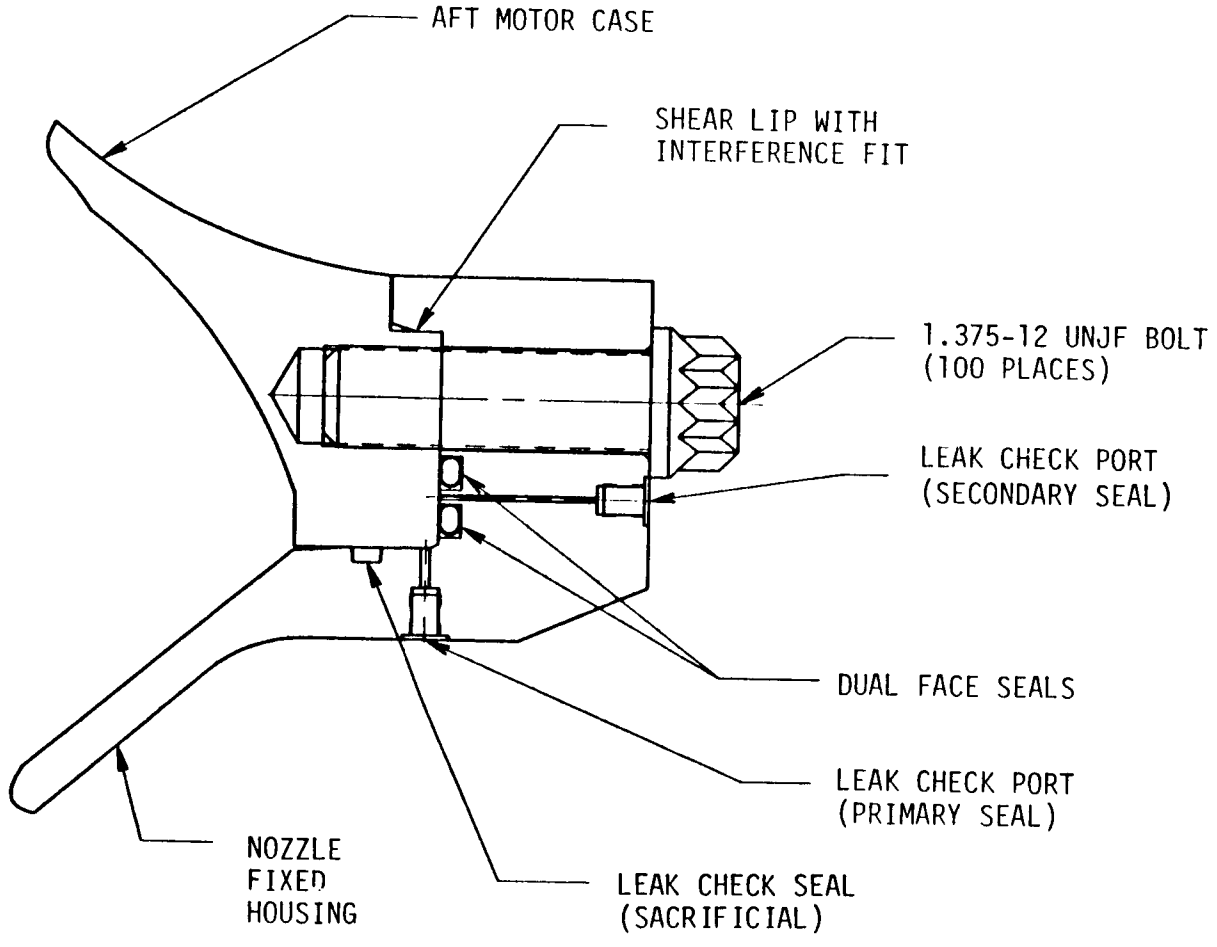

FIGURE 2.3.20. BLOCK II NOZZLE-TO-CASE JOINT DESIGN.

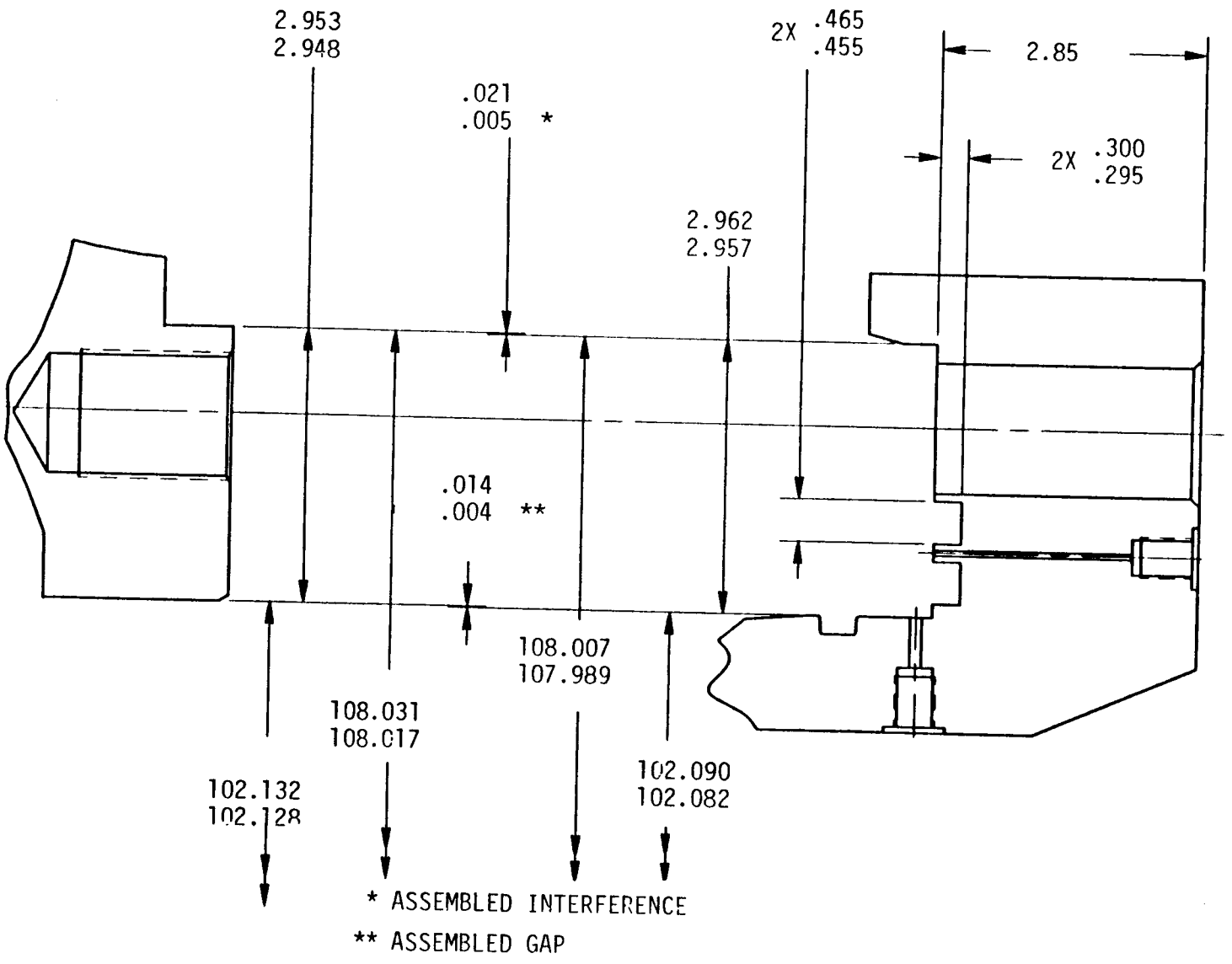

FIGURE 2.3.21. NOZZLE-TO-CASE JOINT CRITICAL DIMENSIONS.

The nozzle is attached using 100 1.375-12UNJF bolts, which are pre-loaded to a total of 16.5×10^6 pounds minimum, approximately 3.9 times the nozzle blow-off load.

2.3.3.3 DESIGN CONDITIONS

Table 2.3.2 lists the primary structural requirements used for the Block II joint design. Maximum pressure and thrust loadings were imposed to ensure the structural integrity of the nozzle fixed housing, the motor aft dome, and the nozzle attachment bolts. Seal deflection requirements were interpreted to mean that gap openings due to the application of limit loads must be kept to less than one-half the seal capability.

2.3.3.4 FINITE ELEMENT ANALYSIS

A PATRAN/NASTRAN three-dimensional finite element model (FEM) of the nozzle-to-case joint was generated for structural analysis and is shown in Figure 2.3.22. The model represents a one-hundredth (3.6 degrees) repeating segment of the motor circumference and utilizes symmetry boundary conditions to simulate the cyclic nature of the structure. The entire length of the nozzle fixed housing and the motor aft dome up to the tangency point were included. This causes the joint area to be sufficiently remote from the axial boundaries so that joint deformations are not significantly affected by rotation and radial deflection boundary conditions of the forward end of the FEM. The attachment bolt was rigidly attached to the motor dome, simulating the threaded condition. The nozzle and motor flanges, and the bolt head and nozzle flange, were connected using only linear contact elements. A radial shear connection was included between the nozzle and motor dome at the shear lip, while no shear connection was included between bolt and nozzle. Joint pre-load was simulated by imposing a reduced temperature (-859°F) on the bolt shank, which was given a coefficient of thermal expansion of 6.6×10^{-6} in-in/°F. The resulting pre-load was 154,200 pounds, which was only slightly less than the 165,000 pounds that was desired. This small difference did not significantly affect the results.

Limit loads were applied to the NASTRAN model according to Table 2.3.2. Pressure was applied along the entire internal surface and in the radial gap between the nozzle and the dome attachment ring, down to the primary seal. A nonlinear analysis was conducted in which contact loads between parts were determined consistent with the relative flange deformations by iteration within the NASTRAN solution procedure.

TABLE 2.3.2. JOINT AND SEAL DESIGN CRITERIA.

JOINT HARDWARE

1. MAXIMUM PRESSURE = 909 PSI (LIMIT).
2. THRUST = 3.31×10^6 POUNDS (LIMIT).
3. APPLIED LOAD AT FORWARD END OF FIXED HOUSING = 1.16×10^6 POUNDS (LIMIT).
4. ULTIMATE SAFETY FACTOR = 1.4.
5. FIELD SAFETY FACTOR = 1.2.
6. PRESSURE ACTS UP TO PRIMARY SEAL.

DEFLECTION AT SEALS (GAPS)

1. SEALS SHALL DEMONSTRATE SEALING CAPABILITY AT:
   A. TWO TIMES MAXIMUM GAP SIZE AT MAXIMUM EXPECTED TRACKING RATE.
   B. TWO TIMES TRACKING RATE AT MAXIMUM EXPECTED GAP SIZE.

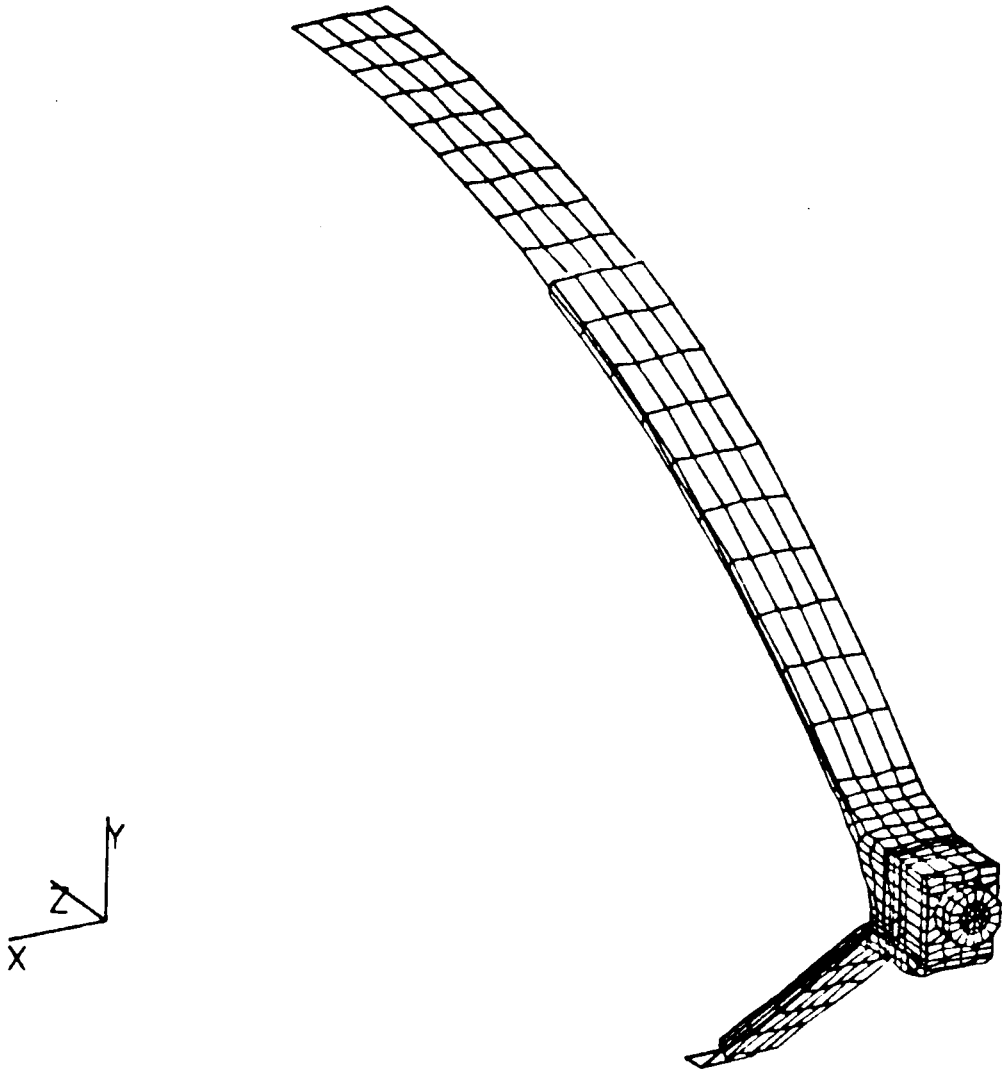

FIGURE 2.3.22. NASTRAN FINITE ELEMENT MODEL OF NOZZLE-TO-CASE JOINT.

The total model deformations for the limit load condition are shown in Figure 2.3.23, while Figure 2.3.24 shows deformations in the joint region. In both of these computer plots, deflections are multiplied by a scaling factor for display purposes. As can be seen from these figures, the nozzle housing tends to move inward while the motor dome tends to deflect outward, which is consistent with the relative pressure loadings. This mismatch in radial deformations is one of the primary causes for the opening of the joint. The other major cause is the eccentricity between the line of action of the blow-off load carried down through the fixed housing and the reaction at the bolted interface. This combination of loads leads to gap opening at the nozzle-to-dome interface as shown in Figure 2.3.25 for the limit load condition. This is a view looking aft at the mating surface, and the numbers shown indicate the axial gap opening at each location. These results show that the gaps are uniform in the circumferential direction with essentially no waviness. This deflection pattern also indicates that the flanges remain in intimate contact outboard of a radius, which is just inboard of the bolt centerline.

Computer-generated contour plots were used to evaluate the maximum stresses that were used in margin of safety calculations. Figures 2.3.26 through 2.3.30 illustrate these stress distributions in critical regions for the limit load condition. Shown in Figures 2.3.26 and 2.3.27 are von Mises stress distributions in the forward and aft faces of the nozzle flange, respectively. Cross-sections of the nozzle housing and the motor dome, with the von Mises stress contours shown, are included in Figures 2.3.28 and 2.3.3.29, respectively. Finally, Figure 2.3.30 is the axial stress distribution in a bolt cross-section. A summary of the stress state in the metal parts is given in Figure 2.3.31, where the maximum stresses are noted at critical locations along with the resulting margins of safety. Critical margins were all positive, which verifies the structural integrity of the joint hardware.

2.3.3.5 JOINT SEALING CAPABILITY

The maximum gap openings of the inboard edge of each seal groove were determined for limit loads to evaluate the joint sealing capability. These gap openings are illustrated in Figure 2.3.32. Also shown in this figure are the seals themselves, 2 0.375-inch-diameter, silver-plated, Inconel metal O-rings. The seals are described more fully in Section 2.3.5. The maximum allowable gap opening (springback) recommended by the manufacturer for these Inconel O-rings in this application is 0.012 inch (see

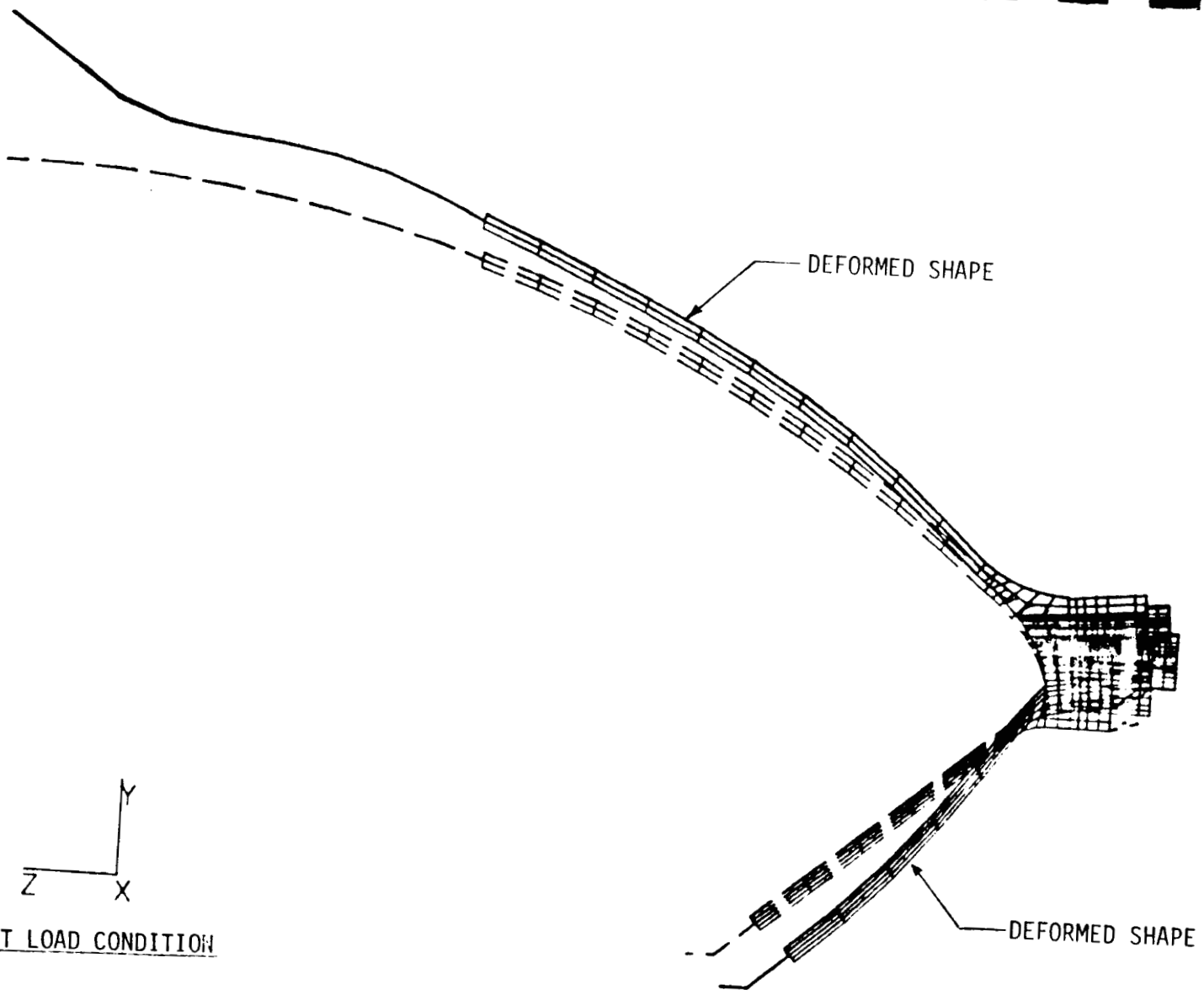

LIMIT LOAD CONDITION

PRESSURE = 909 PSIG

LOAD AT FIXED HOUSING = 1.16×10^6 POUNDS

FIGURE 2.3.23. FINITE ELEMENT MODEL DEFORMED SHAPE.

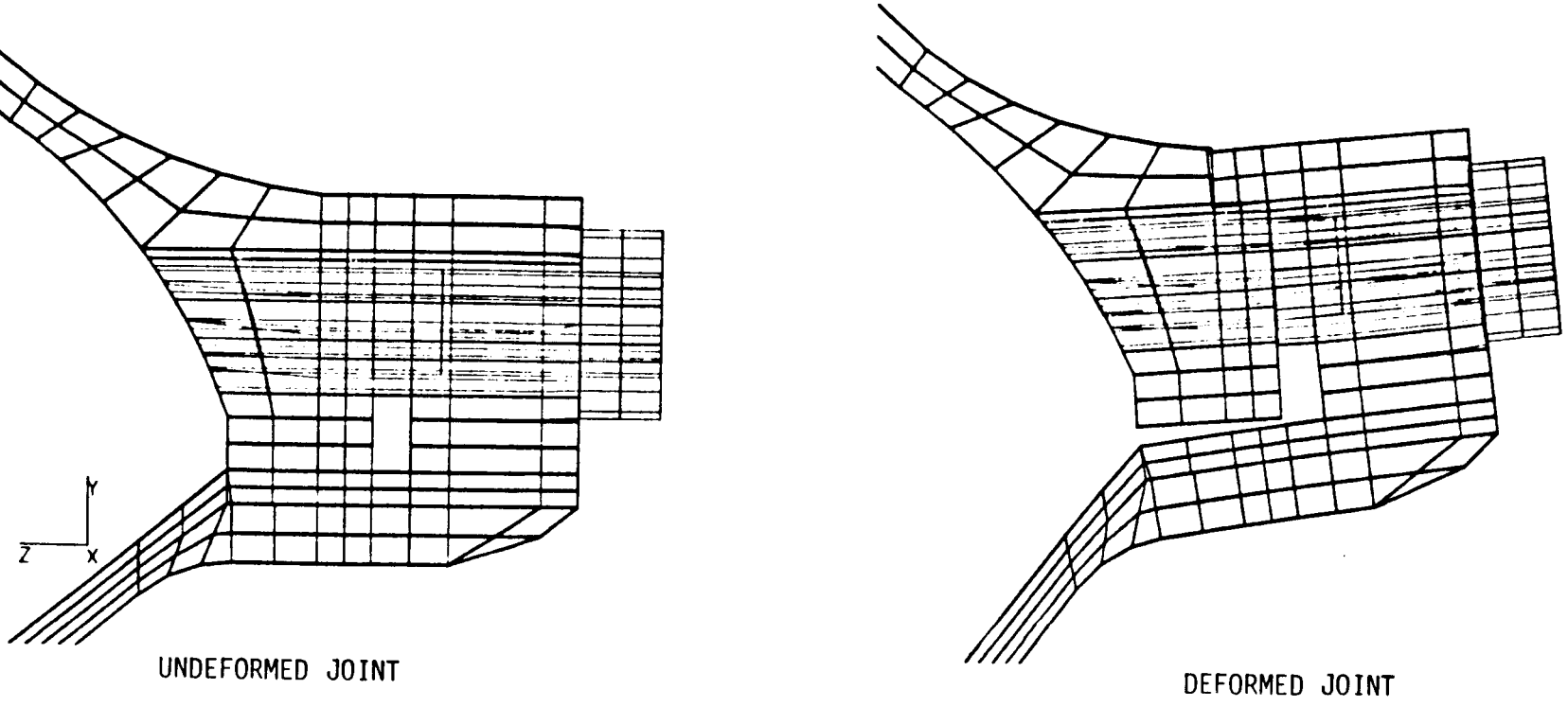

UNDEFORMED JOINT

DEFORMED JOINT

FIGURE 2.3.24. FINITE ELEMENT MODEL LOCAL JOINT DEFORMATIONS.

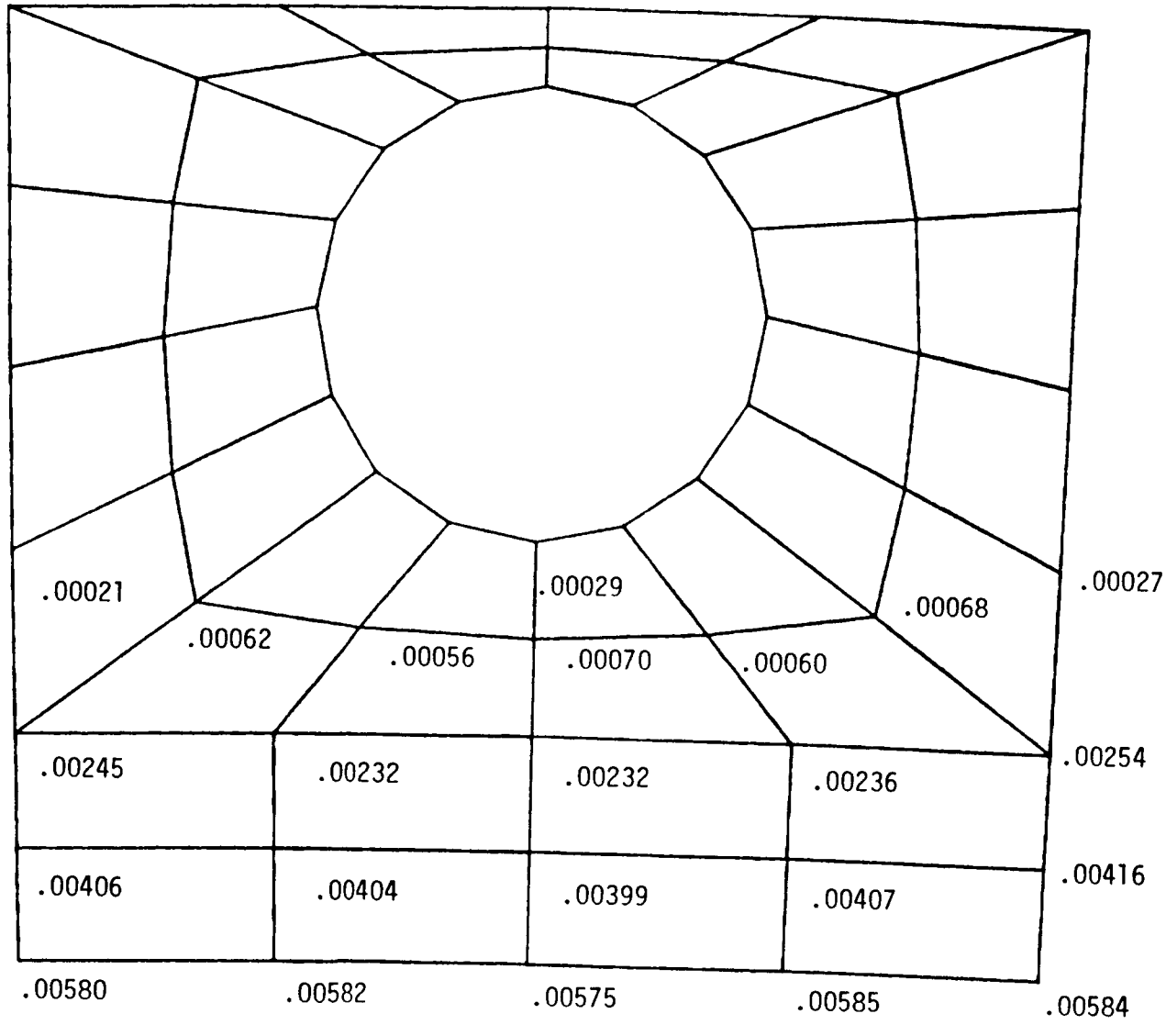

FIGURE 2.3.25. AXIAL GAP PATTERN ON FLANGE MATING SURFACE.

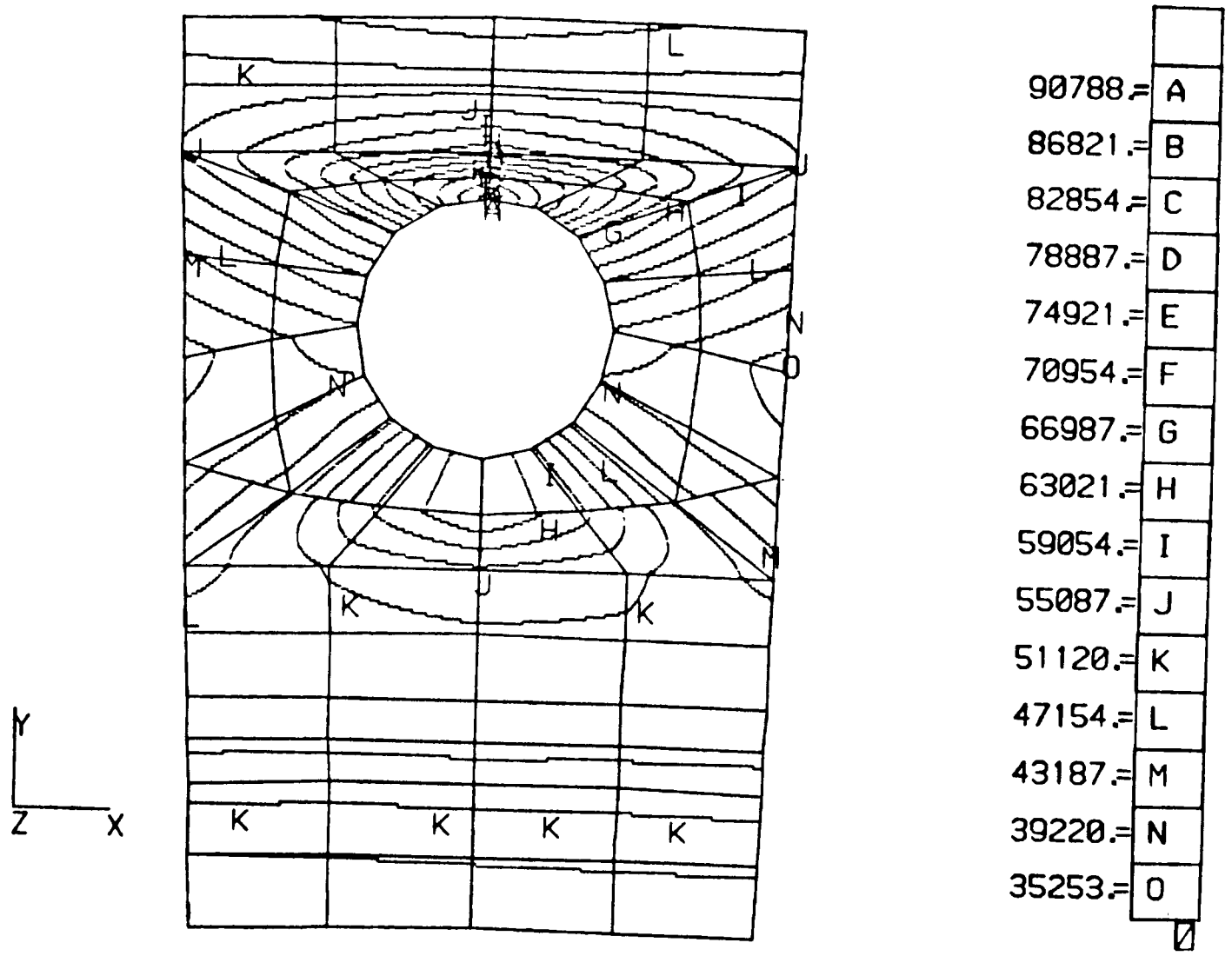

FIGURE 2.3.26. VON MISES STRESS DISTRIBUTION-NOZZLE FLANGE FORWARD FACE.

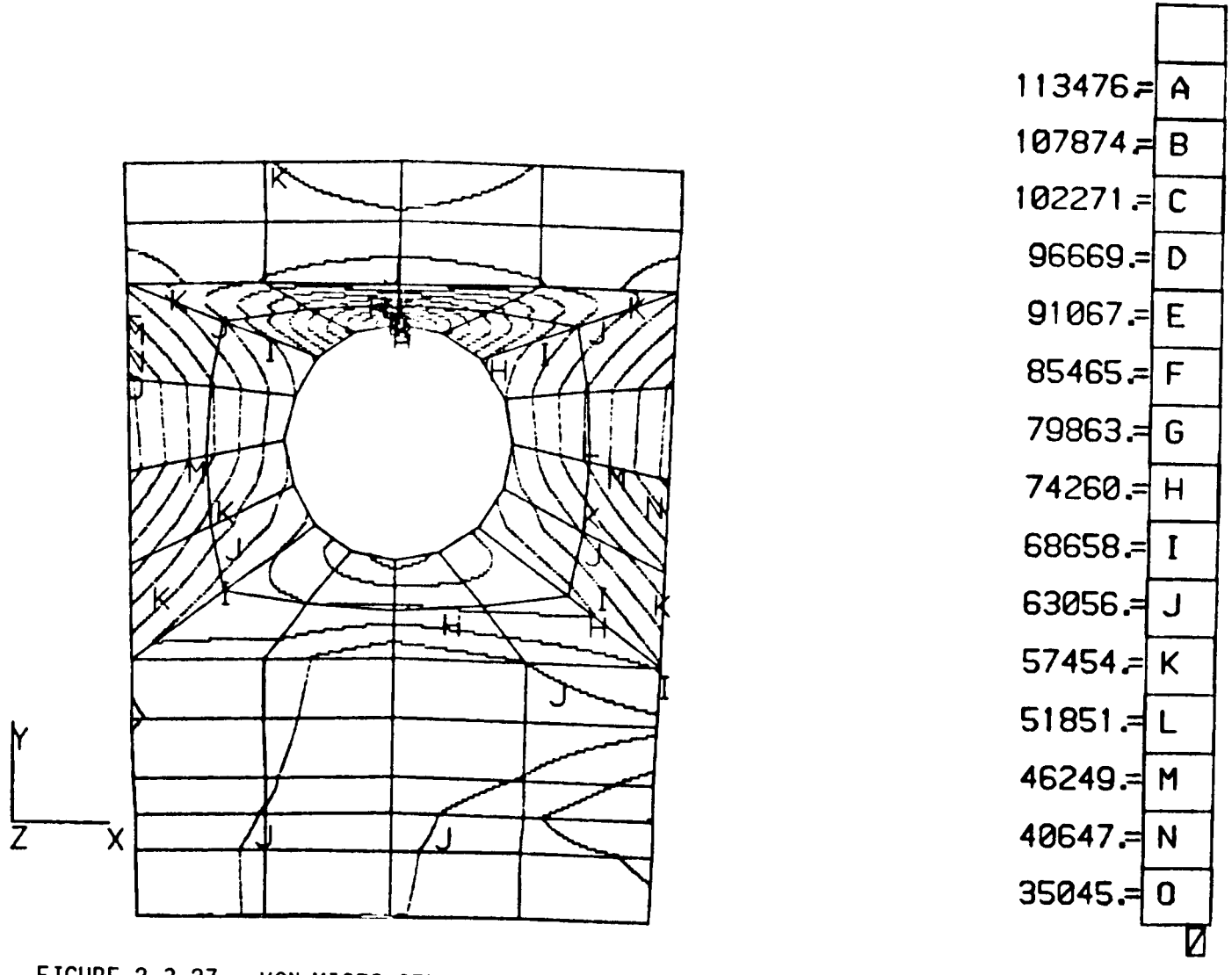

FIGURE 2.3.27. VON MISES STRESS DISTRIBUTION - NOZZLE FLANGE AFT FACE.

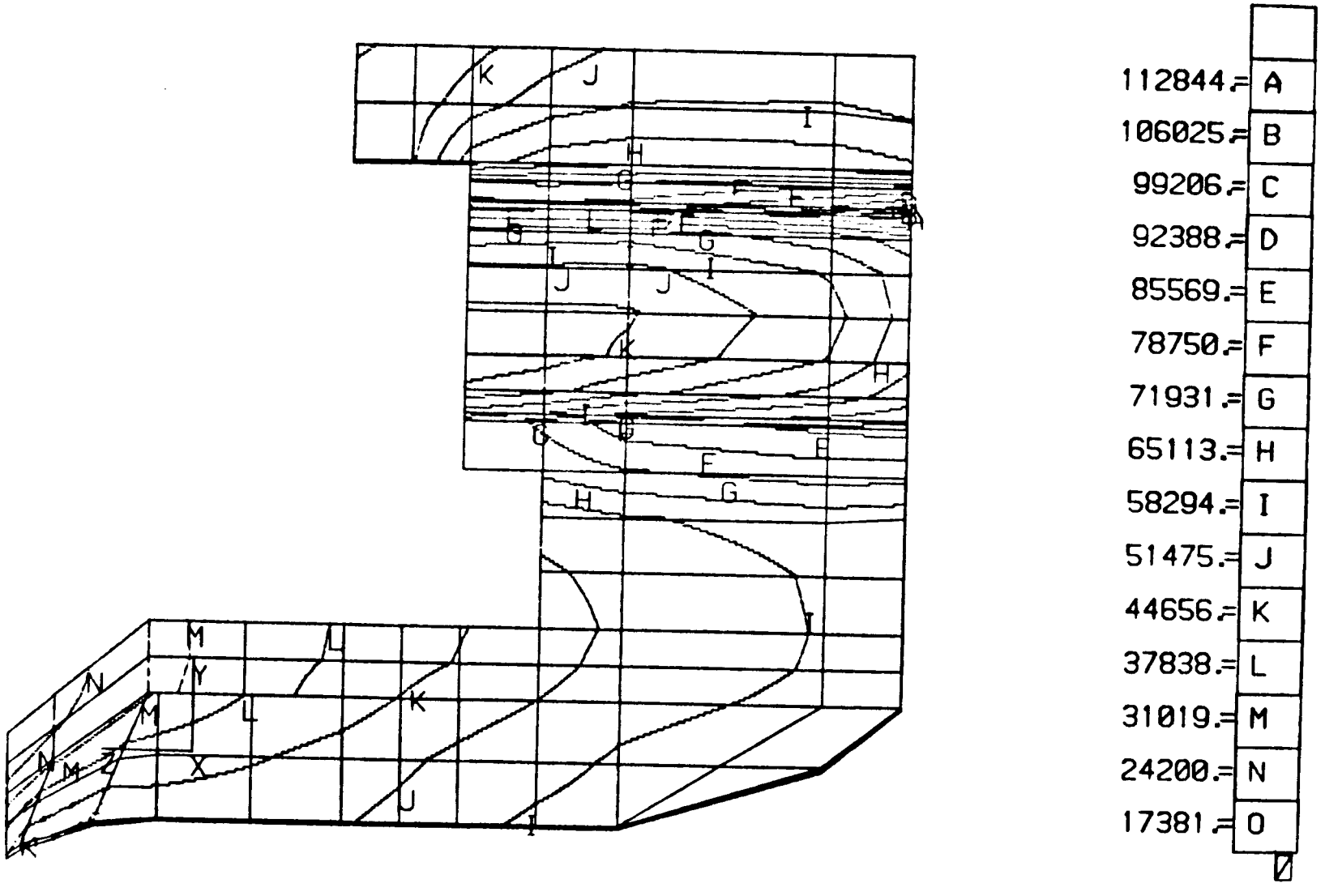

FIGURE 2.3.28. VON MISES STRESS DISTRIBUTION-NOZZLE FLANGE CROSS SECTION.

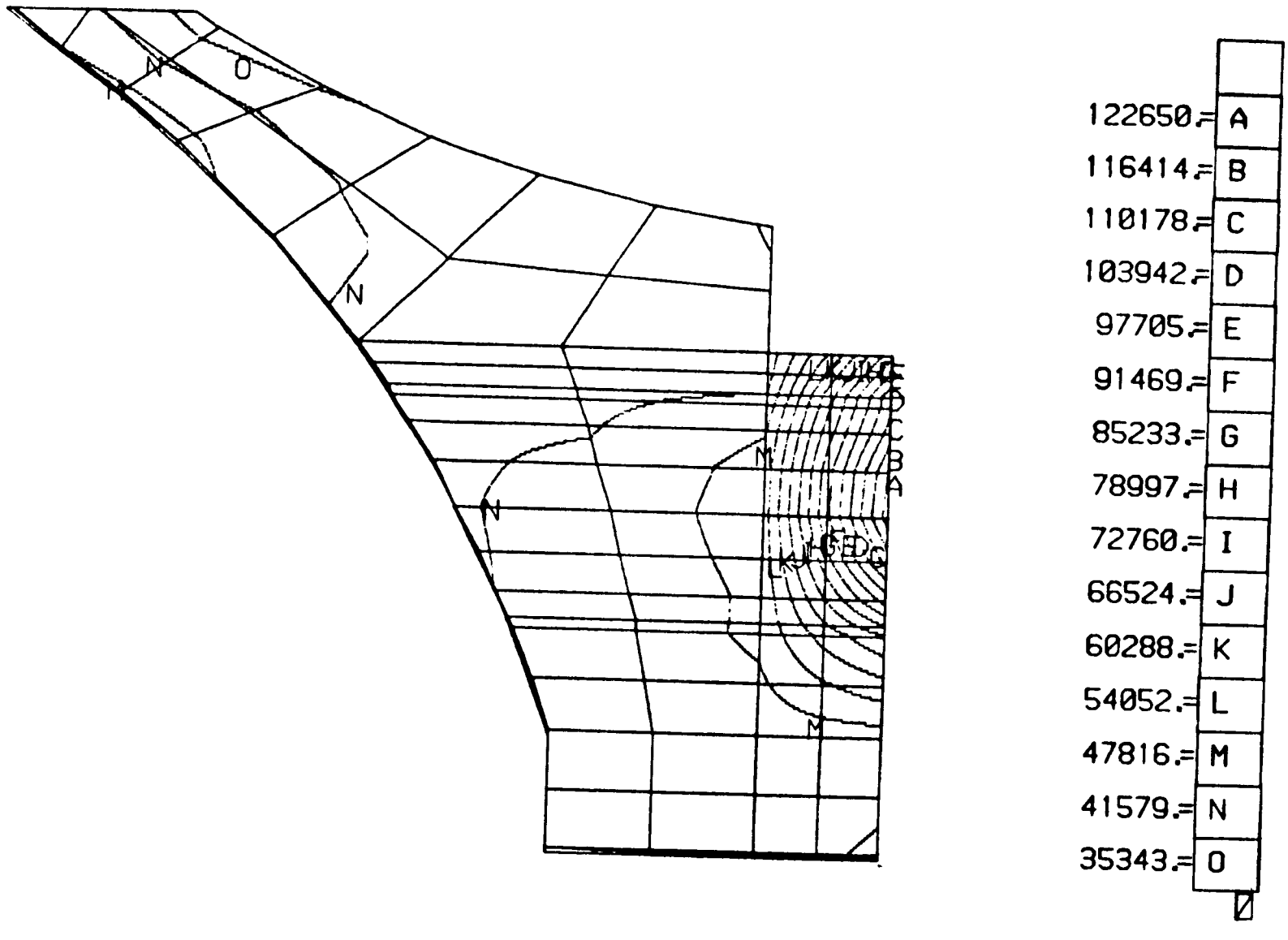

FIGURE 2.3.29. VON MISES STRESS DISTRIBUTION-MOTOR FLANGE CROSS SECTION.

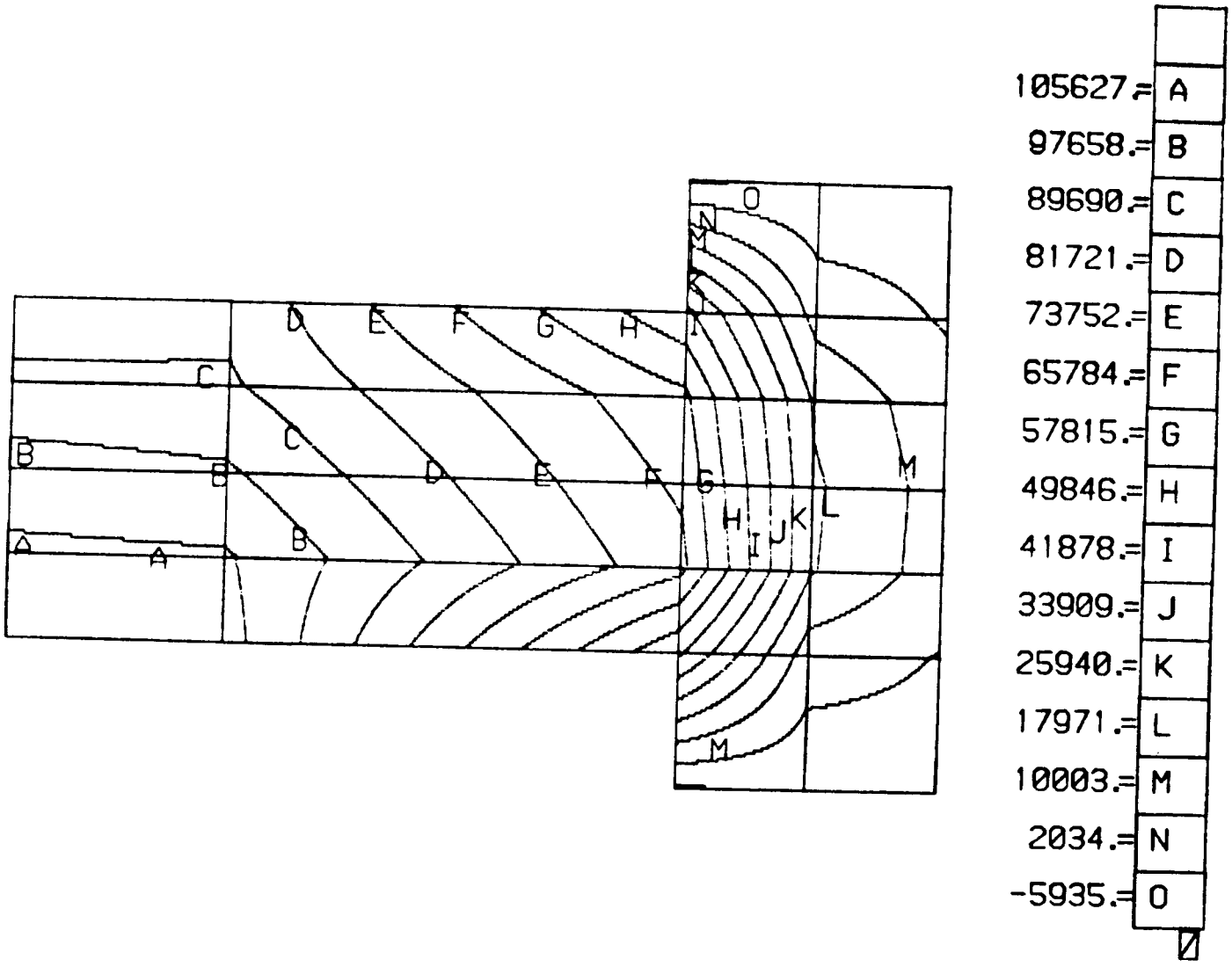

FIGURE 2.3.30. AXIAL STRESS DISTRIBUTION-BOLT CROSS SECTION.

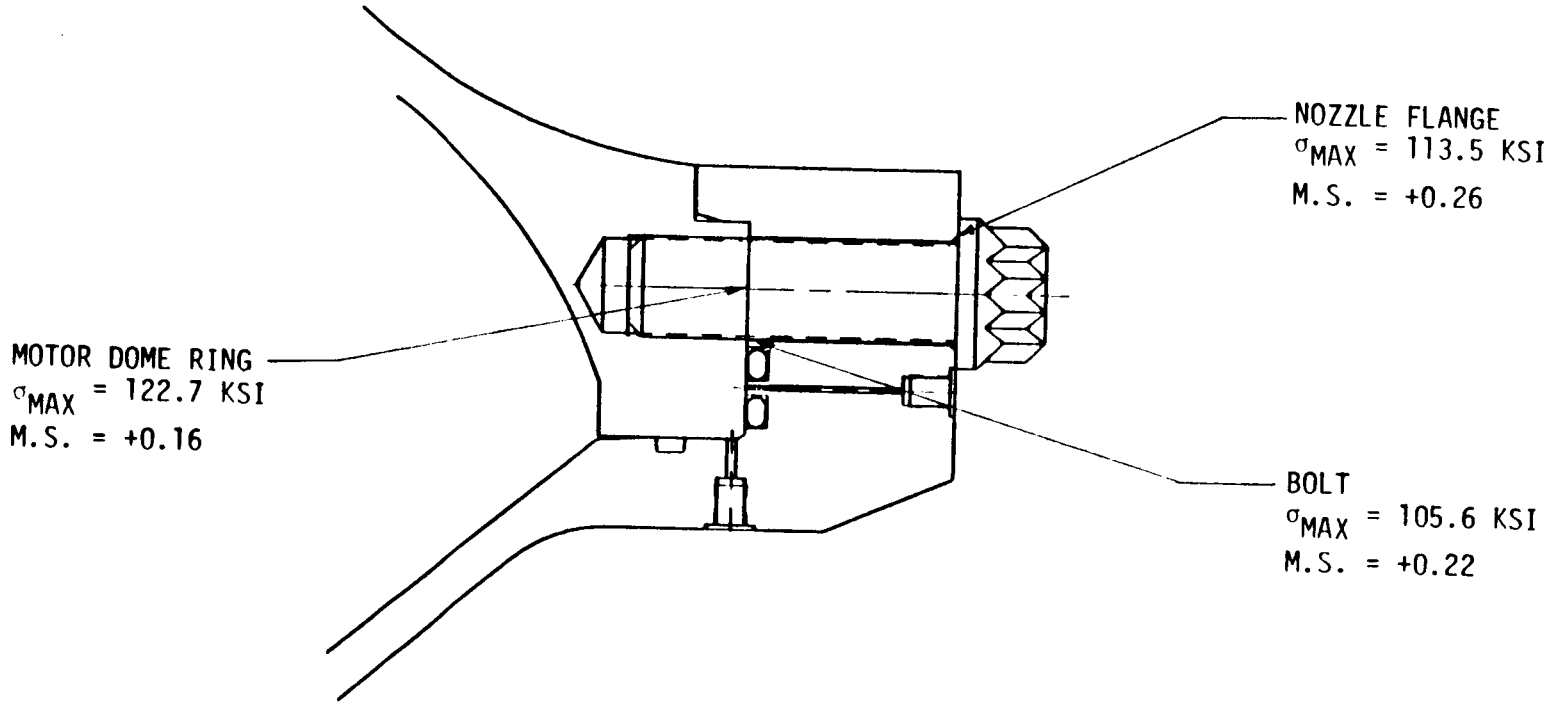

FIGURE 2.3.31. STRESSES AND MARGINS OF SAFETY IN JOINT HARDWARE.

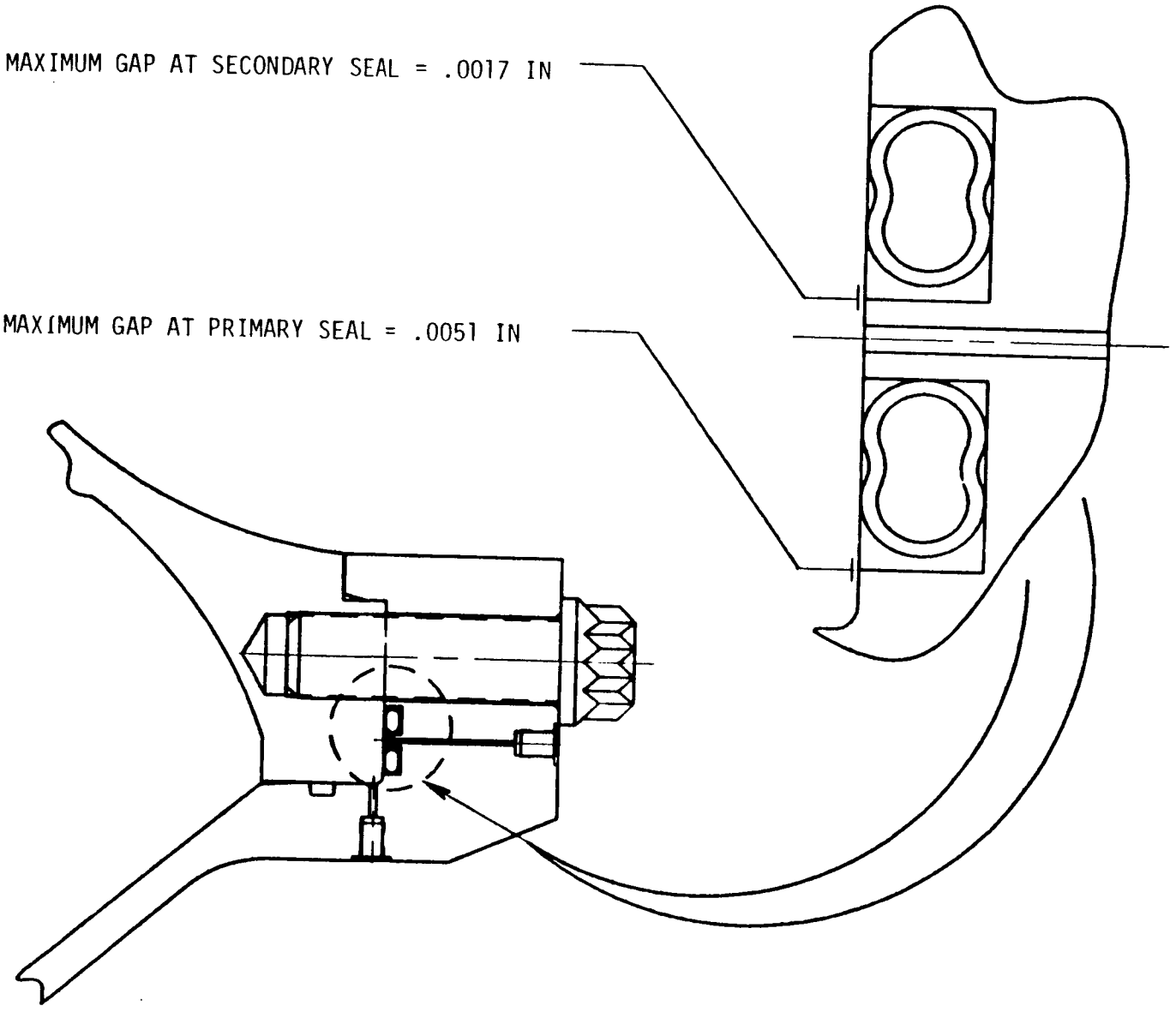

FIGURE 2.3.32. MAXIMUM GAP OPENING AT SEAL LOCATIONS.

Section 2.3.5). As shown in the figure, the maximum gap opening at the primary seal was found to be 0.0051 inch, while the corresponding value for the secondary seal is 0.0017 inch. Since each of these is less than one-half the manufacturer's recommendation, sealing capability at twice the maximum predicted gap is verified. There is some conservatism in this evaluation since the actual springback for the seals has been measured to be 0.033 inch for the 20-percent minimum compression used here.

The gap openings at the nozzle-to-case joint sealing surface are a somewhat nonlinear function of motor pressure. Figure 2.3.33 shows the gaps at the primary and secondary seals as a function of motor pressure. By using these data in conjunction with the ignition pressure transient time history from the DM-1 static firing, the gap openings versus time were found as shown in Figure 2.3.34. Note that these are smooth curves without the sharp discontinuities (jumps) associated with radial slippage (rounding) for a bore seal. The maximum gap opening velocity, shown in Figure 2.3.34 to be approximately 0.029 inch/second, appears to be well within the tracking capability of the metal O-rings used. However, since no hard data exists for this seal characteristic, this area requires some developmental testing to verify the seal's capability.

2.3.3.6 SUMMARY

In summary, the dual face seal approach was found to be a simple, effective design solution for reliably sealing the shuttle SRM nozzle-to-case joint. The primary drawbacks were found to be weight impact and the inability to use existing parts. However, the design presented herein represents a single design iteration, and we believe that further development would yield a design that minimizes these impacts. For example, it appears that utilizing larger bolts on a bigger bolt circle would be a more weight-effective approach, and expanding the bolt circle for the current size bolts might allow the use of existing domes that did not yet have the bolt holes drilled. Design optimization would be part of the Development Program for this approach.

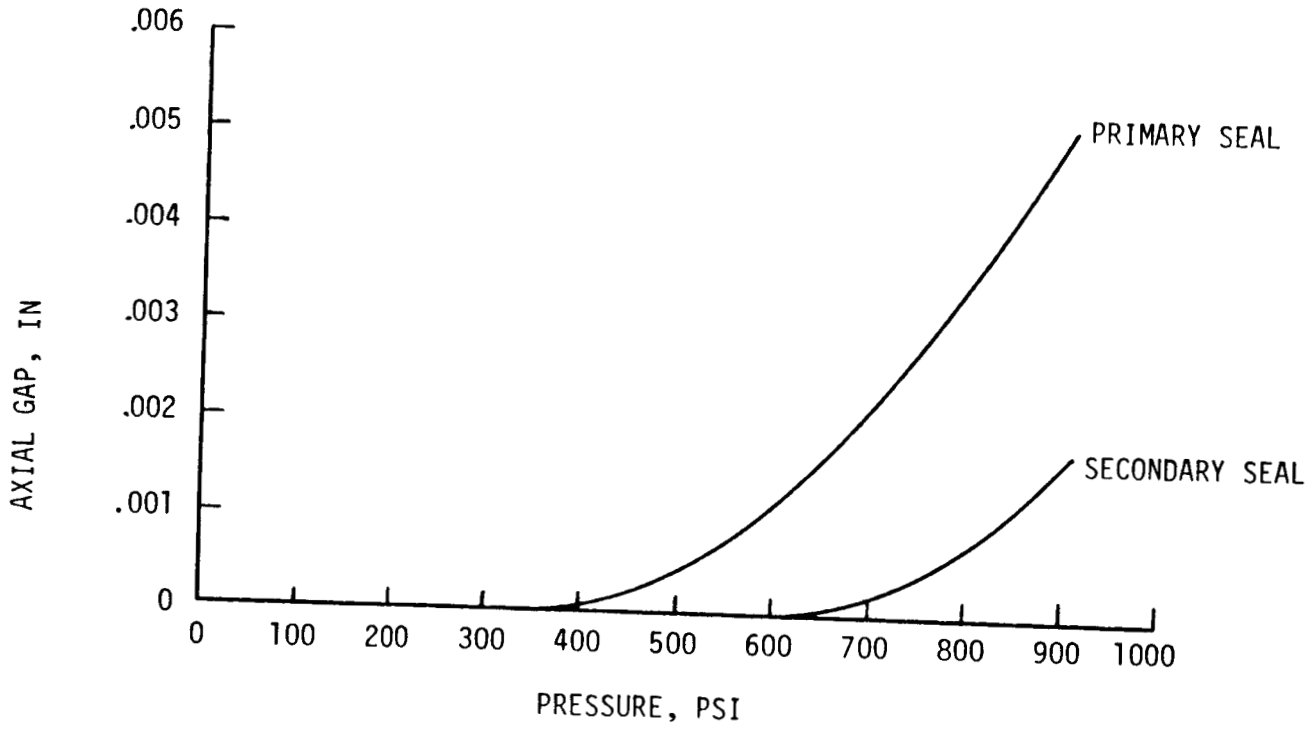

FIGURE 2.3.33. GAP AT SEAL LOCATIONS VERSUS MOTOR PRESSURE.

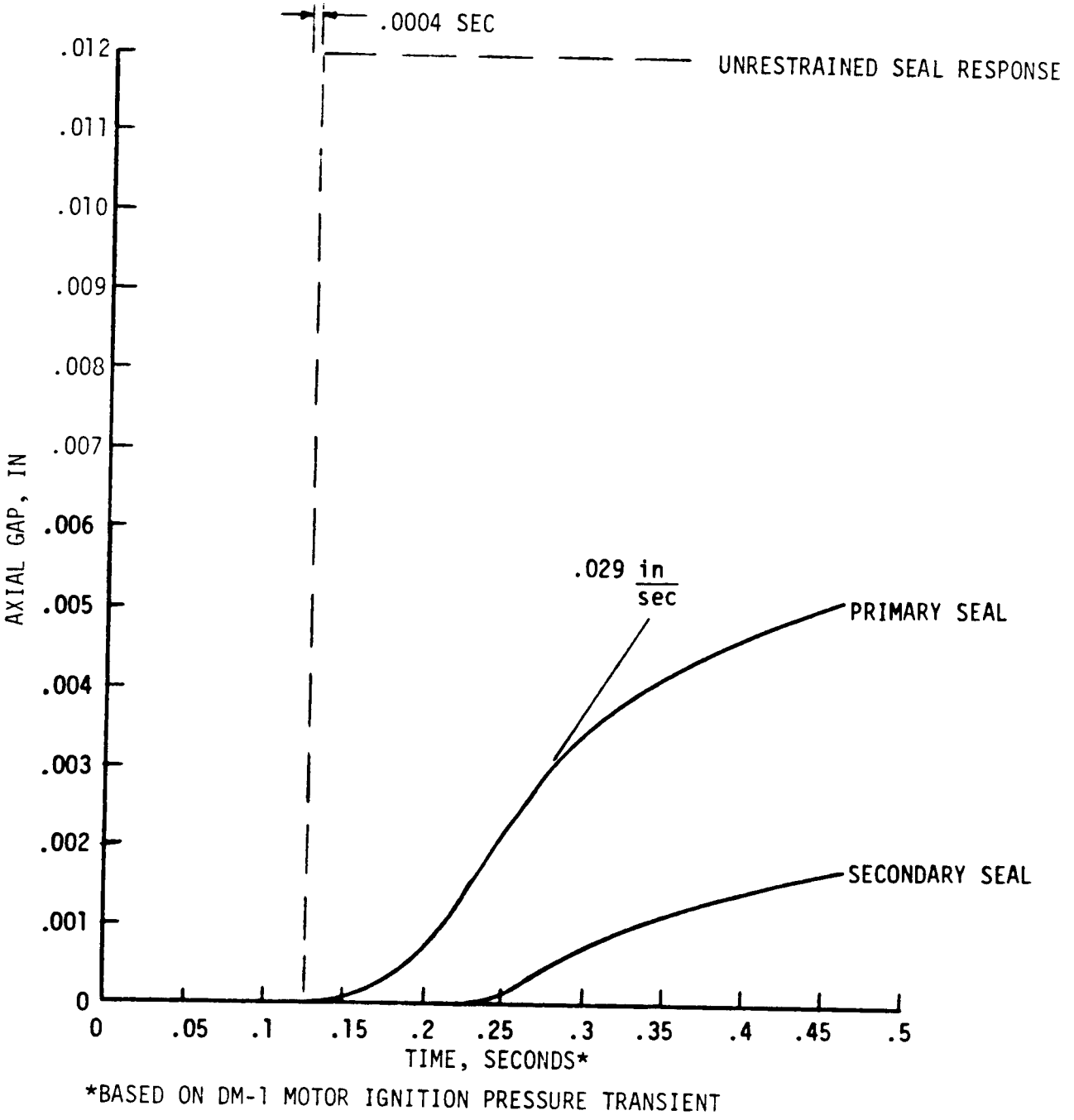

FIGURE 2.3.34. JOINT SEAL DYNAMICS.

2.3.4 NOZZLE-TO-CASE INSULATION JOINT

Trade studies performed during the first phase of this study (documented in Appendix A) selected an Inconel C-ring for the inboard seal and an Inconel O-ring for the outer seal. Neither seal requires pressure to actuate sealing, since both seals are maintained in a compressed state. An unvented nozzle-to-case insulation joint was selected as the best configuration for this sealing system.

The selected nozzle-to-case insulation joint (Figure 2.3.35) is an unvented type filled with a high-strain, ambient-cured RTV adhesive/sealant. An open channel, NBR/ silica stress relief component is vulcanized into the USR-3800 case insulation. Radially oriented oval channels in the stress relief component provide a means for both tensile and compressive deformation while minimizing stresses in the joint and preventing circumferential flow. A silicone foam with a high temperature capability, bonded along the overlap portion of the joint, provides redundant flow baffling while preventing extrusion of the RTV adhesive/sealant into the C-ring groove during assembly. Detailed structural and thermal analyses of this joint are presented below.

Structural analysis of the nozzle-to-case insulation joint was conducted using a two-dimensional TEXGAP finite element model, which is shown in Figure 2.3.36. This simulation included all the critical features of the joint. The steel structure of the Block II SRM design nozzle housing and motor aft dome were modeled along with their respective insulations: NBR/phenolic over a layer of Hypalon for the motor dome and carbon/ phenolic for the nozzle housing. The housing insulation layer of glass/phenolic was neglected, with the carbon/phenolic properties used in that region. A 0.100-inch-thick bondline was placed between the NBR/phenolic and carbon/phenolic at the joint above the step. An open gap was left below the step. The elastomeric stress relief was modeled with an orthotropic material having appropriately reduced R-Z properties and negligible properties in the hoop direction, simulating the open holed geometry. The bolts were modeled by a ring rigidly attached to the motor dome with the correct axial stiffness. This was accomplished using an orthotropic material having the appropriate axial modulus and negligible hoop modulus. Thin, stiff "contact" elements were included under the bolt "head" and between the mating flanges. By iteration, these elements were added or removed until a consistent pattern of compression in the contact elements and separation, where the contact elements are absent, was achieved. Joint pre-load was provided by applying a negative $\alpha \Delta T$ to the bolt to give a net axial pre-load of 16.5×10^6 pounds.

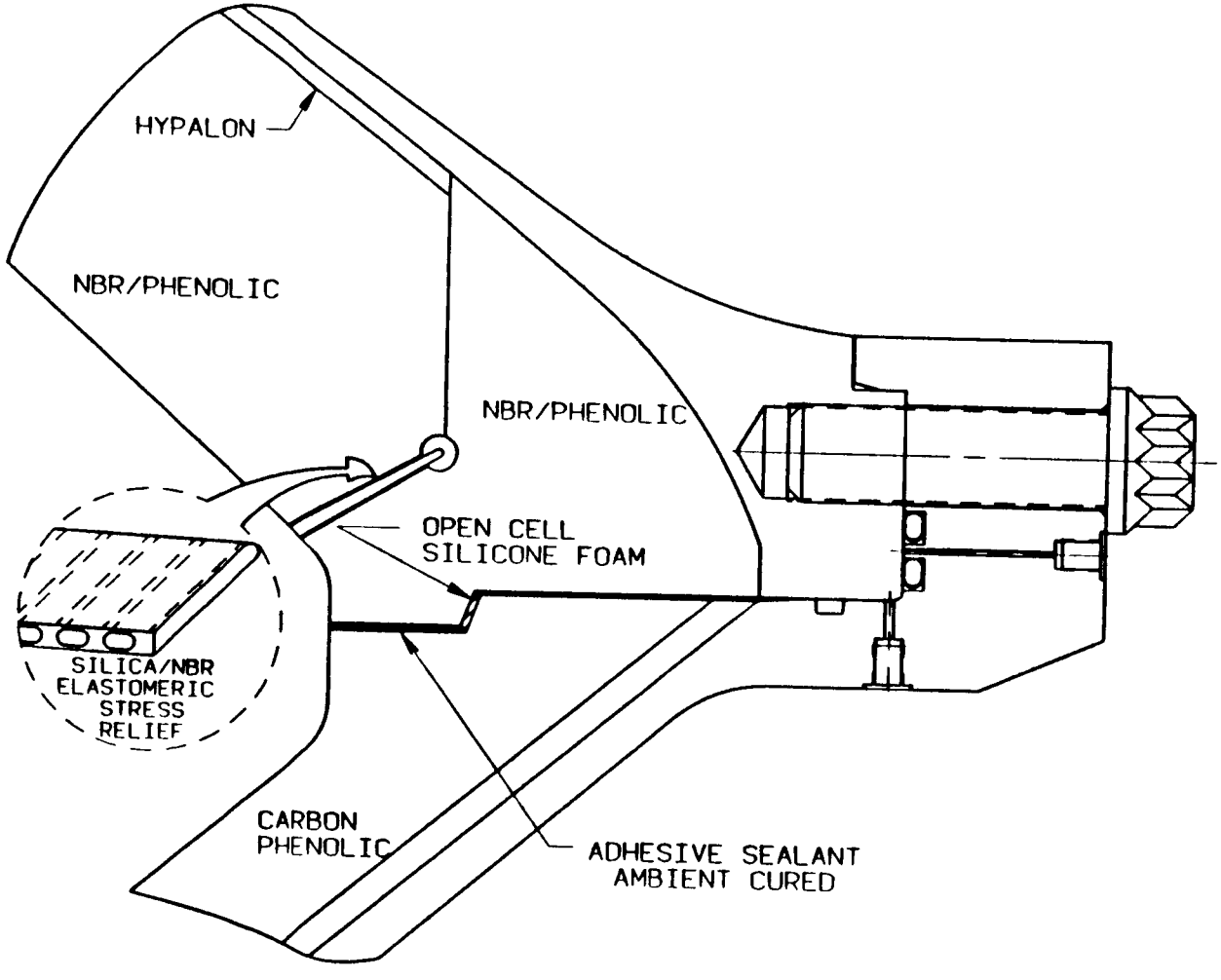

FIGURE 2.3.35. ARC BLOCK II NOZZLE TO CASE JOINT.

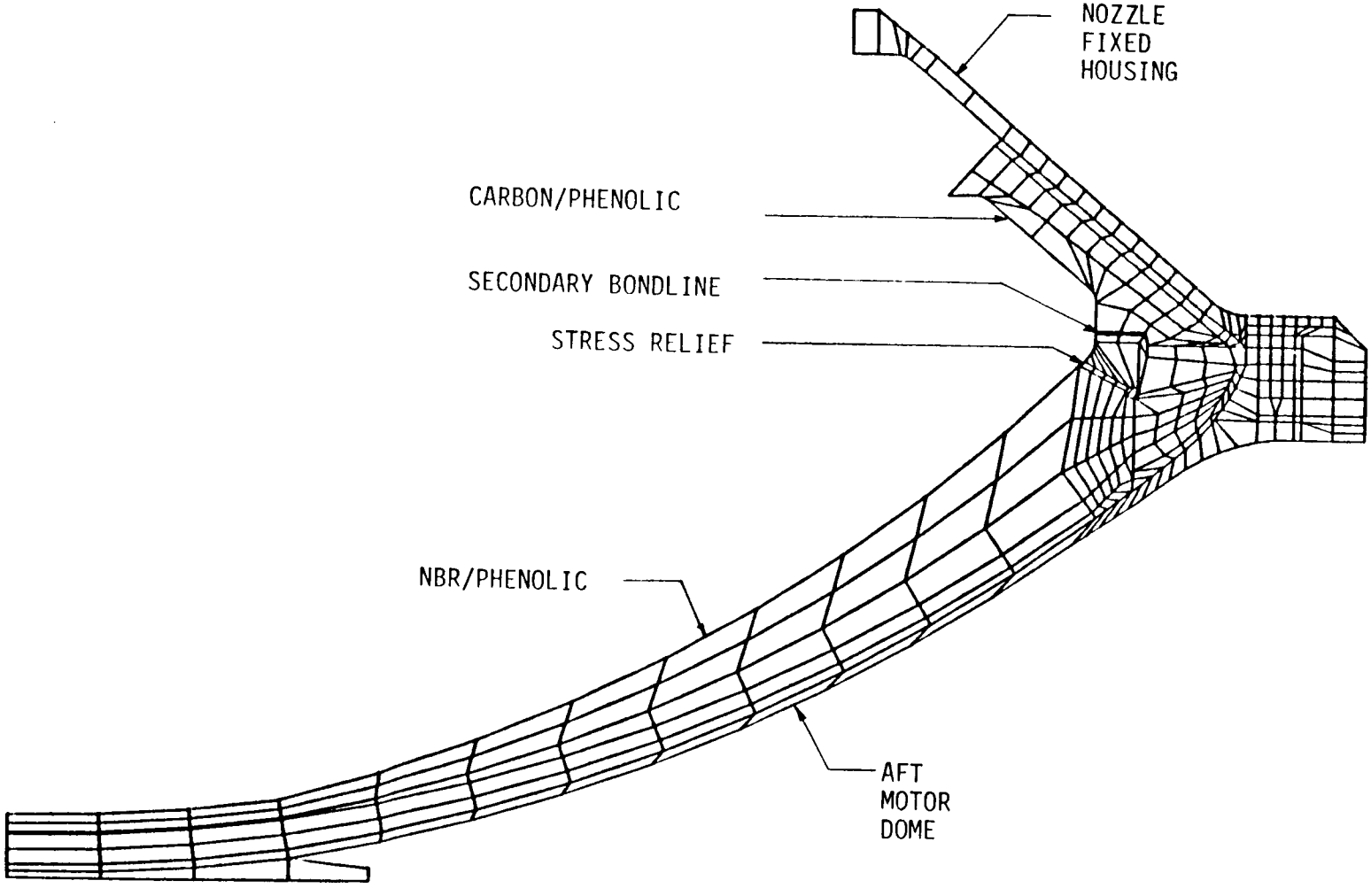

FIGURE 2.3.36. TEXGAP FINITE ELEMENT MODEL OF NOZZLE-TO-CASE INSULATION JOINT.

The model was used to evaluate stresses, strains, and displacements for two distinct loading conditions. The first consisted of limit pressure applied to the interior surface of the insulation and in the stress relief slot. For this condition, it was assumed that the secondary adhesive bond remained intact and, thus, no pressure was applied in the gap between the nozzle and case insulation. The deformed shape of the FEM for this load case is shown in Figure 2.3.37. The deflections in this plot have been multiplied by a factor of 5.0 for presentation purposes. The analysis showed that the deflection across the stress relief is influenced both by the metal joint rotating open and by radial deflection of the nozzle housing and motor dome forward of the joint. The undeformed and deformed slot width at the forward end of the stress relief is shown on the figure to illustrate deflections in this critical region. The stress/strain state in the insulation joint for this load case is summarized in Figure 2.3.38. In most areas of interest, maximum strain is the governing failure criteria; therefore, the maximum strain is shown at critical points along with the associated margin of safety. All margins of safety are positive, which verifies the structural integrity of the joint in the unvented condition.

The other loading condition considered was based on a fail-safe approach. It was assumed that the secondary adhesive bond had failed, allowing the gap between nozzle and dome insulation to open. Therefore, pressure was applied to both faces of the gap down to the primary seal location in addition to the previous loads. The deformed shape of the FEM for this condition is shown in Figure 2.3.39. The stresses and strains in the insulation for this condition are not critical. The original gap width (bondline) and the resulting width after deformation are shown on the figure. The latter is utilized in the following thermal analysis.

The joint must be capable of operating successfully, even if for any reason the joint becomes vented, to ensure positively that adequate reliability exists under all operating conditions. Thermal analyses of the joint in a vented mode were performed for this purpose. Thermal analyses were also performed to evaluate heating in the stress relief channels.

Convective heating rates are substantial in the nozzle-to-case joint region due to the initial high velocity flow between the grain and insulation and due to apparent recirculation in this region upon grain burnback. Flowfield analyses of this region, performed by MTI, were inadequate in predicting the observed insulation material-affected rates. A review of the analytical techniques showed the flowfield calculations were

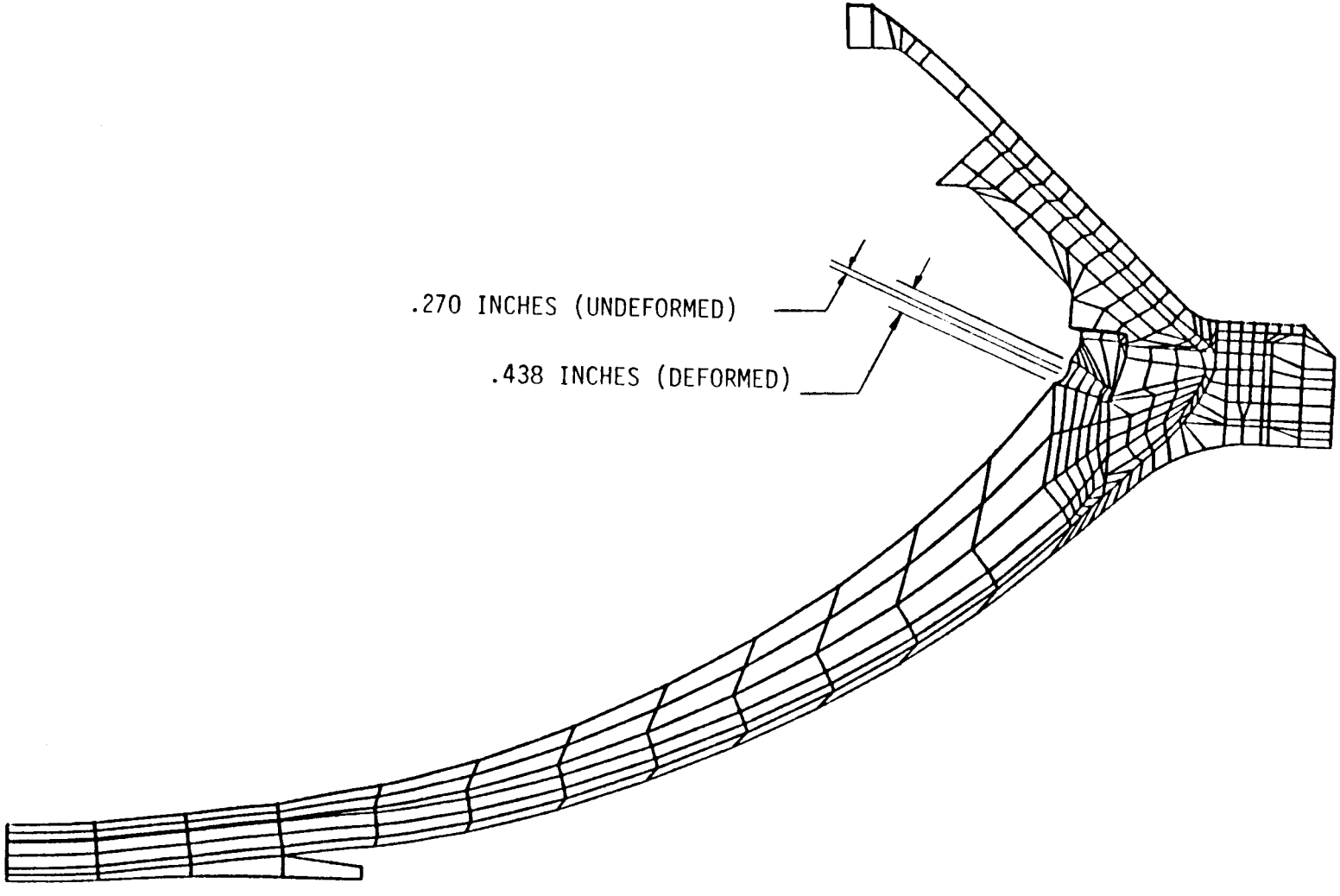

FIGURE 2.3.37. DEFORMED FINITE ELEMENT MODEL-UNVENTED JOINT.

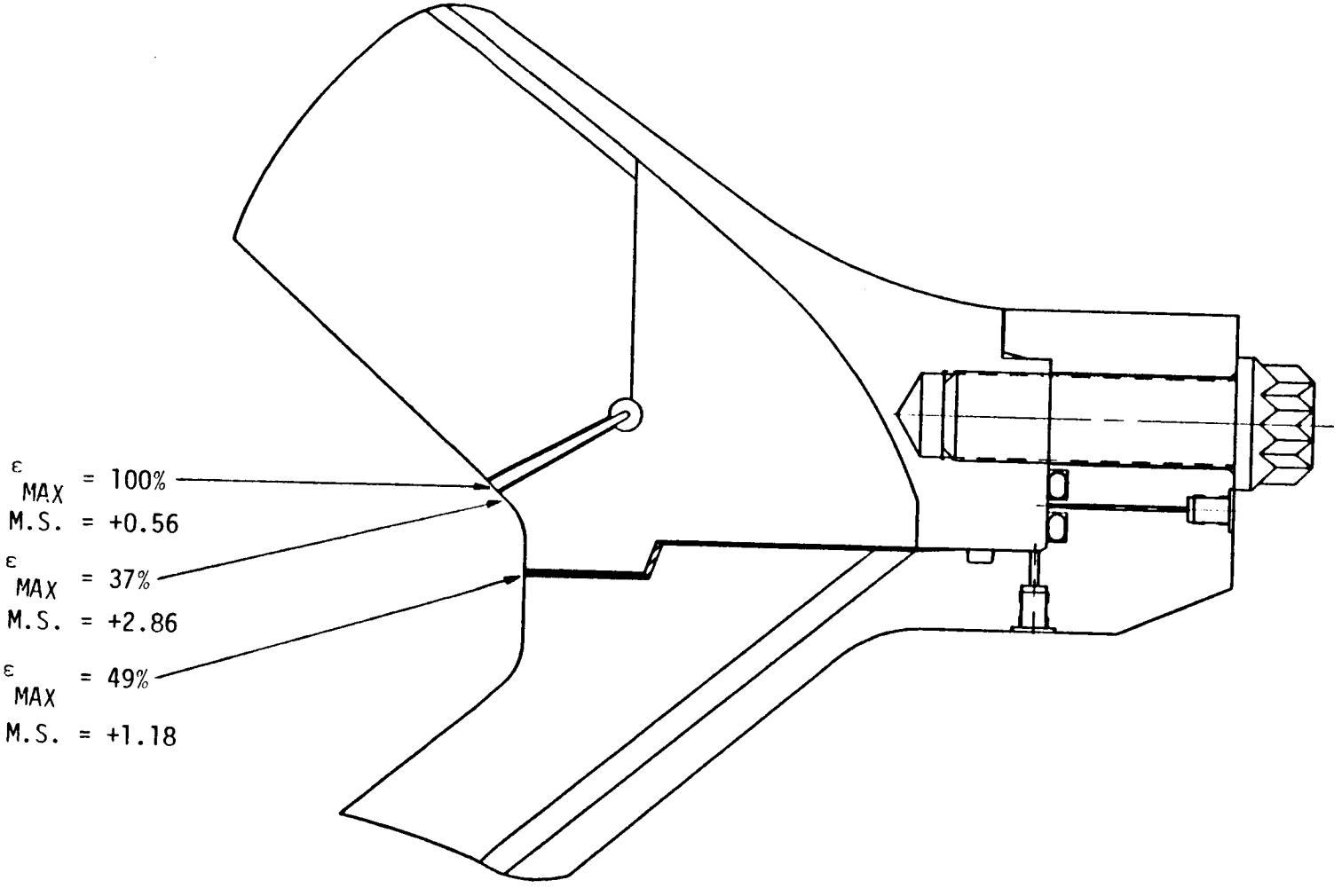

FIGURE 2.3.38. INSULATION JOINT CRITICAL STRAIN LOCATIONS.

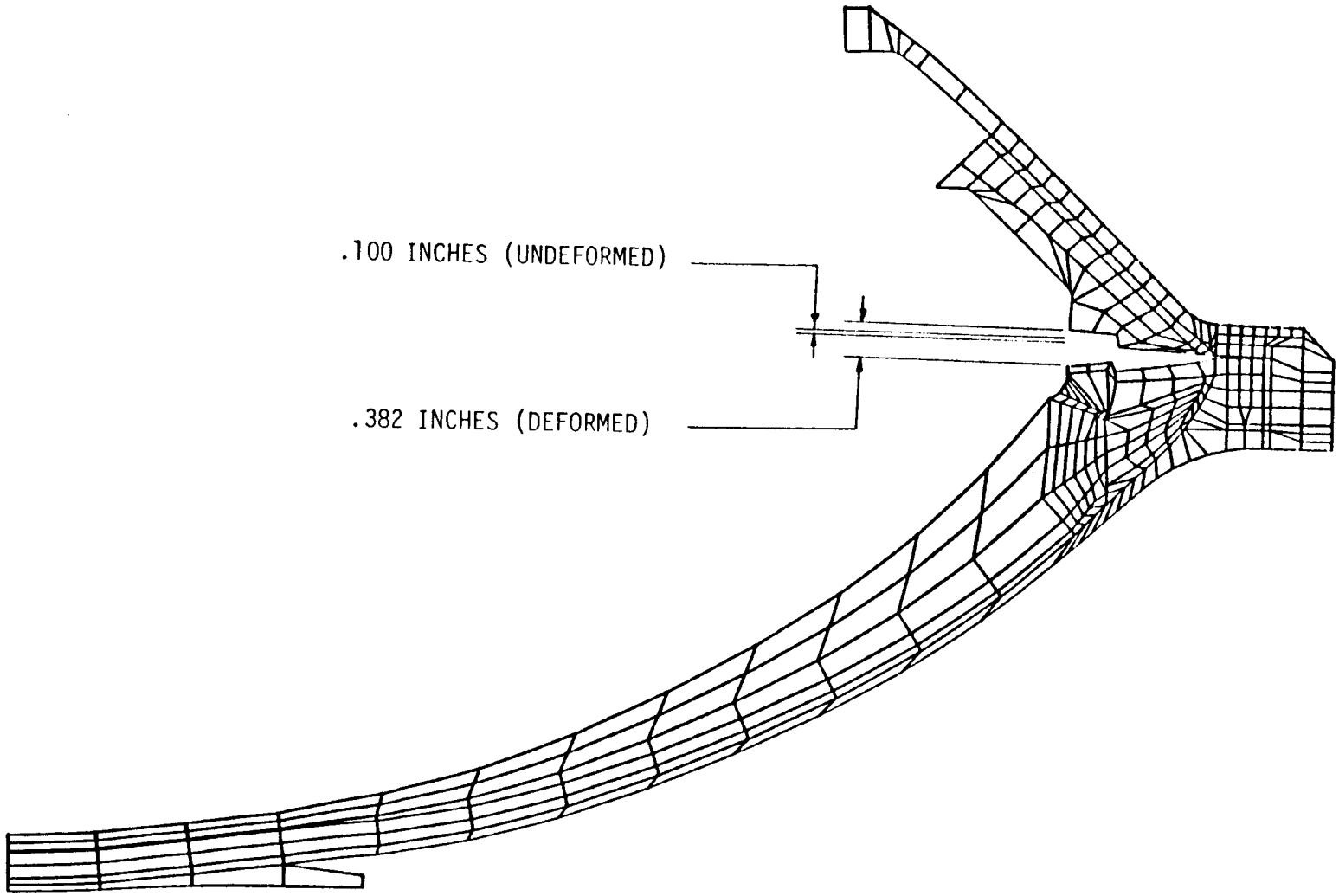

FIGURE 2.3.39. DEFORMED FINITE ELEMENT MODEL-VENTED JOINT.

based upon potential flow; a solution to the elliptical form of the Navier-Stokes is required to properly account for the flow characteristics in recirculation regions. In the absence of meaningful flowfield characteristics and convective film coefficients, the thermal analyses presented below were based upon heating rates determined by emperically fitting measured material-affected rates. Figure 2.3.40 shows the predicted erosion pattern in the aft dome region. The stress relief component is shown to have an adequate length to function properly in the eroded configuration representing burntime conditions.

Heating in the stress relief channels is modeled by coupling a one-dimensional flow module to a two-dimensional conduction solution (see Section 2.3.2). The dominant mode of heating is due to convection from a high velocity influx of gas into the channel such as occurs at ignition. Rapid pressure fluctuations due to vortex shedding from the inhibitors or from rapid changes in recirculation patterns induced by grain burnback were not included in the analyses. The results presented in Figure 2.3.41 show that the channel web erosion is dominated by erosion of the surrounding insulation.

Analytical assessment of the erosion in the joint was based upon venting occurring at ignition. Heating is due to a radial flow of gases at ignition followed by circumferential flow for the remainder of motor operation. A steady 0.5-psi pressure drop was assumed in calculating the mass flux and convective film coefficients resulting from circumferential flow in the joint. Figure 2.3.42 presents the predicted erosion and heat-affected rates in the joint. The erosion is insufficient to cause failure by losing the compressed portions of the nozzle-to-case insulation interface.

The above analyses verify the thermal and structural integrity of the nozzle-to-case insulation joint. Stress relief is shown to minimize both stresses and deflections in the joint. The stress relief component has a sufficient length to properly function throughout motor operation. In addition, the insulation joint is shown to be capable of withstanding the flow should it become vented and capable of maintaining a primary barrier that prevents gases from reaching the compressed Inconel C-ring and O-ring seals.

ORIGINAL PAGE IS
OF POOR QUALITY

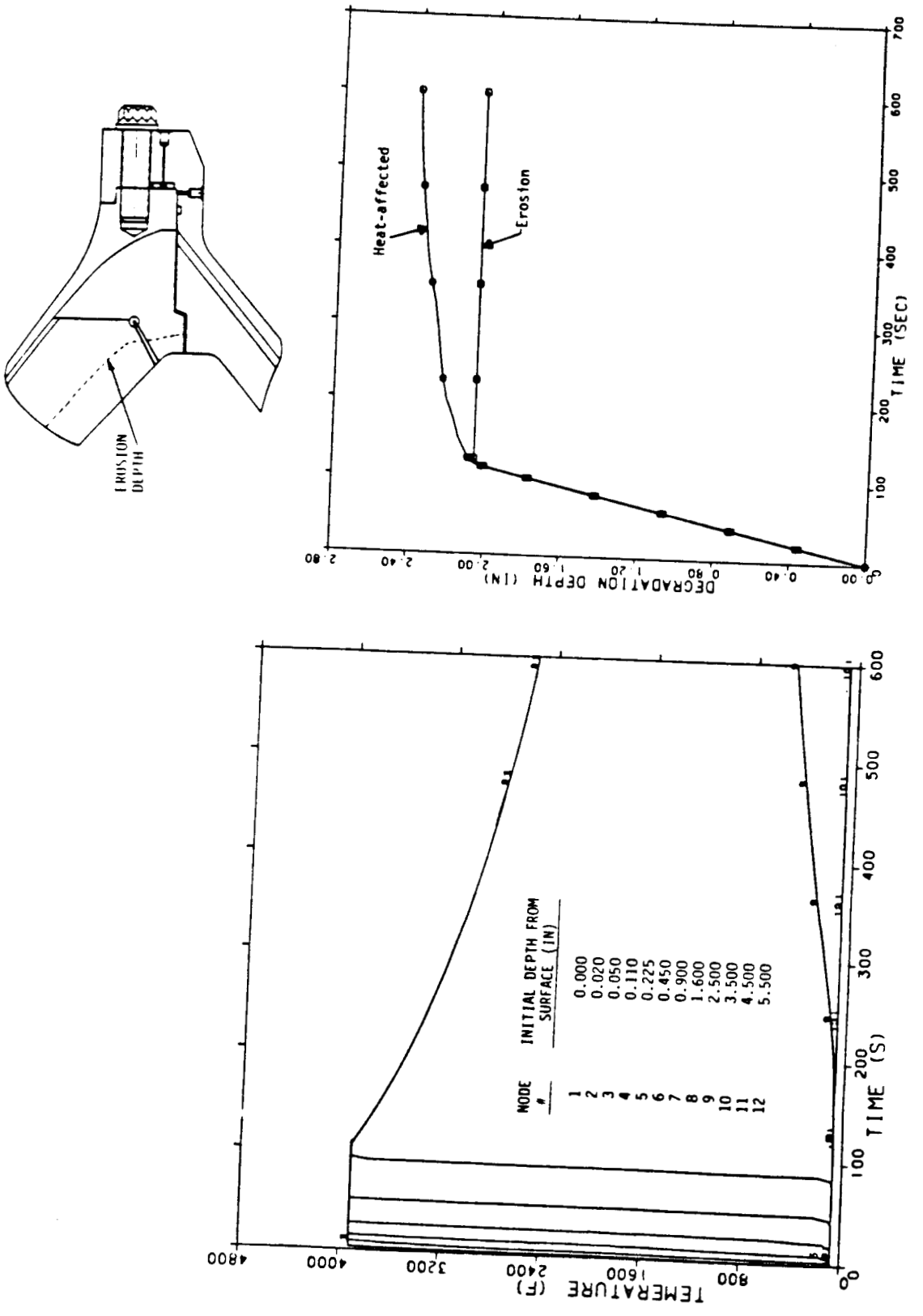

FIGURE 2.3.40. AFT DOME THERMAL RESPONSE AND DEGRADATIOIN PROFILES.

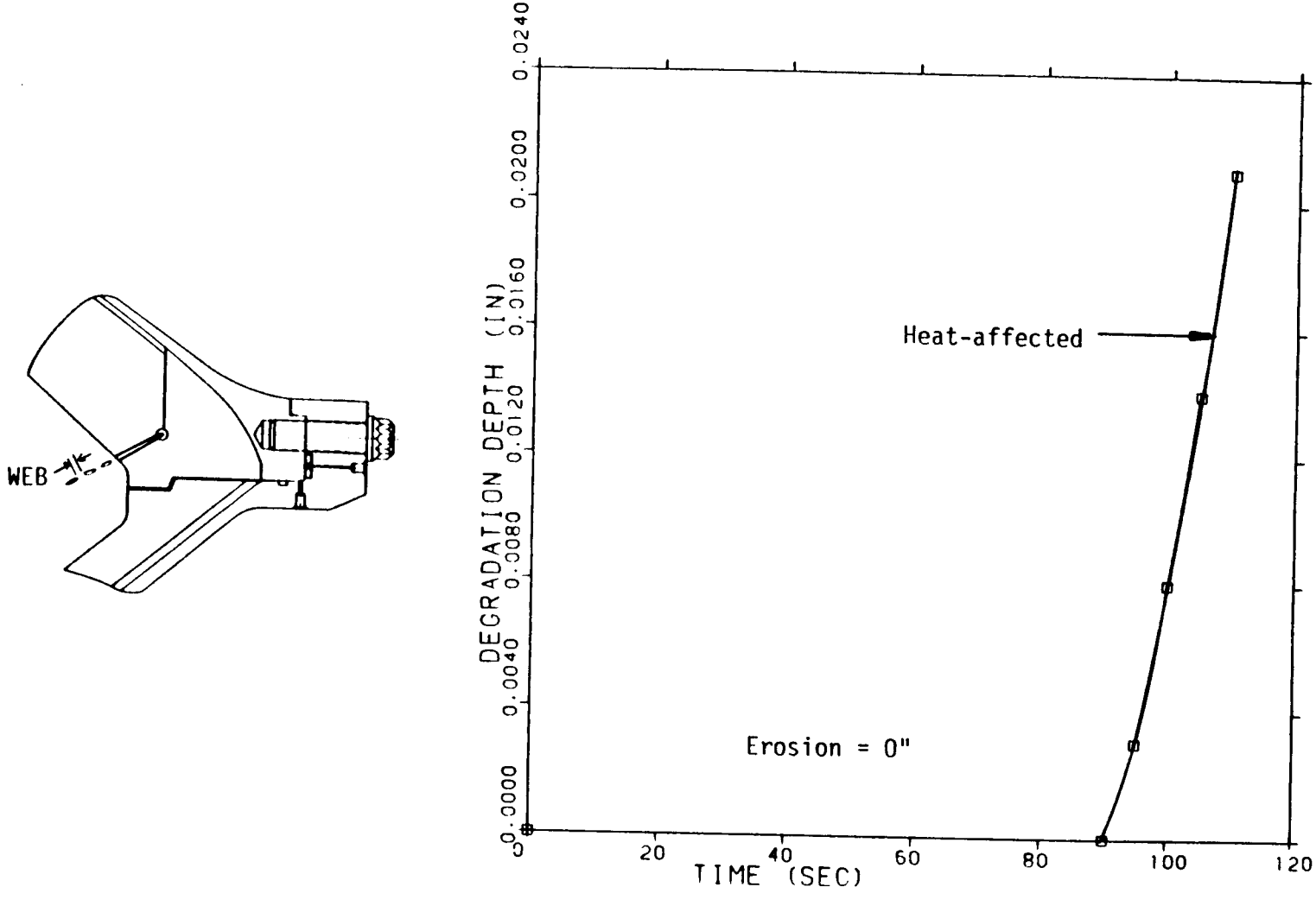

FIGURE 2.3.41. THERMAL DEGRADATION OF CASE/NOZZLE INSULATION STRESS RELIEF CHANNEL WEB.

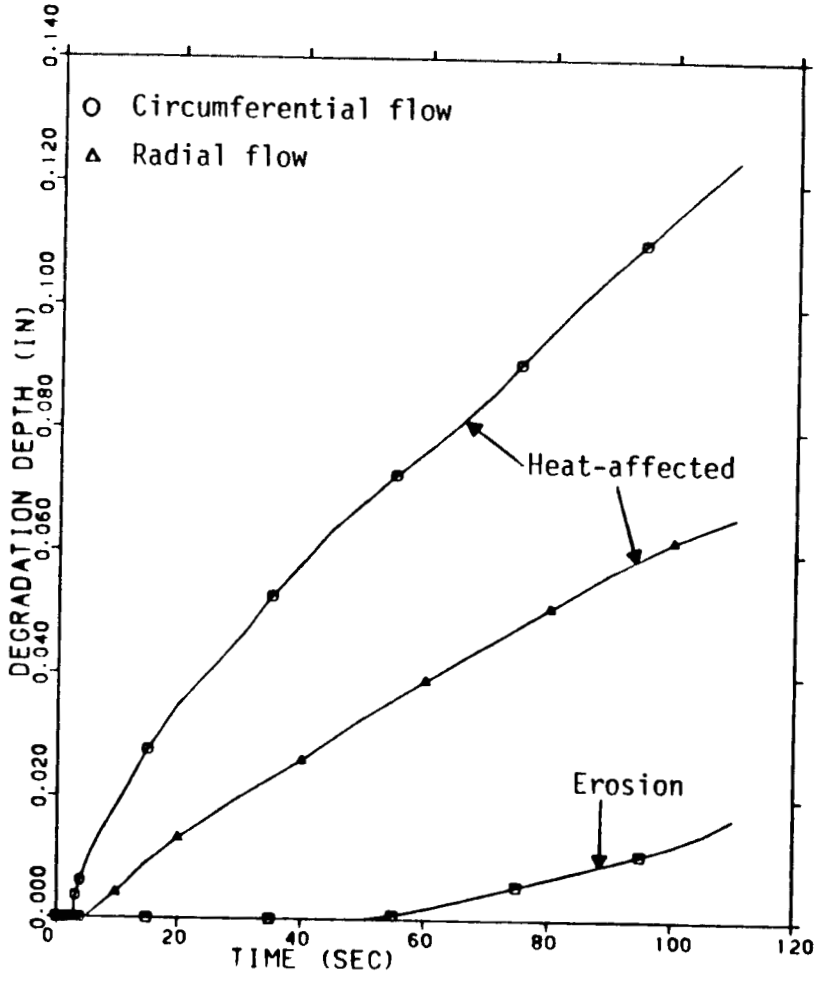

FIGURE 2.3.42. DEGRADATION PROFILES IN THE CASE/NOZZLE INSULATION JOINT.

2.3.5 CASE SEGMENT AND CASE/NOZZLE JOINT SEALS

The results of ARC studies of the subject seals are presented in this section. Highly reliable, commercially available, redundant, metal O-ring seals that meet all design requirements and are well suited to the ARC joint designs are recommended.

2.3.5.1 JOINT/SEAL TRADE STUDY RESULTS

As indicated in ARC's Mid-Term Report (Appendix A), the primary goal of the joint/seal design effort was to improve the reliability of the system and minimize the possibility of failure. Based upon the excellent design and structural/thermal analysis results of NASA LaRC, ARC selected the concept of a bolted, flat flanged joint using face seals to meet this objective. Numerous seal designs (configuration and materials) were investigated as part of the case field joint trade study. The identification of the advantages of redundant metal seals was an important output of this effort.

2.3.5.2 SEAL PRELIMINARY DESIGN CRITERIA

The results of the trade study were utilized to establish the seal design criteria of Table 2.3.3. The listed parameters are rather straightforward with the exception of the following environmental values:

- Maximum Pressure - MEOP for the topmost case field joint is 1,004 psia; design pressure is 1.4 x 1,004 = 1,406 psia. The corresponding design pressure for the case/nozzle joint is 1.4 x 909 = 1,273 psia. For preliminary discussions with seal manufacturers, 1,410 psia design pressure was used for all case seals.

- Maximum Temperature - a value of 1,400°F was used. No physical significance was attached to the value; it enabled discussions with seal manufacturers without overly constraining them.

- Maximum Gap - a maximum gap (i.e., flange face lift-off) of 3.5 mil was used. This value proved to be representative of actual results (a range of 0 to 5.7 mils, as indicated in Section 2.3.5.4).

- Maximum Gap Rate - no a priori values of this parameter were available. (See Section 2.3.5.4.)

It is to be noted that the seal criteria of Table 2.3.3 are preliminary in the sense that these are judged necessary but not sufficient conditions. In addition to the

TABLE 2.3.3. SEAL DESIGN CRITERIA
CASE FIELD JOINTS AND
NOZZLE/CASE JOINT.

REDUNDANCY:	TWO SEALS MINIMUM, VERIFIABLE BY TEST
PRESSURE ASSISTANCE:	SEALS TO ACCOMMODATE, BUT TO RETAIN SEALING CAPABILITY WITHOUT, PRESSURE ASSISTANCE
DESIGN COMPATIBILITY:	SEALS TO BE COMPATIBLE WITH BOLTED FLAT SEALING JOINT DESIGN AND ATTENDANT DISPLACEMENT AND TRACKING VELOCITY REQUIREMENTS(1)
RELIABILITY:	SEAL BEHAVIOR TO BE WELL UNDERSTOOD AND DEMONSTRATED OVER THE RANGE OF DESIGN OPERATION CONDITIONS
COMMERCIAL:	DEMONSTRATED FABRICATION AND UTILIZATION HISTORY OF SIMILAR EQUIPMENT
ASSEMBLY:	EASE OF INSTALLATION AND SEGMENT ASSEMBLY; RESISTANT TO DAMAGE; COMPATABILITY WITH BOLT TENSION REQUIREMENTS
ENVIRONMENTAL:	MAXIMUM PRESSURE (PSIA): 1410 MAXIMUM TEMPERATURE (°F): 1400 MINIMUM TEMPERATURE (°F): 20 MAXIMUM GAP (MILS): 3.5(2) MAXIMUM GAP RATE: TBD(3)

---

(1) SEALING CAPABILITY TO BE DEMONSTRATED AT TWO TIMES MAXIMUM GAP AT MAXIMUM TRACKING VELOCITY AND TWO TIMES TRACKING RATE AT MAXIMUM GAP.

(2) A MAXIMUM OPENING OF THE JOINT SEALING SURFACES OF 3.5 MIL WAS ESTABLISHED BASED UPON PRELIMINARY WORST CASE STRESS ANALYSIS RESULTS. SEE SECTION 2.3.5.4 FOR FINAL RESULTS.

(3) GAP RATES, WHICH ESTABLISH REQUIRED TRACKING RATE TO ENSURE SEALING, ARE PROVIDED IN SECTION 2.3.5.4.

parameters listed, numerous additional requirements exist relating to the manufacturing, transportation, assembly, and testing operations; joint design and performance (both static and dynamic) specifics provide additional seal requirements. Some of these additional requirements were derived from the analysis of joint performance and information from the seal manufacturers and are provided in Section 2.3.5.4.

2.3.5.3 RELATED SEAL EXPERIENCE

The use of metal seals in rocket motor applications has undergone an interesting evolution. A number of SRMs of the 1950 to 1960 timeframe incorporated "Flexatallic" type gasket seals. These seals are widely used, even today, in industrial and utility applications characterized by heavy flanges, high clamping (static) loads, and low dynamic loadings. The development of lighter, more highly stressed cases ended the use of these seals in rocket motor applications. Elastomeric O-ring seals were employed in the overwhelming majority of rocket motor case seal applications. Concurrently, aerospace manufacturers and their seal vendors were developing high performance metal seals. It is to be noted that Rocketdyne is in this group, and has made extensive use of advanced, pressure-assisted metal seals throughout the SSME. These seals have been found to provide very high reliability in high pressure service over a range from cryogenic liquid to high temperature gas applications.

The widespread use of rubber O-rings in rocket motor applications is well documented. The catastrophic failure of the 51-L seals is, in and of itself, not sufficient to eliminate their use (especially when used with improved joint designs). Both metal and elastomeric seals were investigated in the trade study (Appendix A). Metal seals were found to have superior static and dynamic performance characteristics in this study. Metal seal superiority over rubber seals was notable in the area of reliability: breaching of the insulation seal would result in rapid and catastrophic loss of a rubber seal, while metal alloy seals offer much higher sealing reliability; low ambient (and resultant cold joint) temperatures do not result in metal seal impairment, whereas the static and dynamic sealing characteristics of rubber seals suffer severe impairment; metal seals offer improved analysis tractability/predictability over rubber seals.

As indicated in the trade study (Appendix A), the metal-jacketed gasket primary and metal C-ring secondary seal configuration was highly rated for the joint designs investigated. The ARC modified in-line joint with this seal configuration was reviewed by the seal manufacturer with extensive design and manufacturing background in providing seals to similar requirements. In summary, the Fluorocarbon Gasket

Division* did not recommend (and declines to bid) the use of a gasket type seal and both the Fluorocarbon Components Division and the Advanced Products, Inc. recommended the use of silver plated, Inconel 718 O-rings for both primary and secondary seals. These two manufacturers share the supply of seals for utility nuclear reactor vessel head closures. Their manufacturing considerations and recommendations coupled with relevant utilization experience resulted in prime consideration being given to a dual metal O-ring seal at case segment joint and case-nozzle joint locations.

Design data for various metal seal designs were provided by Advanced Products, Inc. and are included in Tables 2.3.4 through 2.3.7. Table 2.3.4 provides yield strength versus temperature data for a number of seal alloys; the superior high temperature strength characteristics of age-hardened Inconel 718 is apparent. Design pressure ranges for various seal designs are included as Table 2.3.5; as indicated, vented metal O-ring nominal design range is from 10^{-6} Torr. to 3,000 psia (standard, i.e., 10 percent, wall thickness). Nominal design temperature upper limit for Inconel 718 is 1,400°F as indicated in Table 2.3.6. Recommended materials for various seal configurations are also indicated in Table 2.3.6. Seal plating maximum working temperatures and recommended sealing loads for a variety of materials are provided in Table 2.3.7. A design temperature ceiling of 1,500°F and a minimum flange loading of 250 pounds/circumferential-inch are indicated for silver plating.

2.3.5.4 SEAL DESIGN AND PERFORMANCE SPECIFICS

Based upon a review of the ARC preliminary joint design and performance requirements, Fluorocarbon, Inc. recommended the following seals:

RANKING	DESCRIPTION
HIGHEST	2 METAL** O-RINGS, 1/2" DIAMETER
SECOND	2 METAL** O-RINGS, 3/8" DIAMETER
THIRD	2 METAL** C-RINGS, 3/8" DIAMETER

---

* Fluorocarbon, Inc., Metallic Gasket Division of Houston, Texas; Fluorocarbon, Inc., Components Division of Columbia, S.C.; and Advanced Products, Inc. of North Haven, Connecticut.

** Inconel 718 with silver plating, 10 percent wall

TABLE 2.3.4. METAL SEAL MATERIAL DESIGN DATA
(ADVANCED PRODUCTS, INC.)

Yield Strength (psi) for Various Materials at Various Temperatures (000 Omitted)

Material	Code	72°F. 20°C.	200°F. 93°C.	400°F. 204°C.	600°F. 316°C.	800°F. 427°C.	1000°F. 538°C.	1200°F. 649°C.	1400°F. 760°C.	1600°F. 871°C.	1800°F. 982°C.	2000°F. 1093°C.
Type 304SS	1	34	27	20	17	15	14	12	11	9	5	2
316SS	2	38	35	29	26	23	21	19	18	14	7	3
321SS	3	33	31	28	25	22	20	18	15	11	6	3
347SS	4	39	37	33	32	31	29	26	22	15	9	6
Monel 400	5	47	48	49	50	51	24	28	34	40	54	
Inconel 600	6	38	34	32	30	29	28	24	20	10	6	
Inconel X-750 Annealed	7	36	35	33	31	29	28	26	17	9	4	
Age Hardened	7	124	122	120	118	116	116	115	94	30	10	
Inconel 718 Age Hardened	14	164	162	160	158	154	148	142	106	42	15	6
Haynes 25	9	68	58	48	40	39	36	36	38	34	26	12

TABLE 2.3.5. PRESSURE RANGES FOR VARIOUS METAL SEALS.
(ADVANCED PRODUCTS, INC.)

DESIGN RANGE FOR METAL VENTED O-RING

Pressure	M-W-R	M-O-R	M-V-R	M-C-R	M-SE-R
100,000 psi		BV			A
50,000		BV		B	A
25,000	A	BV	A	B	A
10,000	A	BV	A	B	A
5,000	A	BV	A	B	A
3,000	A	AV/B	A	A	A
1,000	A	AV/B	A	A	A
500	A	AV/B	A	A	A
15	A	A	A	A	A
10^{-1} Torr	A	A	A	A	A
10^{-2}	A	A	A	A	A
10^{-3}	A	A	A	A	A
10^{-4}	A	A	A	A	A
10^{-5}	A	A	A	A	A
10^{-6}	A	A	A	A	A
10^{-7}	A	B		B	A
10^{-8}	A	B		B	A
10^{-9}	A			B	A
10^{-10}	A			B	A
10^{-11}				B	A
10^{-12}					A
10^{-13}					A
See Also	NA	See Page 15	NA	See Page 12	NA

LEGEND:

A = STANDARD WALL
B = HEAVY WALL
V = VENTED
M-W-R = WIRE RING
M-O-R = O-RING
M-V-R = V-RING
M-C-R = C-RING
M-SE-R = SPRING-ENERGIZED RING

TABLE 2.3.6. METAL SEAL MAXIMUM TEMPERATURE DESIGN DATA
(ADVANCED PRODUCTS, INC.)

Material	Max. Temp.	M-W-R	M-O-R	M-V-R	M-C-R	M-SE-R
Nickel	2200°F	•				
Haynes 25	2000°F		•			
Hastelloy	1800°F			•	•	
Gold	1700°F	•				
Copper	1700°F	•				
Inconel 718	1400°F		•		•	•
Inconel-X-750	1400°F	•	•	•	•	•
Inconel-600	1200°F	•	•			
300 Series-SS	800°F	•	•			•
Aluminum	400°F	•				•

LEGEND:

M-W-R = WIRE RING
M-O-R = O-RING
M-V-R = V-RING
M-C-R = C-RING
M-SE-R = SPRING-ENERGIZED RING

TABLE 2.3.7. METAL SEAL LOADING AND PLATING DESIGN DATA
(ADVANCED PRODUCTS, INC.)

Maximum Working Temperature	Plating/Coating Type	Recommended Load Range for Sealing (lbs./circum. in.)
150° F	Indium	75-350
450° F	Teflon	150-450
300° F	Lead	100-400
1500° F	Silver	250 Up
1700° F	Copper	250 Up
1700° F	Gold	200 Up
2200° F	Nickel	400 Up

The springback characteristics for the 3/8-inch outside diameter O-ring are included as Figure 2.3.43. This figure presents load versus compression data for a 4-inch-long specimen. The characteristic indicated as "20% COMP" corresponds to a flange groove height of 0.300 inch, i.e., 80 percent of a 0.375-inch diameter; the resultant compression is 0.075 inch. The springback for this configuration is 33 mils, i.e., the difference between the 75-mil compression and the 42-mil permanent set of the ring. The springback value of 12 mils quoted by Fluorocarbon, Inc., therefore, incorporates a good margin of conservatism. In addition, the 12-mil quoted springback is more than twice the worst-case nozzle-to-case joint gap of 5.7 mils and nearly four times the 3.1-mil maximum gap at any case segment field joint.

The 3/8-inch-diameter O-ring configuration was selected by ARC since it requires less room and therefore enables a smaller groove (and hence flange); the smaller O-ring also required a smaller compression load (about 80 percent of the 1/2-inch ring); at 0.012 inch, the springback for the 3/8-inch rings is, in all cases, more than twice the maximum design flange gap. While requiring higher flange loading and offering less springback than the comparable C-ring designs, the O-ring offers more seal area and is more forgiving to distortion in seal or flange bearing surface.

The revised Contract End Item (CEI) requirement is that "each seal shall demonstrate sealing capability at two times maximum gap size at maximum expected tracking velocity and two times tracking rate at maximum expected gap size." Neither of the seal manufacturers were able to provide tracking rate data or mathematical model results for any metal seals. The extremely rapid response rate of the metal O-ring seals had negated the manufacturers' need for such information; both Fluorocarbon and Advanced Products did, however, indicate a willingness to discuss test programs to acquire the information.

Lacking this tracking rate data, two mathematical modeling efforts were initiated. A highly simplified model establishing a "seal characteristic" based upon calculated natural frequencies and resultant average cyclic velocities was prepared. The resultant envelope was then "halved" to establish an "operating ceiling" as per the above CEI requirement. These results were then plotted along with the joint operating maps from the detailed structural analysis efforts. These results are included in Figures 2.3.44 and 2.3.45 for the case/nozzle and case field joints, respectively. As indicated, due to the very high seal tracking rates and large springback, seals at both locations provide wide "operating margin" even at worst-case conditions.

ORIGINAL PAGE IS
OF POOR QUALITY

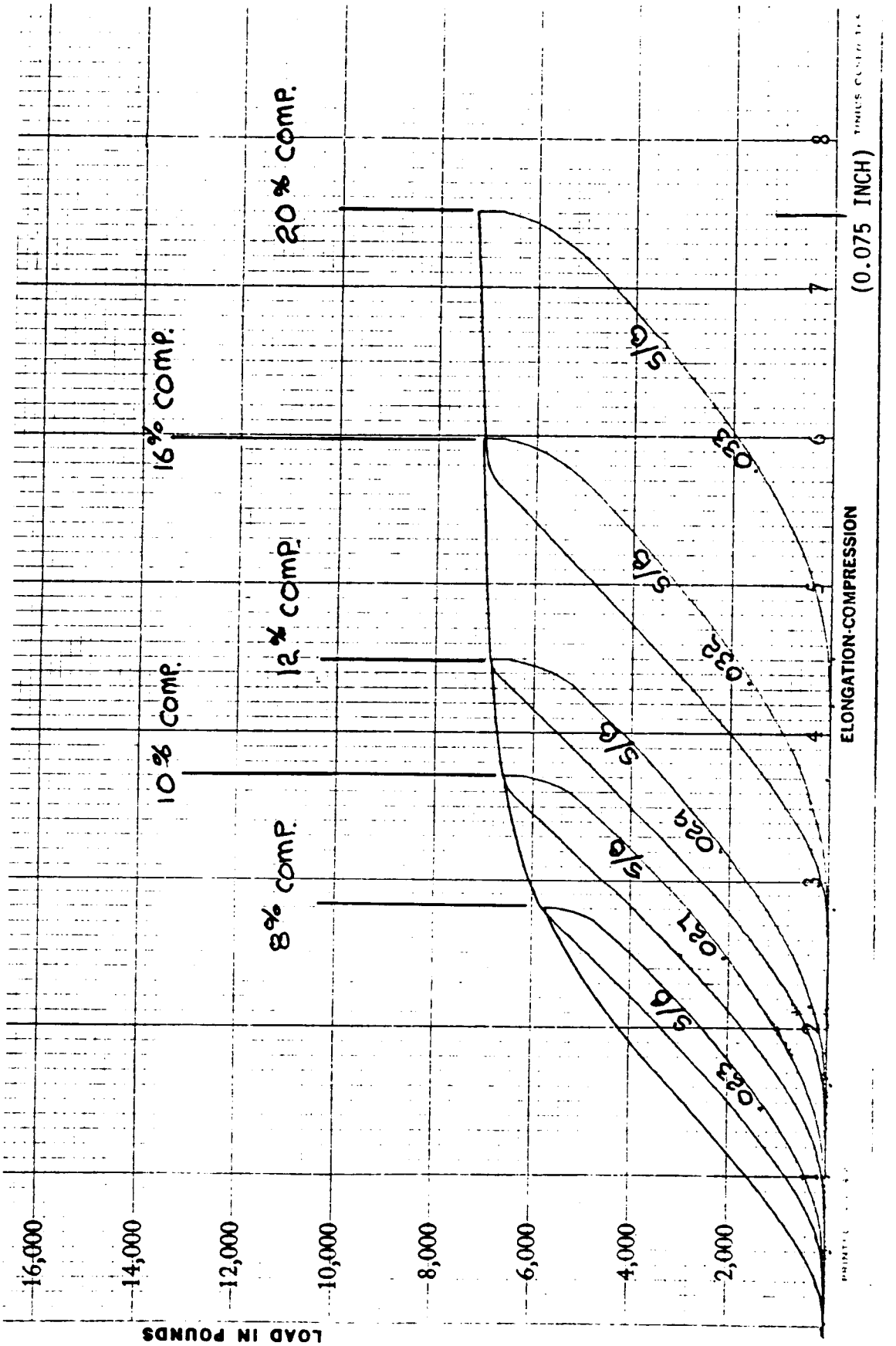

FIGURE 2.3.43. SEAL SPRINGBACK CHARACTERISTICS
3/8-INCH INCONEL 718 O-RING, 0.037-INCH WALL
THICKNESS, SAMPLE LENGTH OF 4.000 INCHES.
(FLUOROCARBON, INC.)

ORIGINAL PAGE IS
OF POOR QUALITY

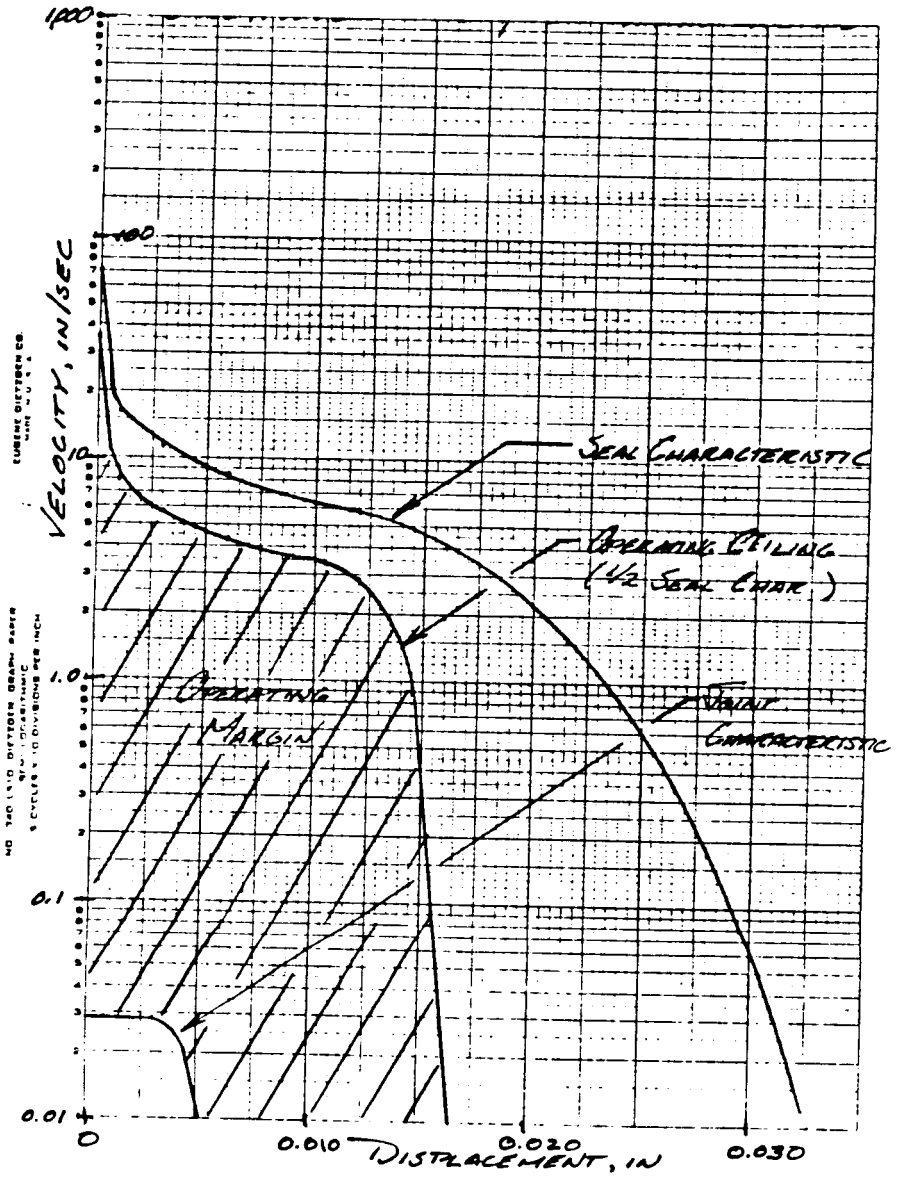

FIGURE 2.3.44. CASE/NOZZLE JOINT AND SEAL CHARACTERISTICS.

ORIGINAL PAGE IS
OF POOR QUALITY

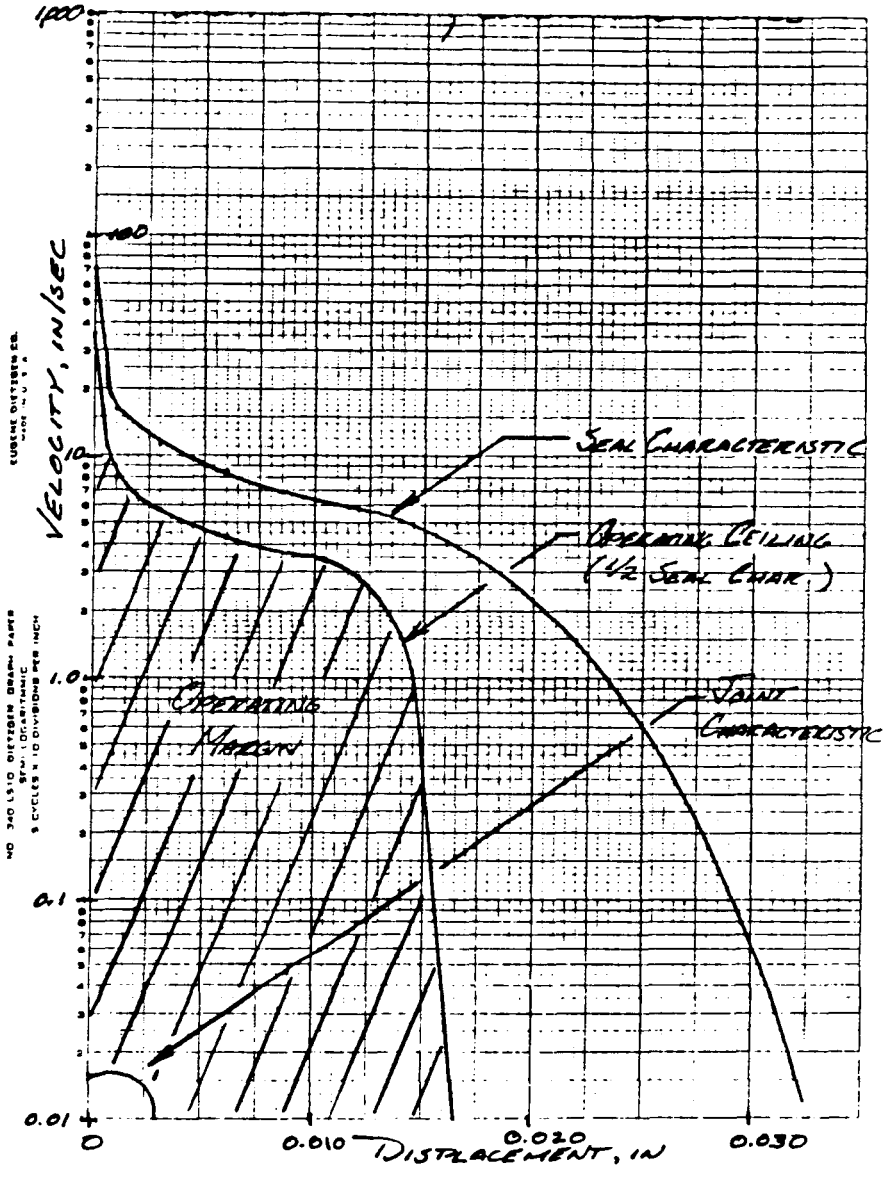

FIGURE 2.3.45. CASE FIELD JOINT AND SEAL CHARACTERISTICS.

The joint structural model dynamic results provided the joint characteristics presented in Figures 2.3.44 and 2.3.45. Detailed results are presented in Sections 2.3.1 and 2.3.3 for the case field joint and case/nozzle joints, respectively.

The design and performance specifics for the dual metal O-ring seals are provided in Table 2.3.8. Backup information on the seals is included in Appendix B.

2.3.5.5 SEAL SUMMARY

A review of the dual metal O-ring seal design and performance information of the previous section with the criteria of Table 2.3.3 reveals that the design conforms with requirements in each area. In the evaluation of this design, the demonstrated fabrication and utilization history for seals of this type is a very important consideration. Also most important is the fact that these seals lend themselves well to the joint designs. Finally, the selection of the design followed from the review and recommendations of the leading seal manufacturers.

Among candidate topics for further study are design, fabrication, shipping, assembly, inspection, etc. Careful review by ARC and the leading suppliers of these seals has led ARC to the conclusion that, for the system proposed, each of these obstacles can be overcome in straightforward, cost-effective fashion with a high degree of reliability.

TABLE 2.3.8. SEAL DESIGN DATA.

JOINT	SEAL	NOMINAL SEAL OD (IN)
CASE SEGMENT	PRIMARY	141.1
CASE SEGMENT	SECONDARY	142.4
CASE/NOZZLE	PRIMARY	103.1
CASE/NOZZLE	SECONDARY	104.4

NOTES

(1) GROOVE OD EQUALS SEAL OD + 0.014/.029.

(2) GROOVE HEIGHT AND WIDTH ARE 0.300 INCH AND 0.445 INCH RESPECTIVELY AT ALL LOCATIONS.

(3) ALL SEALS ARE 3/8-INCH DIAMETER, INCONEL 718, SILVER PLATED (0.004/0.006 INCH), 0.038-INCH WALL, VENTED DESIGN.

(4) REQUIRED SEAL COMPRESSION IS 2500 LBF/IN-SEAL (FLUOROCARBON VALUE VS. 1700 ADVANCED PRODUCTS).

(5) DESIGN SPRINGBACK IS 0.012-INCH (FLUOROCARBON VALUE VS. 0.011 ADVANCED PRODUCTS).

(6) SEAL SURFACES TO BE 32 MICRO-INCHES (RMS) FINISH; MACHINE TOOL MARKS TO BE CONCENTRIC. LUBRICATION NOT REQUIRED.

(7) SEALS NOT TO BE REUSED.

2.4 ASBESTOS-FREE INSULATION

The insulation trade studies were presented in the Mid-Term Report, which is submitted as Appendix A of this document. These trade studies resulted in an asbestos-free insulation design for the Block II SRM. This section will present this overall insulation design and the supporting rationale. In addition, the available material database will be presented followed by the thermal analyses that have been performed since the Mid-Term Report was issued. These analyses were used to verify the adequacy of the materials selected to achieve the desired insulation performance safety factors.

The specific design descriptions and rationale for the insulation at the case segment joints and the case-to-nozzle joint were presented in Sections 2.3.2 and 2.3.4, respectively.

2.4.1 INSULATION DESIGN DESCRIPTION

The case insulation trade studies resulted in selection of a hybrid insulation system for the case segments. This system uses a Kevlar/silica-filled Hypalon as the material used next to the steel case wall to provide the required thermal protection. The aft portion of the motor case segments near the joints and the portion of the aft case segment that is exposed during much of the motor firing have a layer of USR-3800 NBR/phenolic insulation placed between the Hypalon and the propellant combustion gas path. This material provides high erosion resistance in these critical areas in the aft case and at the joints. The Mid-Term Report described the automated ribbon winding technique that has been chosen as the best method for applying the insulation into the case segments.

USR-3800 has also been selected as the material for the molded inhibitors located at the forward end of each casting segment. These inhibitors would be formed during the case segment insulation automated layup.

The propellant liner and the castable inhibitors on the aft end of the grain segments will be made from the same material. The trade studies performed during the first phase of the work identified that the best option would be to retain the current liner material and replace only the asbestos filler. This choice would keep intact the proven compatibility of the CTPB liner with the PBAN propellant and provide known bonding and

aging characteristics. A number of fibrous materials, including silicates similar to asbestos, were identified as candidates. These include PBI, carbon fibers, ceramic fibers, silica fibers, and mineral wool. The advantages and disadvantages of these fillers and a relative ranking are shown in Table 2.4.1.

Carbon fiber was given the highest score due to its ability to maintain maximum char strength at high temperatures, although to achieve maximum strength it must be used in conjunction with a silicate that can melt and inhibit surface oxidation. All the fibrous silicate materials behave similarly in the high temperature environment and cannot be differentiated on that basis. A laboratory study would be needed to differentiate on the basis of processing and liner mechanical properties. PBI fiber was given the lowest score due to lack of an experience base.

The selected liner retains the current binder system with the asbestos being replaced 50 percent by carbon fiber and 50 percent by a silicate fiber. Cab-O-Sil (another silicate) would be added to control the thixotropic behavior for processing purposes.

As discussed in the Mid-Term Report, replacement materials for the asbestos-containing portions of the safe and arm (S&A) device were also identified. The S&A clutch disc material will be replaced with a Kevlar phenolic, while the S&A commutator material will be replaced with ceramic phenolic.

A silica NBR material will be used to fabricate the stress relief flaps at the aft end of each casting segment and to form a component of the joint insulation. This material was selected because of the need for a low modulus and compatibility with the PBAN propellant.

2.4.2 INSULATION MATERIAL DATABASE

USR-3800 is an existing NBR/phenolic material that uses boric acid as a filler. USR-3800, a Uniroyal product, has been produced for close to 20 years and was used in both the POLARIS and POSEIDON missiles. In addition, the material has been tested as part of insulation studies for large motor applications (References 1 and 2) and been found to exceed the performance of the currently used NBR/asbestos material. Table 2.4.2 presents the thermal and mechanical properties of this material that have

C-2

TABLE 2.4.1. LINER MATERIAL ALTERNATIVES.

MATERIAL/MANUFACTURER	ADVANTAGES	DISADVANTAGES	SCORE
CARBON FIBER BASF, HITCO, HERCULES, UNION CARBIDE, CORTAULDS	DEMONSTRATED IN INSULATION FORMULATIONS TO MAINTAIN EXCELLENT CHAR STRENGTH; DOESN'T MELT	CAN BE OXIDIZED AT HIGH TEMPERATURES	7.5
CERAMIC FIBER (SILICATE) NEXTEL - 3M FIBERFRAX - H.I. THOMPSON	MELTS AND PROVIDES CORROSION PROTECTION	HIGHER COST	7.0
FIBROUS SILICA REFRASIL - H.I. THOMPSON	MELTS AND PROVIDES CORROSION PROTECTION		7.0
MINERAL WOOL (SILICATE)	MELTS AND PROVIDES CORROSION PROTECTION		7.0
PBI FIBER CELANESE	DEMONSTRATED IN INSULATION FORMULATIONS TO GIVE GOOD HIGH TEMPERATURE PERFORMANCE.	NO PROCESSING DATA AVAILABLE ON LINER FORMULATIONS. LONG TERM AGING CHARACTERISTICS NOT ESTABLISHED.	5.0

TABLE 2.4.2. USR-3800 MECHANICAL AND THERMAL PROPERTIES.

TEMPERATURE		SPECIFIC HEAT		CONDUCTIVITY	
(°K)	(°R)	(kJ/kg-K)	(Btu/Lbm-R)	(W/m-K)	(Btu/ft-sec-R)
256	460	0.711	0.170	0.031	0.50 E-5
283	510	1.091	0.261	0.083	1.33 E-5
311	560	1.463	0.350	0.138	2.22 E-5
339	610	1.831	0.438	0.167	2.68 E-5
367	660	2.044	0.489	0.175	2.81 E-5
394	710	2.136	0.511	0.180	2.89 E-5
422	760	2.153	0.515	0.182	2.92 E-5

MECHANICAL PROPERTIES AT AMBIENT CONDITIONS

STRESS		STRAIN	MODULUS	
(MPa)	(PSI)	(%)	(MPa)	(PSI)
7.6	1100	200	179.3	26,000

been obtained from the literature. Figure 2.4.1 presents the results of a thermogravimetric (TGA) analysis of both USR-3800 and the current NBR/asbestos material. The TGA analysis is used to determine the decomposition characteristics of the material. As can be seen from the figure, the residual char material for USR-3800 is greater than that for NBR/asbestos, which is an indication of improved char strength. Table 2.4.3 shows data from Reference 1, which compare the erosion characteristics of USR-3800 and NBR/asbestos. As can be seen from the data, USR-3800 outperforms NBR/asbestos. These data were used to create an analytical model of this material to aid the thermal analysis discussed in Section 2.4.3. All additional required data needed to validate the use of this material will be obtained in the Development and Verification Phase of the Block II program.

The Kevlar/silica-filled Hypalon material is a recently developed material currently being used by ARC as an asbestos replacement insulation in a surface-to-air missile system. This rocket motor is currently in the qualification phase. Performance, bond, and aging data have been and are being generated in this program and will be available for the Block II Program. Table 2.4.4 presents the thermal and mechanical properties of this material. Figure 2.4.2 presents the results of a TGA analysis of the Kevlar/silica-filled Hypalon. A validated thermal model of this material existed before this current study program began and has been used to verify the adequacy of the proposed design.

Table 2.4.5 contains the mechanical and thermal properties of the silica NBR material selected for the stress relief flaps and a joint insulation component.

The trade studies performed indicated that a hybrid insulation system using a Kevlar-filled EPDM material in place of the USR-3800 also was a viable alternative to the current NBR/asbestos insulation. ARC believes that it is good design practice to carry a backup insulation material into the Development and Verification Phase of the program. Kevlar-filled EPDM is recommended as a backup insulation material for the USR-3800. ARC has an established database with the Kevlar-filled EPDM material (References 3 and 4). Table 2.4.6 presents the thermal and mechanical properties of this material. Figure 2.4.3 shows the results of a TGA analysis of Kevlar-filled EPDM. Figure 2.4.4 shows the type of erosion data that have been obtained using the ARC Insulation Test Motor (ITM). As can be seen from the figure, both instantaneous and average erosion data as a function of Mach number are available for use in the design process.

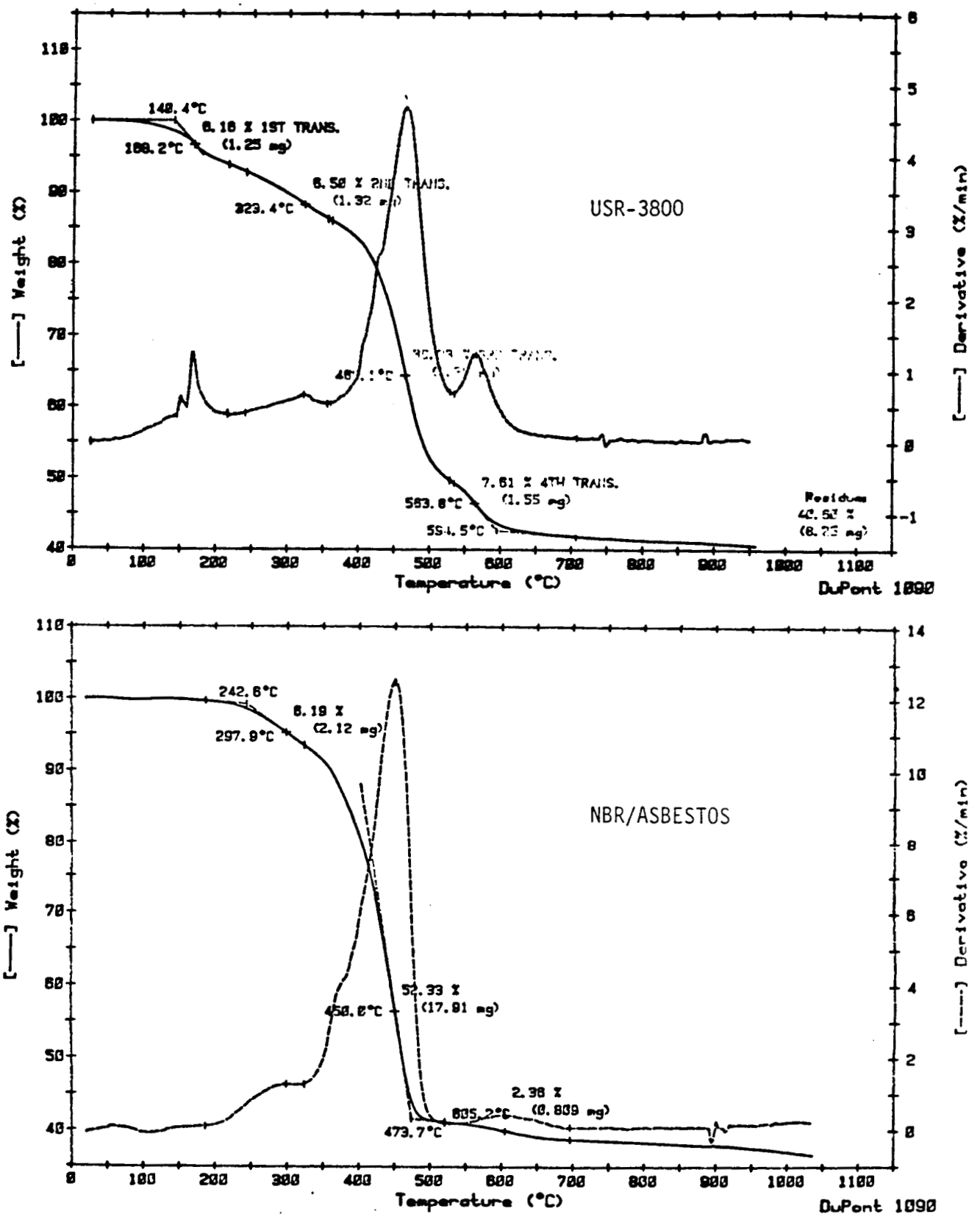

FIGURE 2.4.1. THERMOGRAVIMETRIC ANALYSIS RESULTS FOR USR-3800 AND NBR/ASBESTOS.

TABLE 2.4.3. COMPARISON OF EROSION DATA FOR USR-3800 AND NBR/ASBESTOS[1].

INITIAL MACH NUMBER	EROSION RATE DATA[2] USR-3800 (mm/sec)	USR-3800 (in/sec)	NBR/ASBESTOS (mm/sec)	NBR/ASBESTOS (in/sec)
0.05	0.102	0.004	0.229	0.009
0.10	0.152	0.006	0.508	0.020
0.15	0.076	0.003	0.660	0.026
0.20	0.076	0.003	0.787	0.031
0.25	0.051	0.002	0.864	0.034

1 DATA FROM REFERENCE 2.4.1. PROPELLANT HAD 15% ALUMINUM, 88% SOLIDS.

2 AVERAGED EROSION BASED ON INITIAL MACH NUMBER.

TABLE 2.4.4. HYPALON MECHANICAL AND THERMAL PROPERTIES.

TEMPERATURE		SPECIFIC HEAT		CONDUCTIVITY		
(°K)	(°R)	(kJ/kg-K)	(Btu/Lbm-R)	(W/m-K)	(Btu/ft-sec-R)	EMISSIVITY
200	360	0.732	0.175	0.122	1.95 E-5	0.80
294	530	1.484	0.355	0.112	1.80 E-5	0.80
422	760	1.848	0.442	0.099	1.59 E-5	0.80
644	1160	1.986	0.475	0.077	1.23 E-5	0.80
811	1460	2.048	0.490	0.069	1.10 E-5	0.80
1367	2460	2.090	0.500	0.069	1.10 E-5	0.80
2478	4460	2.090	0.500	0.069	1.10 E-5	0.80
3589	6460	2.090	0.500	0.069	1.10 E-5	0.80

MECHANICAL PROPERTIES AT AMBIENT CONDITIONS

STRESS		STRAIN	MODULUS	
(MPa)	(PSI)	(%)	(MPa)	(PSI)
11.0	1600	28	58.6	8,500

ORIGINAL PAGE IS
OF POOR QUALITY

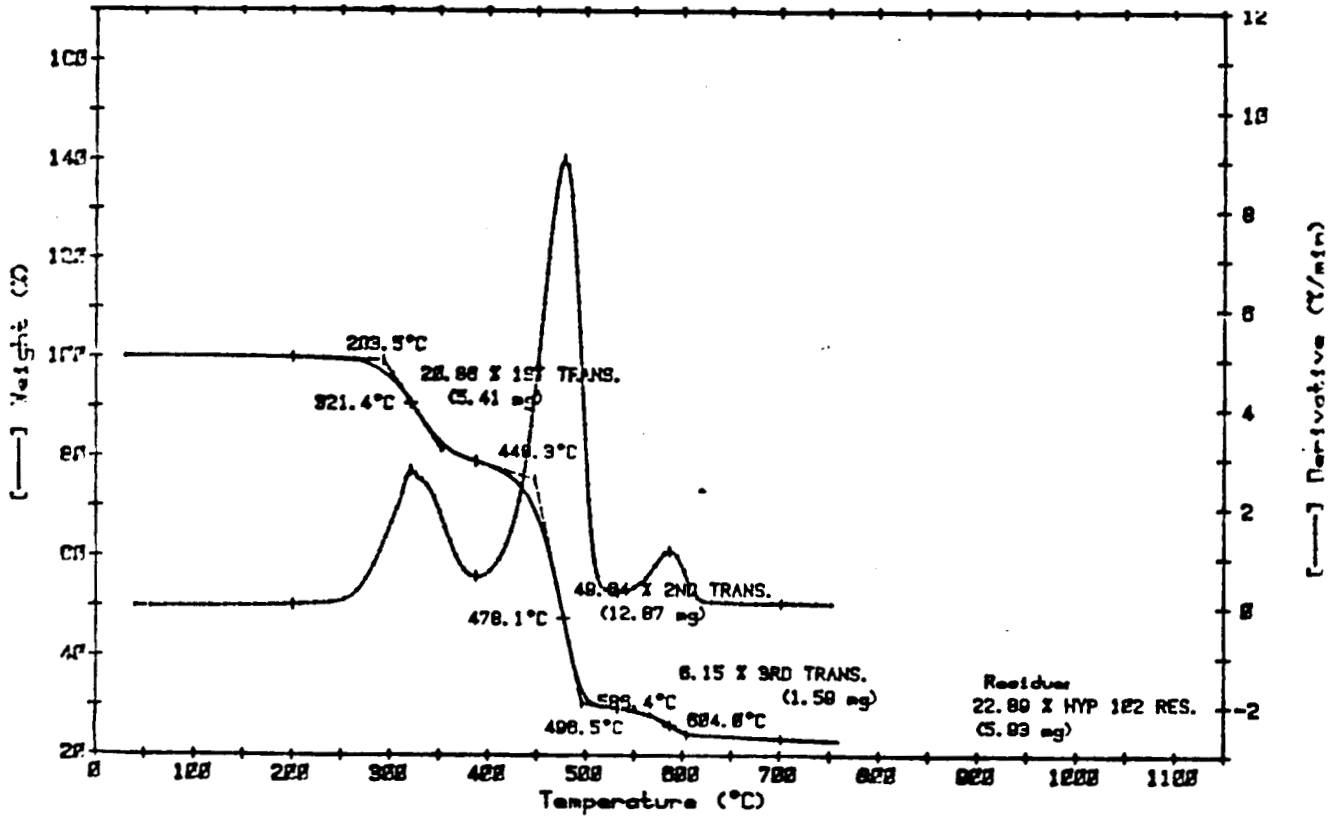

FIGURE 2.4.2. THERMOGRAVIMETRIC ANALYSIS RESULTS FOR KEVLAR/SILICA-FILLED HYPALON.

TABLE 2.4.5. SILICA NBR MECHANICAL AND THERMAL PROPERTIES.

TEMPERATURE		SPECIFIC HEAT		CONDUCTIVITY	
(°K)	(°R)	(kJ/kg-K)	(Btu/Lbm-R)	(W/m-K)	(Btu/ft-sec-R)
256	460	1.818	0.435	0.242	3.89 E-5
283	510	1.881	0.450	0.242	3.89 E-5
311	560	1.923	0.460	0.242	3.89 E-5
339	610	1.986	0.475	0.248	3.98 E-5
367	660	2.048	0.490	0.260	4.17 E-5
394	710	2.111	0.505	0.262	4.21 E-5
422	760	2.174	0.520	0.267	4.28 E-5

MECHANICAL PROPERTIES AT AMBIENT CONDITIONS

STRESS		STRAIN	MODULUS	
(MPa)	(PSI)	(%)	(MPa)	(PSI)
13.5	1960	470	14.8	2150

TABLE 2.4.6. KEVLAR/EPDM MECHANICAL AND THERMAL PROPERTIES.

TEMPERATURE		SPECIFIC HEAT		CONDUCTIVITY		
(°K)	(°R)	(kJ/kg-K)	(Btu/Lbm-R)	(W/m-K)	(Btu/ft-sec-R)	EMISSIVITY
217	390	1.038	0.2483	0.196	3.15 E-5	.90
256	460	1.170	0.2800	0.190	3.05 E-5	.90
350	630	1.492	0.3570	0.162	2.60 E-5	.90
422	760	1.714	0.4100	0.162	2.60 E-5	.90
644	1160	1.756	0.4200	0.125	2.01 E-5	.90
722	1300	1.756	0.4200	0.112	1.80 E-5	.90
1367	2460	1.756	0.4200	0.112	1.80 E-5	.90
3589	6460	1.756	0.4200	0.112	1.80 E-5	.90

MECHANICAL PROPERTIES AT AMBIENT CONDITIONS

STRESS		STRAIN	MODULUS	
(MPa)	(PSI)	(%)	(MPa)	(PSI)
7.8	1125	19	72.4	10,500

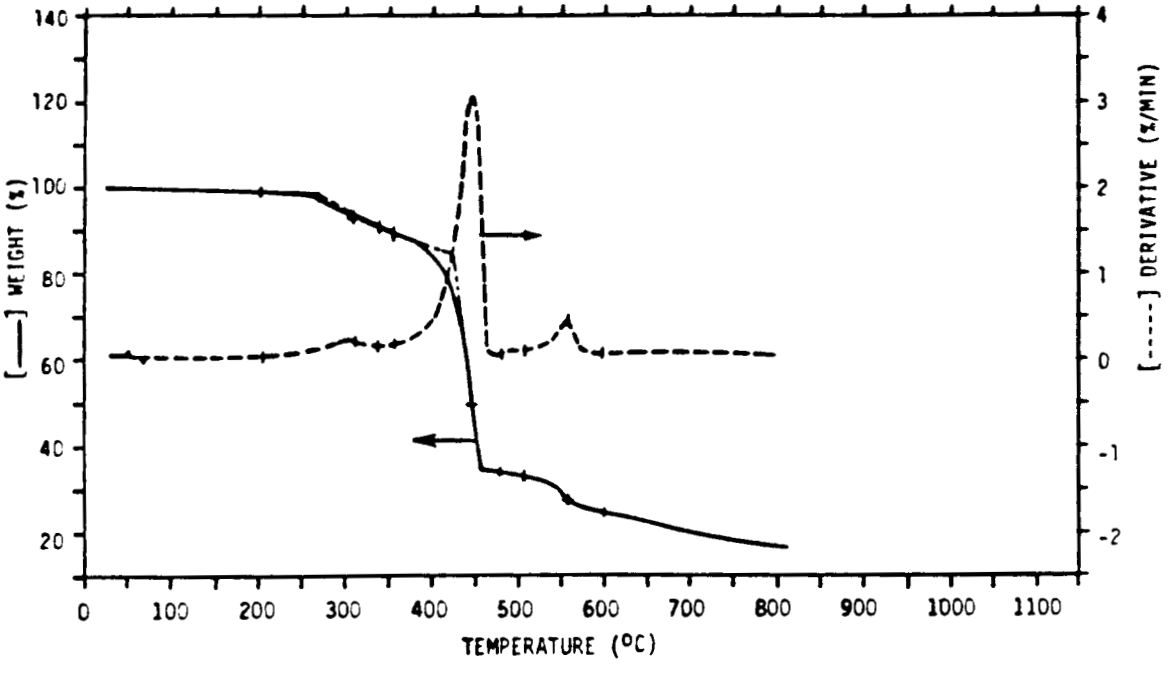

FIGURE 2.4.3. THERMOGRAVIMETRIC RESULTS FOR KEVLAR FILLED EPDM.

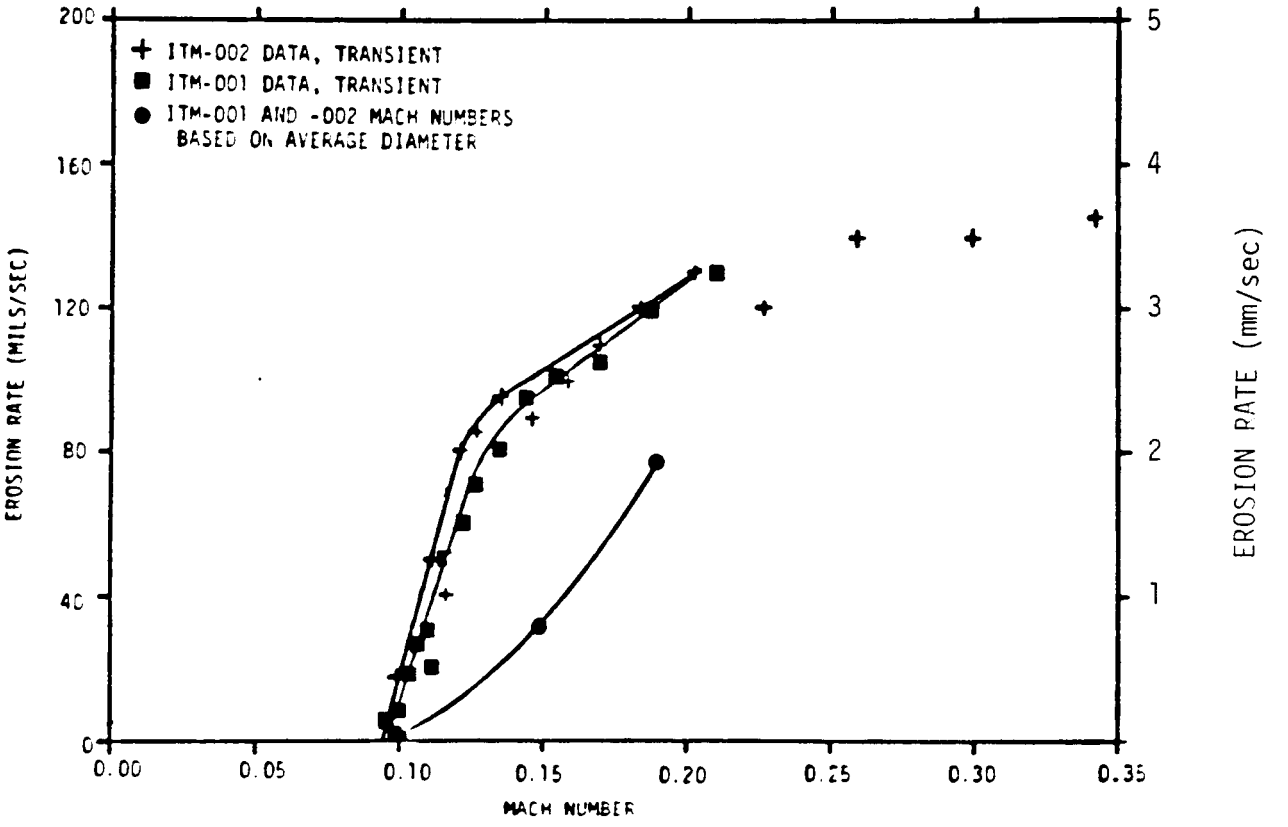

FIGURE 2.4.4. EROSION DATA FOR KEVLAR-FILLED EPDM OBTAINED FROM THE ARC INSULATION TEST MOTOR.

2.4.3 CASE INSULATION THERMAL ANALYSES

One-dimensional thermal analyses were conducted on the center segment of the SRM motor. This section was chosen because performance data were available at this location from the Morton Thiokol Inc. thermal report on the high performance motor (HPM) design (Reference 5). The Aerotherm Chemical Equilibrium (ACE) and the Charring Material Thermal Response and Ablation (CMA3) computer programs were used in these analyses. These programs are standard industry tools for insulation analysis.

ACE is used to perform a series of thermochemical calculations involving varying mixtures of propellant combustion gas, insulator pyrolysis gas, and insulator char constituents. The thermochemical calculations quantitatively describe the equilibrium reaction state (i.e., species, temperature), chemical energies, and energies associated with mass transfer occurring at the heated surface of the insulator for each mixture.

CMA3 uses this matrix of energy descriptions in performing a heated surface energy balance. CMA3 incorporates this surface energy balance in a finite difference solution of the one-dimensional, axisymmetric parabolic heat conduction equation which calculates transient in-depth temperatures, erosion recession rates, pyrolysis gas generation rates, and the density gradient within the insulator. Remaining parameters required by CMA3 include the geometric configuration, material properties, and boundary conditions. The internal boundary conditions consist of three components: convection, chemical energy, and luminous radiation. The convective conditions were identical to those in Reference 5.

The thermal analyses performed on the center motor segment used the current HPM insulation thicknesses so that a direct comparison of the resulting safety factors could be made to the current asbestos-containing material. The portion of the overall thickness allotted to the Hypalon material was that required for thermal protection of the case. The remainder was analyzed as USR-3800. The results of these analyses are presented in Figure 2.4.5. As can be seen from the figure, the USR-3800/Hypalon hybrid design outperforms the current NBR/asbestos material, resulting in higher safety factors for the same insulation thickness.

Because of differences in the specific gravity of the selected insulation materials when compared to the current NBR/asbestos, a weight savings of 806 kg (1,774

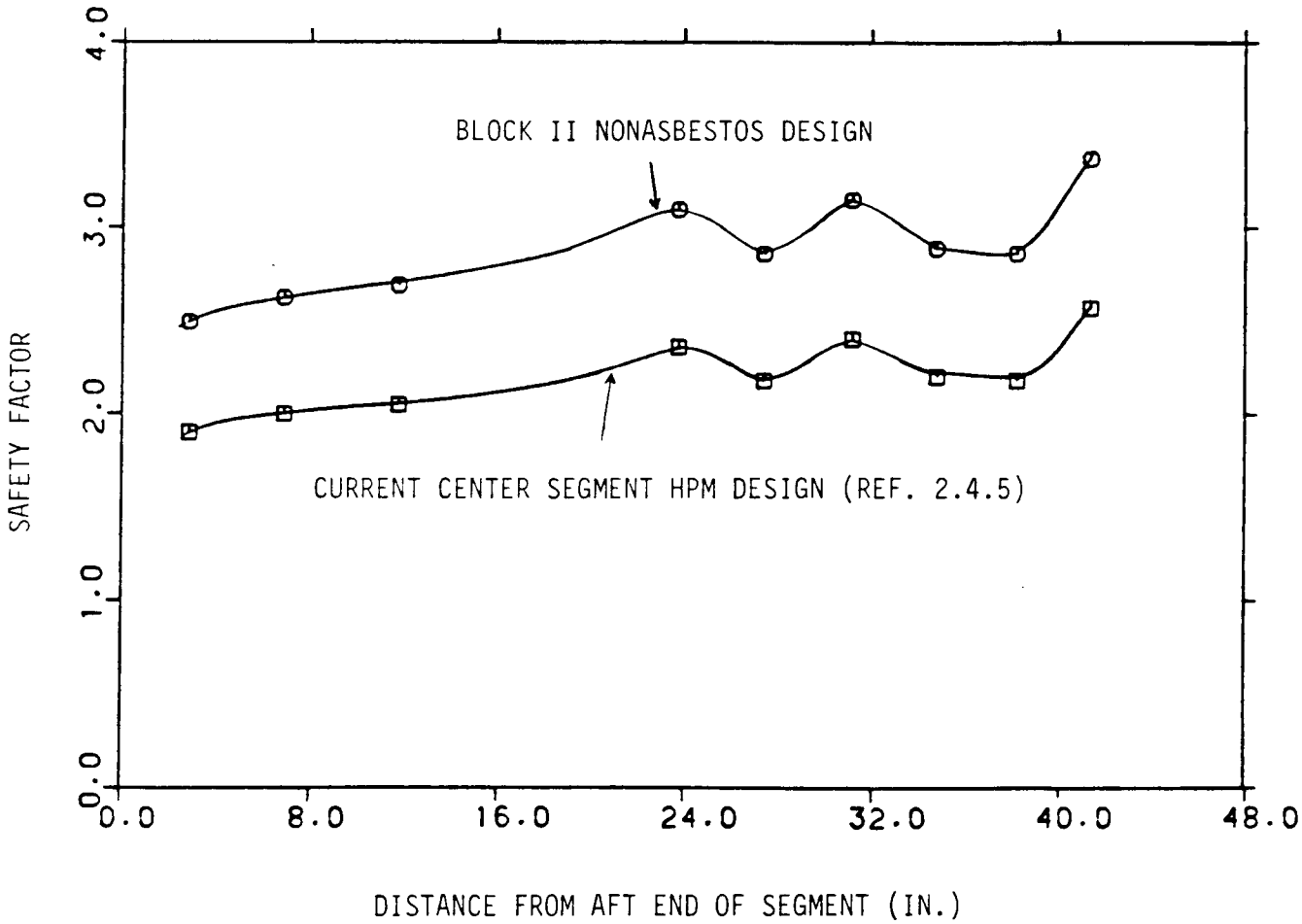

FIGURE 2.4.5. THERMAL ANALYSIS SAFETY FACTOR COMPARISON FOR THE CENTER SEGMENT.

pounds) over the HPM design has been calculated when insulation thicknesses are held at the current values.

Because of the improved safety factors for the proposed design, the potential exists for the Block II design to thin the insulation thickness and obtain a larger volume for propellant loading while maintaining the current insulation safety factors. This reduction in insulation thickness reduces the insulation weight an additional 1,163 kg (2,559 pounds). The ballistic performance impact of this weight reduction is discussed in Section 3.0.

In summary, the insulation materials selected as a result of the trade studies have been found to have an adequate database of properties. These properties have permitted the creation of thermal analytical models that have been used to analyze the proposed Block II design. These preliminary analyses have established that the selected nonasbestos materials are viable replacements for the current asbestos materials. The additional data necessary to finalize the Block II design will be obtained in the Development and Verification Phase of the program.

REFERENCES

1. Simmons, B. A., and D. L. Nachbar, "Development of Cost-Optimized Insulation System for Use in Large Rocket Motors," Vols. I-III, Aerojet-General Corporation, NASA CR-72581, CR-72582, and CR-72583, 1969.

2. Bradley, W., J. DeAcetis, A. Stenersen, et al., "Investigation and Evaluation of Motor Insulation for Multiple Restart Application," Final Report, AFRPL-TR-67-287, 1967.

3. Yezzi, C. A., and B. B. Moore, "Characterization of Kevlar/EPDM Rubbers for Use as Rocket Motor Case Insulators," AIAA Paper 86-1489, 1986.

4. Spear, G. B., T. L. Ludlow, J. F. Sparks, B. B. Moore, and T. F. Davidson, "Thermally Stable Elastomeric Insulations for Tactical Applications," presented at the JANNAF Propulsion Conference, August 1986.

5. Eddy, N. F., K. Eckhart, S. B. Pendleton, et al., "High Performance SRM Internal Insulation Design Report," Morton Thiokol, Inc., TWR-13065 Rev. B Amendment 2, 1984.

2.5 NOZZLE DESIGN

At the beginning of the Block II SRM Study Program, the decision was made to retain the current nozzle concept to take full advantage of the years of design, development, and testing invested in that approach. Thus, alternative approaches to the basic nozzle geometry and assembly techniques, the flex bearing, and the thrust vector control system were not considered directly. Impacts in these areas were considered only when driven by the results of the study in other areas. One item identified for study was the nozzle liner material, which has exhibited some anomalous erosion in the past (STS-8). In addition, the Block II requirements dictated that redundant seals be included at nozzle internal assembly joints and that asbestos-containing materials be eliminated. The results in each of these study areas is discussed in the following section.

2.5.1 NOZZLE LINER MATERIAL

Liners used on the current SRM nozzle are fabricated from rayon-based carbon cloth/phenolic tape. The performance of this liner material has been adequate with the exception of anomalous gouging and "pocketing erosion", which was first noted on STS-8. NASA and the current nozzle fabricator have spent considerable effort investigating the solutions to this problem and, as a result of stringent material/processing controls and revised processing/fabrication techniques, have virtually eliminated the incidence of pocketing erosion in the six flights preceding 51-L.

The goal of the program study in this area was to investigate the use of state-of-the-art liner materials to further reduce the possibility of pocketing erosion. A material trade study was, therefore, initiated and the preliminary results were given in the Mid-Term Report (Appendix A). Since that time, the study was completed and the final results are included as an addendum to Appendix A. Contrary to the preliminary findings, the final conclusion was that the current material should be retained. In short, none of the materials investigated meet the requirements of offering a positive gain in reliability and having an extensive database to back them. The most promising material was found to be multidirectionally reinforced carbon-carbon advanced composites. While carbon-carbon composites are most certainly the material of the future in this application, it was not yet considered sufficiently mature for the shuttle SRM. Refer to the addendum to Appendix A for the details of the trade study and, in particular, for the results of a design study submitted by Societe Europeenne de Propulsion (SEP), a leading

French propulsion company. SEP investigated two carbon-carbon ITE approaches utilizing nondegradable backup insulative materials, which are certainly viable options for the future, particularly in applications where performance requirements dictate the use of the most advanced materials available.

2.5.2 NOZZLE SUBASSEMBLY JOINT SEALS

A redundant seal design study was conducted for the five joints in the nozzle subassembly shown in Figure 2.5.1. The details of that study are included in Appendix A. As reported there, the selected joint/seal configuration is the face seal and bore seal combination. The selected design at each joint is shown in Figure 2.5.2.

The seals chosen for use at each location are elastomeric O-rings. This type of seal is currently used; it appears to have performed adequately in this application in the past, as no record of any problems has been found. In addition, potential joint opening that dictated the design at the case and nozzle-to-case joints is less of a problem for these joints, which are typically in compression and are not subject to the load eccentricities of the two "major" joints. As previously reported, the incorporation of redundant scale at nozzle subassembly joints result in 247.5 pounds.

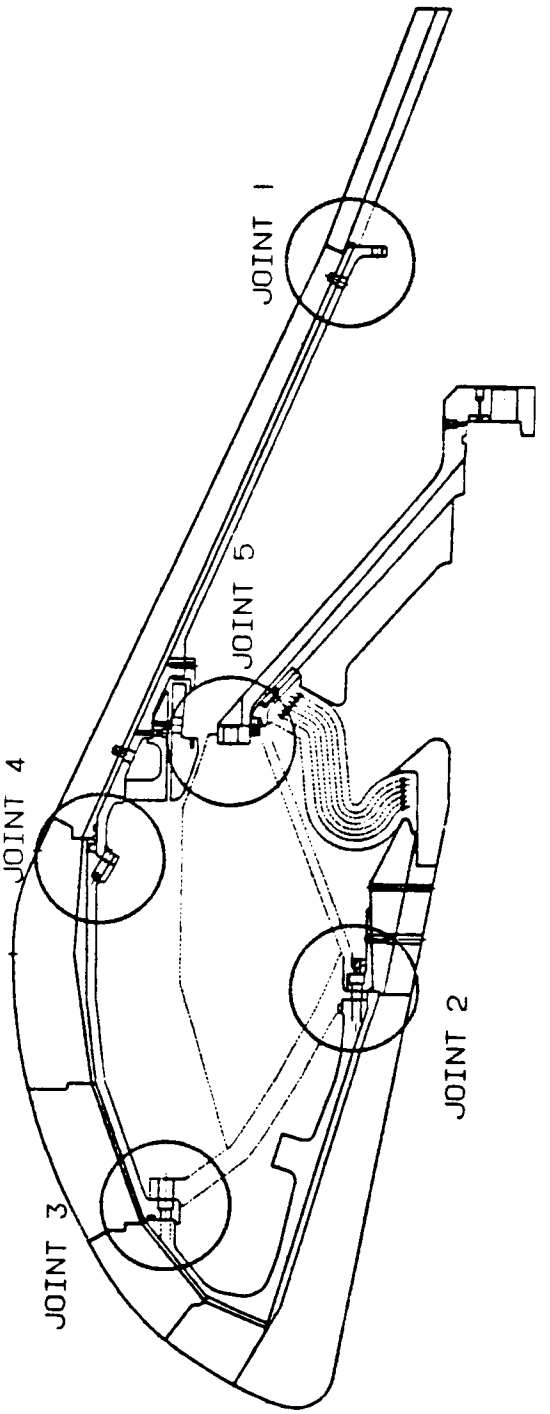

FIGURE 2.5.1. SRM NOZZLE SUBASSEMBLY JOINTS.

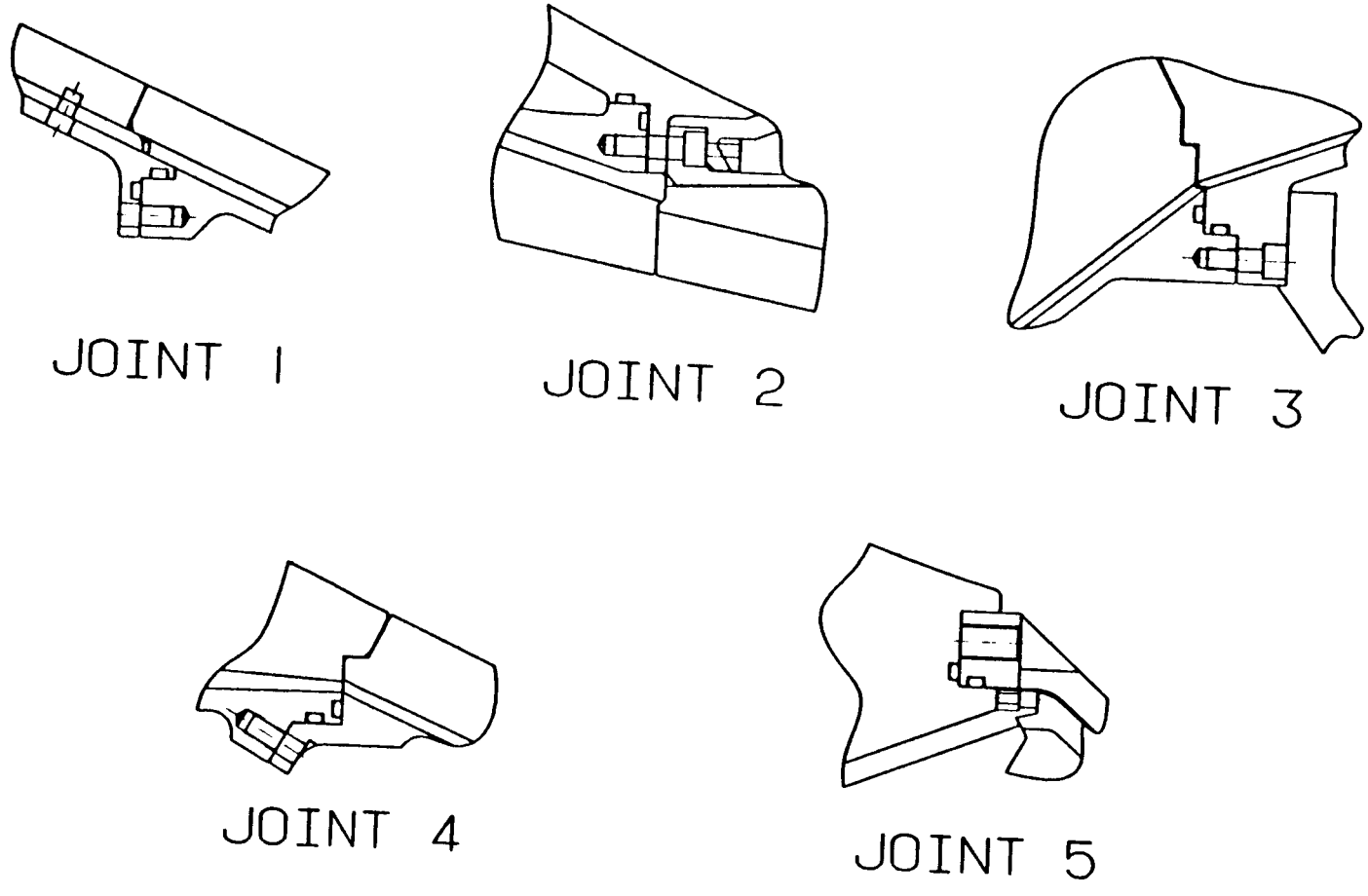

FIGURE 2.5.2. BLOCK II NOZZLE SUBASSEMBLY JOINT DESIGNS.

2.5.3 FLEX BEARING BOOT

Replacement of the silica and asbestos-filled NBR in the nozzle flex bearing boot presents numerous design challenges due to the unique structural and thermal requirements imposed upon it. Low flexural stiffness is mandatory to minimize thrust vector control actuation torque. The current stacked wafer approach using carbon cloth between wafers (for venting purposes) helps achieve the low flexural stiffness. Replacement materials must be able to be processed in the same manner. Boot deflections resulting from pressurization and thrust vectoring stress the char and may cause char spallation, which increases the affected rates.

Thermal environments imposed on the boot are severe due to the configuration and location. The bent or recessed portion of the boot can trap aluminum oxide particles in the combustion gas. Heat is rapidly conducted from the aluminum oxide to the boot. In addition, flow of aluminum oxide along the wall will cause gouging of the boot.

Candidate materials with a sufficient database for the boot include NBR filled with silica; silica and polybenzimidazole (PBI) fiber; or silica and Kevlar fiber. Other candidate materials are USR-3800 (NBR/phenolic), Kevlar-filled EPDM, and DC 93-104. Basic properties of these elastomeric insulations are presented in Table 2.5.1.

Each of the parameters influencing the operation of the flex bearing boot must be properly accounted for to select the optimum material. Thus, a trade study was performed to evaluate the relative performance of candidate materials. Relative weighting factors used in the trade study emphasized reliability as the most important parameter. Table 2.5.2 shows the results of the trade study. DC 93-104 is shown to have properties that best satisfy the requirements for the flex bearing boot.

As previously mentioned, DC 93-104 has a strong char that adheres well to the virgin insulation. This strong char is fairly brittle and can spall when subjected to significant deflections. To alleviate spallation problems, a through-the-thickness braided structure impregnated with DC 93-104 is used in the first three outer layers of the boot. Carbon fibers in the braided structure provide an integral retention mechanism for the char layer and have sufficient play to accommodate boot deflections. Figure 2.5.3 shows the basic design details of the flex bearing boot.

TABLE 2.5.1. NOZZLE FLEX BOOT CANDIDATE MATERIAL PROPERTIES.

PROPERTY	CANDIDATE MATERIALS					
	NBR/SILICA PBI	NBR/SILICA	USR-3800 NBR/PHENOLIC	EPDM/ KEVLAR	NBR/SILICA KEVLAR	DC 93-104
SPECIFIC GRAVITY	1.23	1.21	1.146	1.163	1.24	1.45
TENSILE STRENGTH (PSI)	600	1,960	1,100	1,125	1,730	210
ELONGATION (%)	275	470	200	19	41	45
TENSILE MODULUS (PSI)	10,500	2,150	26,000	10,500	10,500	110
THERMAL CONDUCTIVITY (BTU/FT-SEC-R)	2.78 E-5	3.89 E-5	1.33 E-5	2.60 E-5	3.65 E-5	5.10 E-5

TABLE 2.5.2. NOZZLE FLEX BOOT MATERIAL CANDIDATE TRADE STUDY.

RATING PARAMETER	WEIGHTING FACTOR	NBR/SILICA PBI	NBR/SILICA	USR-3800 NBR/PHENOLIC	EPDM KEVLAR	NBR/SILICA KEVLAR	DC 93-104	SILICA-ASBESTOS NBR
LOW STIFFNESS	0.25	1.75	2.00	0.75	1.75	1.75	2.50	2.25
GOOD EROSION RESISTANCE	0.30	1.50	0.60	2.70	2.10	1.50	3.00	1.50
GOOD PROCESSIBILITY	0.20	1.40	2.00	0.80	1.40	1.40	1.60	1.60
LOW WEIGHT	0.15	1.20	1.20	1.50	1.35	1.20	1.05	1.20
COST	0.10	0.80	0.80	1.00	0.90	0.80	0.70	0.80
TOTAL RATING =		6.65	6.60	6.75	7.50	6.65	8.85	7.35

* RATING VALUE = WEIGHT FACTOR x RELATIVE PERFORMANCE

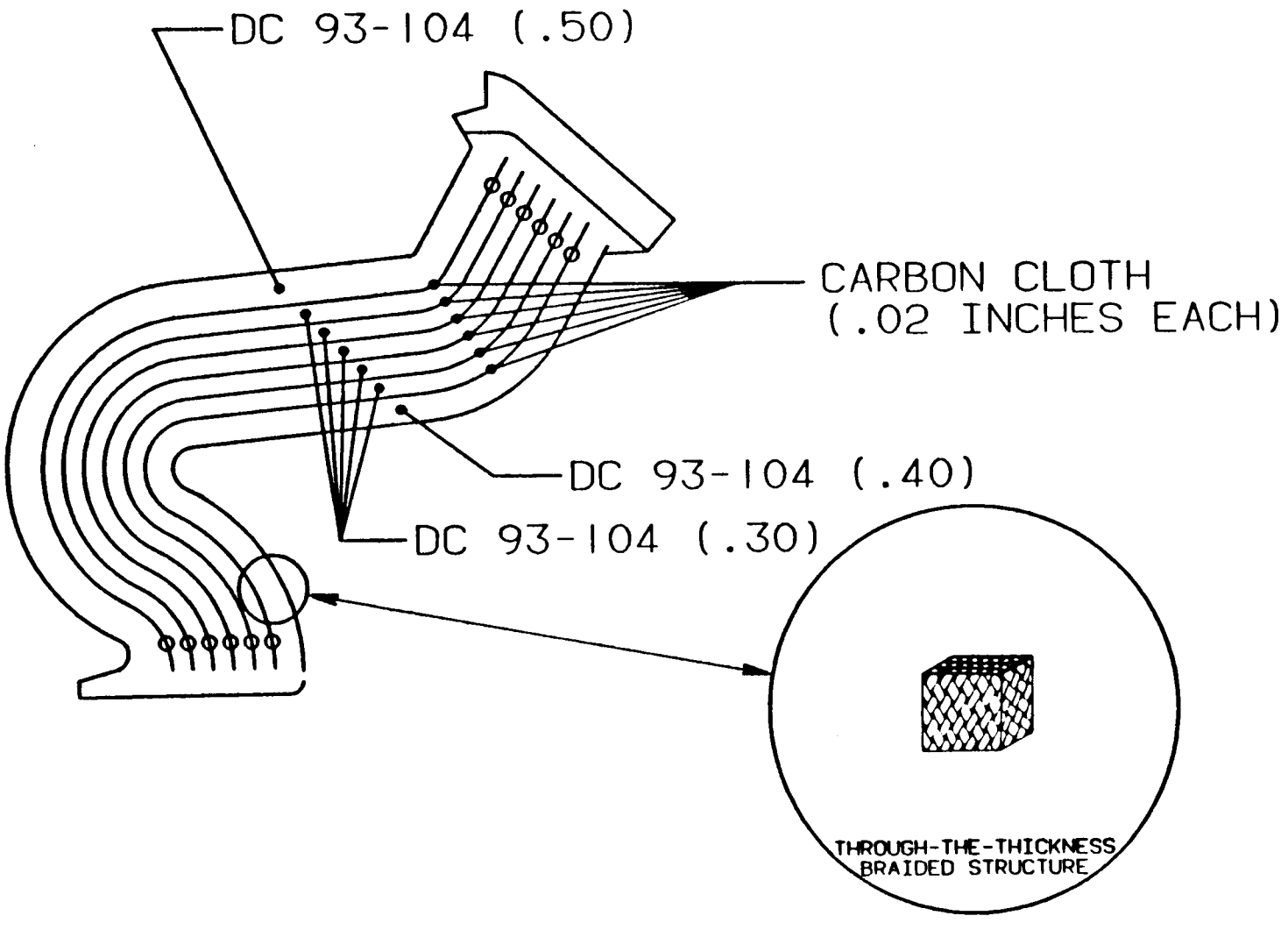

FIGURE 2.5.3. NOZZLE FLEX BEARING BOOT.

2.5.4 ADHESIVES

Two asbestos-filled adhesives used in the nozzle assembly are EA-934 and EA-913. Adhesive replacement studies performed on various programs at ARC resulted in selecting nonasbestos versions of the above adhesives, designated as EA-934 NA and EA-913 NA. Table 2.5.3 presents a comparison of basic properties between the current and the asbestos-free adhesives.

TABLE 2.5.3. ADHESIVE PROPERTIES.

	EA-934	EA-934 NA	EA-913	EA-913 NA
VISCOSITY (POISE) AT 24°C				
PART A	7500	1760	3000-6500	2000-8000
PART B	30	30	3-6	3-6
TENSILE SHEAR STRENGTH* (MPA)				
24°C	21.3	24.6	30	34
149°C	6.9	10.0	-	-
204°C	5.2	4.6	-	-
POTLIFE (MINUTES) AT 24°C	40	40	480	480

* BONDED TO CHROMIC ACID ETCHED 2024-T3 ALCLAD.

2.6 IGNITER

2.6.1 INTRODUCTION

The primary purpose of the igniter design study was to minimize potential leak paths in the igniter-to-adapter and adapter-to-motor case interfaces. Secondary objectives were to evaluate igniter propellant and ballistic design, evaluate expendable versus reusable hardware, and replace the igniter insulation with an asbestos-free material.

The constraints on this design study were to maintain ignition performance and reproducibility without degrading structural and thermal margins. In order to have a high degree of confidence in any design changes, the database for the design change must exist or be created through a test program.

2.6.2 CURRENT SRM IGNITER DESIGN

The current shuttle igniter design is depicted in Figure 2.6.1. The SRM ignition system is a forward end, internally mounted solid rocket type (pyrogen) igniter and is approximately 44.5 inches long by 20 inches in diameter. The flight grain is a 40-point star configuration approximately 16.9 inches in diameter by 32.8 inches long. The propellant grain consists of approximately 137 pounds of a 10 percent aluminized PBAN propellant and it is cast into a D6AC steel case insulated internally and externally with asbestos and silica-filled NBR. A molded silica phenolic throat insert controls the igniter pressure and directs the igniter plume to the main SRM propellant grain.

The igniter chamber is bolted to the igniter adapter (D6AC steel) with 36 3/4-inch bolts. Each bolt uses a special washer and pressure sealing packing. The main seal between the igniter chamber and the igniter adapter is a dual O-seal gasket. The adapter bolts to the main SRM chamber with 40 5/8-inch bolts utilizing a washer and pressure sealing packing on each bolt. The primary seal between the adapter and the SRM chamber is also a dual O-seal gasket.

The ignition initiator is a small, multinozzled asbestos- and silica-filled NBR insulated steel cased rocket motor containing 1.4 pounds of propellant in a 30-point star configuration. The initiator case and the safety and arming (S&A) device attach to the

ORIGINAL PAGE IS
OF POOR QUALITY

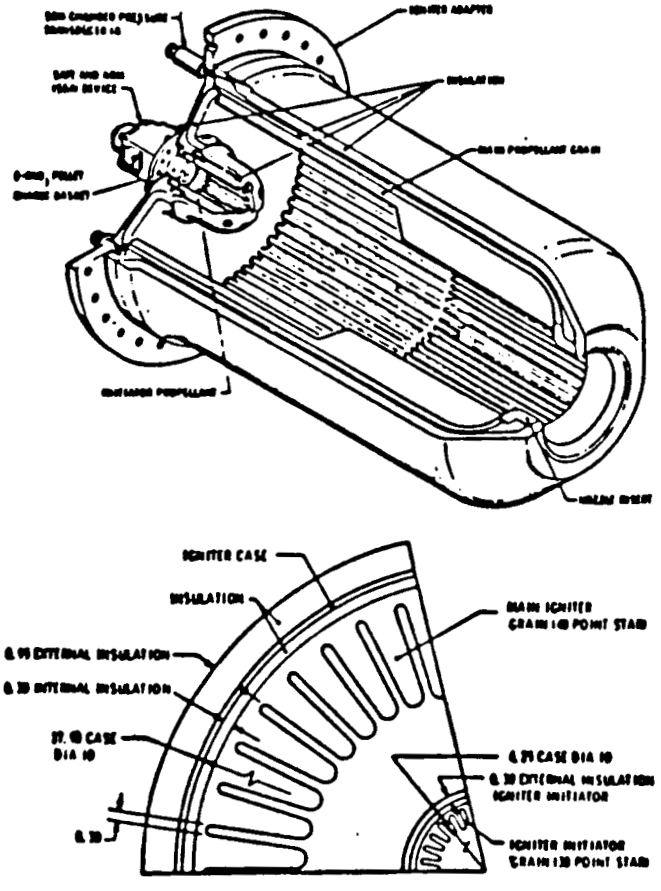

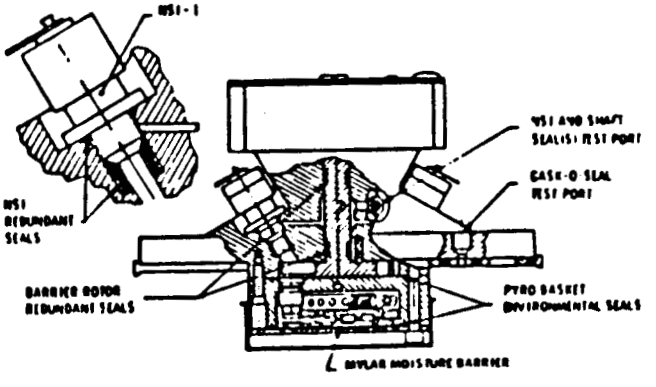

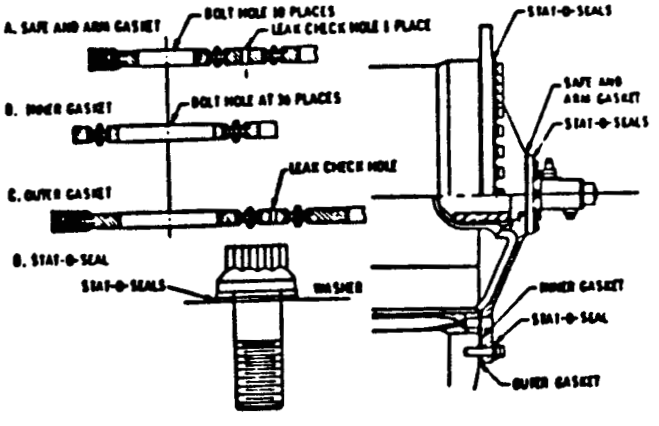

FIGURE 2.6.1. CURRENT IGNITER AND SEALS.

igniter adapter. The S&A is bolted to the adapter using 10 bolts. A dual O-seal gasket forms the dual redundant seals with special packing on each bolt as an environmental seal.

The S&A device consists of a reusable actuating and monitoring (A&M) and an expendable booster-barrier assembly containing a mixture of $BKNO_3$ pellets and granules. Two redundant NASA standard initiators (NSIs) provide positive ignition. The NSIs utilize dual redundant seals and the A&M uses dual O-ring seals on the barrier rotor shaft.

Totaling up the seals in the igniter/S&A, there are 6 primary seals, 42 secondary seals, and 88 environmental seals. The primary seals are the fundamental seals that hold igniter or motor gas pressure while secondary seals would seal against gas pressure only if the primary seals failed. The environmental seals are used for sealing out the environments except for the bolt seals on the bolts that attach the igniter chamber to the igniter adapter. These seals are secondary seals and environmental seals.

2.6.3 IMPROVED SRM IGNITER SYSTEM

The improved SRM igniter is depicted in Figure 2.6.2. This system is a forward end, internally mounted solid rocket type (pyrogen) igniter. The igniter is approximately 19 inches in diameter by 34 inches long, overall. The flight grain is a 40-point star configuration that is 16.4 inches in diameter by 21.6 inches long. The propellant grain consists of 119 pounds of 18 percent aluminized HTPB propellant cast into a 200 maraging steel case with an integral welded igniter adapter and a removable aft closure held in place using 36 high strength 3/4-inch bolts. The case is insulated internally and externally with Kevlar and silica-filled Hypalon. A molded silica phenolic throat insert controls the igniter pressure and directs the igniter plume to the main SRM propellant grain.

The igniter adapter is bolted to the main SRM chamber with 40 5/8-inch bolts that have a washer and an environment seal on each bolt. The primary seal consists of a radially compressed aerospace G-T ring that seals against high pressures with larger clearances than an O-ring. This design is utilized for dynamic rod and piston seals and will not twist under installation. The secondary seal is a resilient metal C-ring mounted as a face seal between the adapter and the main SRM chamber. Metal C-ring seals are

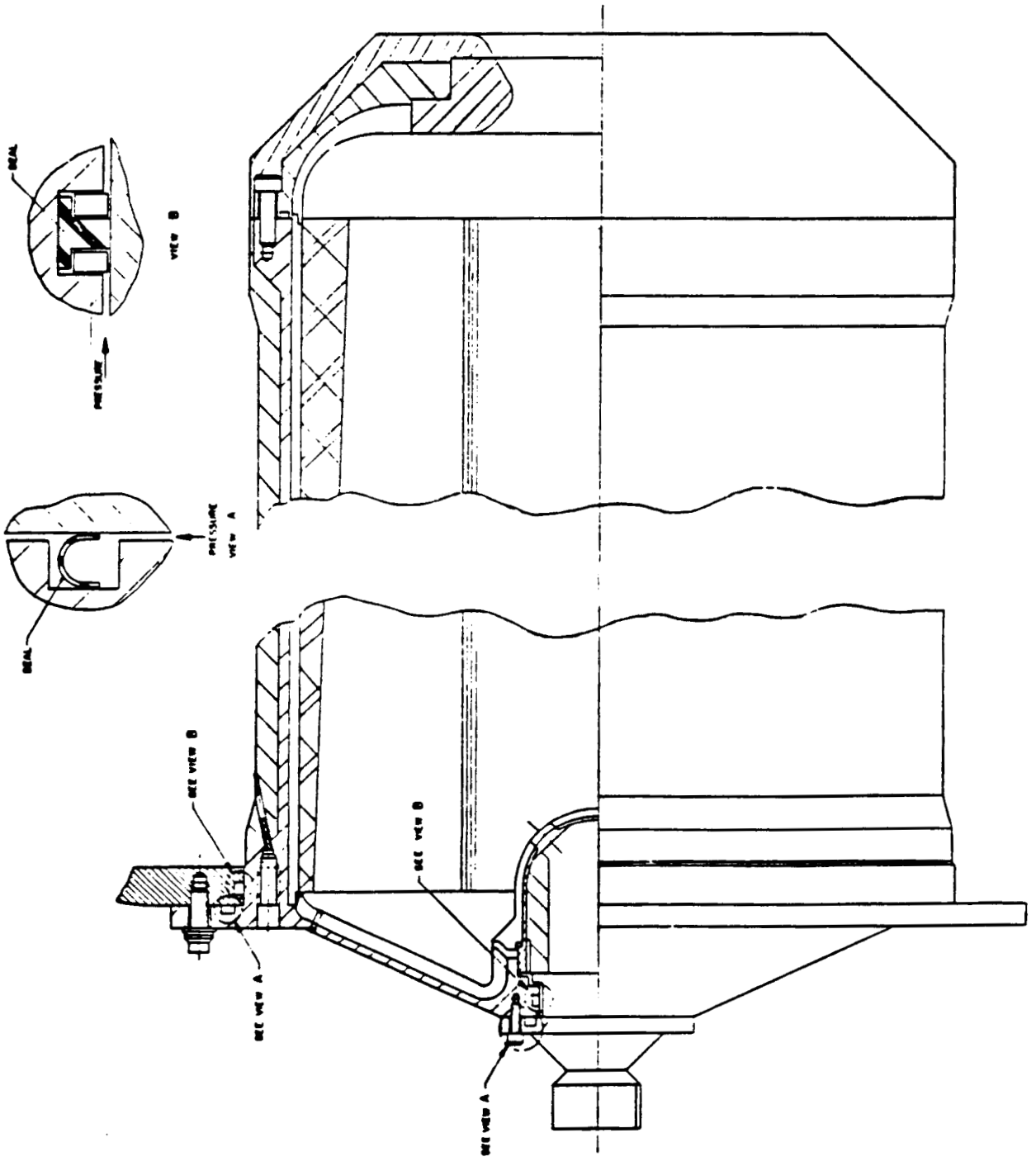

FIGURE 2.6.2. IMPROVED SRM IGNITER.

very high temperature seals (up to 2,000°F) and they are resilient seals that maintain sealing in the event of flange separation caused by thermal or pressure shock or by bolt creep. Both types of seals are also much more compression set resistant than O-rings and have a higher recovery rate than O-rings, allowing them to maintain constant contact with the sealing surfaces as the gap opens.

At the forward end of the igniter, mounted to the igniter adapter, is the ignition initiator. The initiator utilizes the same hardware that is used in the current design but it is loaded with ARCADENE 360A HTPB propellant to maintain compatibility with the main igniter propellant. The grain design is also the same as in the current design since the 360A propellant is tailored to have the same burn rate as the TP1178. The initiator case will be insulated with Kevlar and silica-filled Hypalon to the same thickness that the abestos-silica NBR is applied on the current design.

The S&A device will remain the same as that used on the current design with the asbestos containing parts replaced with nonasbestos materials. The S&A clutch disc material will be replaced with Kevlar phenolic while the S&A commutator material will be replaced with ceramic phenolic.

The S&A is attached to the igniter adapter using 10 bolts with a washer and special packing used as an environmental seal. The S&A is sealed to the adapter using a radially squeezed G-T ring and a face sealing metal C-ring, the same as in the adapter to main SRM case. The dual O-ring seals on the A&M main rotor will remain the same as will the seals on the NSIs. For the external environmental seals, either an O-ring type seal or a formed in-place gasket material (i.e., RTV) can be used on the igniter adapter to SRM case and the S&A to igniter adapter.

Total weight savings for the improved versus the production igniter are approximately 110 pounds. The reduced grain length (32.8 inches vs. 21.6 inches) and the thinner insulation on igniter case account for this weight reduction.

2.6.4 IGNITER PROPELLANT

The igniter propellant selected for the improved igniter is ARCADENE 360A, which is detailed in Table 2.6.1. ARCADENE 360A is an 88 percent solids-loaded HTPB

TABLE 2.6.1. ARCADENE 360A.

INGREDIENT	WT %
R-45 HT BINDER	10.0
DOA	2.0
Al POWDER	18.0
Fe_2O_3	1.5
AP (60/40 200μ/MA)	68.5
	100.0

TOTAL SOLIDS	88%
I°sps	260.7 lbf-sec/lbm
DENSITY	0.0655 lb/cu-in
EQUILIBRIUM T_c	3508°K
C*	5123 ft/sec
E	10.74
GAMMA	1.166
BURNING RATE (1000 PSI)	0.70
PRESSURE EXPONENT	0.48

MECHANICAL PROPERTIES (2 in/min x head)

	70°F	-40°F	+160°F
MAX. STRESS (PSI)	201	514	128
% STRAIN AT MAX. STRESS	30	43	26
TANGENT MODULUS (PSI)	1540	12,100	1010

propellant with a bimodal blend of ammonium perchlorate (AP) and 18 percent aluminum. This propellant is a variant of the MLRS propellant of which ARC has loaded over 28 million pounds into MLRS motors. The higher burn rate necessary for the SRM igniter application is achieved by increasing the percentage of iron oxide (~1 percent vs. 1.5 percent) and by varying the percentage of fine versus course AP in the bimodal blend. This propellant is completely characterized for use through the MLRS Program and represents very low risk in the SRM igniter application. Prior to casting the propellant, the insulated case will be barrier coated with EA-946 and then lined with ARL-151 liner. Both of these materials have been well characterized for use with this propellant in the MLRS Program.

2.6.5 IGNITER GRAIN DESIGN

The igniter grain is shown in Figure 2.6.3 and described in Table 2.6.2. The grain design is a 40-point star design with the web between star points varying from 0.20 inch at the head end to 0.05 inch at the aft end. The star tip radii are 4.90 inches from the igniter centerline. The maximum nominal mass flow rate is approximately 65 percent of the DM-1 igniter firing. The molded cellulose phenolic nozzle has a throat diameter of 6.60 inches and will have a projected 0.030-inch total erosion on the diameter during the igniter firing. Maximum expected operating pressure (MEOP, $+3\sigma$ condition) is projected to be 1,660 psia.

This grain design matches very closely the performance from the current production igniter. Igniter MEOP and mass flow rates compare very favorably with SRM firings QM-1 and QM-2 as shown in Figure 2.6.4. Igniter plume contact with the SRM will therefore match the current production igniter and ignition times for the SRM should remain the same.

2.6.6 IGNITER INSULATION

The improved igniter insulation selected for replacing the current asbestos and silica-filled NBR is Kevlar and silica-filled Hypalon. This selection comes from the extensive trade studies documented in Section 2.4. Preliminary estimates of insulation requirements, based upon reported Material Affected Rates (MARs) for the igniter in QM-2, using a 2.0 MAR safety factor, and reducing the igniter length results in a total igniter assembly insulation weight reduction of approximately 78 pounds. On the

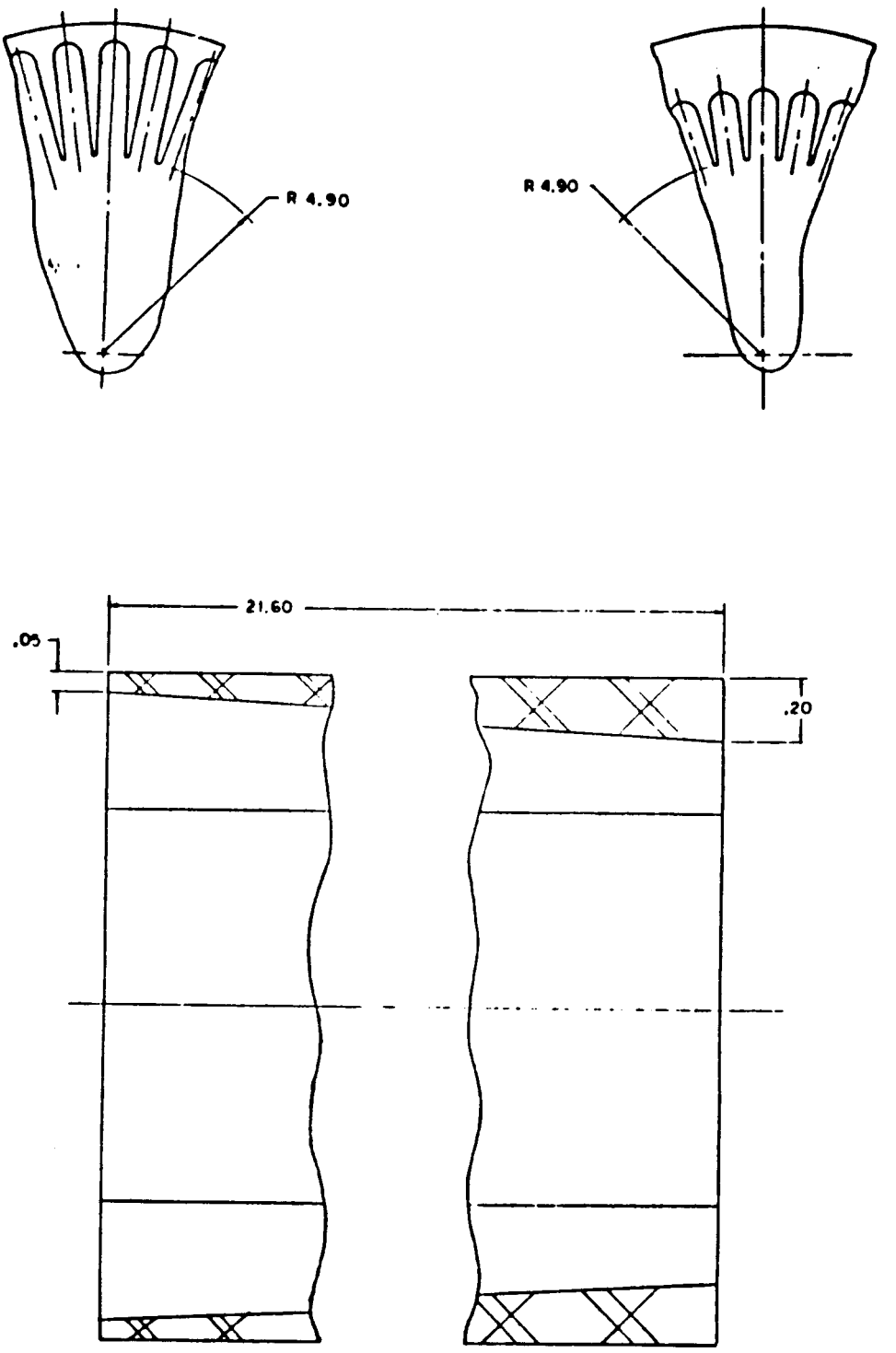

FIGURE 2.6.3. IMPROVED SRM IGNITER GRAIN.

TABLE 2.6.2. SRM IGNITION SYSTEM.

PROPELLANT

- HTPB/AP/Al
- r_{1000} = 0.70 ips @ 60°F

GRAIN CONFIGURATION

- 119 lb. GRAIN WEIGHT
- 40-POINT STAR, 21.6 IN. LONG BY 16.4 IN. OD
- 4.90 IN. RADIUS TO STAR TIPS
- 0.20 IN. TO 0.05 IN. WALL WEB TAPER FORWARD TO AFT

NOZZLE

- CELLULOSE PHENOLIC
  0.030 IN. TOTAL PREDICTED EROSION ON DIAMETER
- 6.60 IN. THROAT DIAMETER

PERFORMANCE

- 323 lbm/s MAXIMUM NOMINAL MASS FLOW RATE
- 1660 PSIA MAXIMUM EXPECTED OPERATING PRESSURE (90°F, $+3\sigma$ CONDITIONS)

ORIGINAL PAGE IS
OF POOR QUALITY

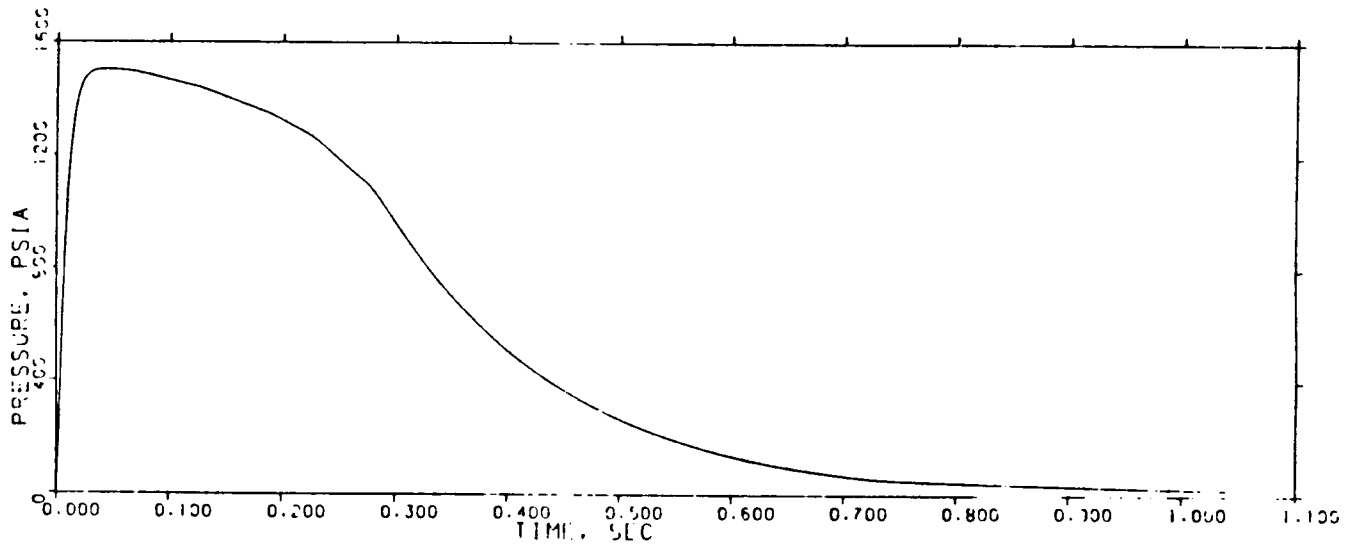

FIGURE 2.6.4. IMPROVED IGNITER PRESSURE TRACE
SRM IGNITER NOMINAL PERFORMANCE @ 60°F.

average, external igniter case insulation is reduced in thickness by 20 percent while the internal case insulation is reduced by 33 percent. The igniter initiator insulation thickness was not changed.

The silica phenolic throat insert will be replaced with a lower cost, higher performance cellulose phenolic. Estimated cost savings of the cellulose versus the silica phenolic are approximately 85 percent for the raw material. The cellulose phenolic is also predicted to have 80 percent of the erosion experienced in the silica phenolic and 15 percent less weight due to a lower density.

These insulation thicknesses keep the igniter hardware below the required 300°F during SRM action time and 400°F following SRM web burnout per specification CPW1-3300.

2.6.7 IGNITER SEALS

The primary objective of this design study is to reduce potential exhaust gas leak paths from the igniter assembly. To achieve that goal, various hardware configuration concepts were examined to reduce the overall number of primary and secondary gas seals. In the current production igniter, there are 6 primary, 42 secondary, and 88 environmental seals as detailed in Table 2.6.3. In the proposed design, the case and adapter will be manufactured from 200 maraging steel and welded together, eliminating all case-to-adapter seals in the production design (Figure 2.6.2). Using this design, the total number of seals is reduced to 5 primary, 5 secondary, and 52 environmental. This provides a delta of 1 primary seal and 37 secondary seals. The secondary seals are drastically reduced due to the elimination of the bolts and the special bolt packing (stato-seals) in the igniter case to adapter joint.

A trade study was conducted to determine what type or types of primary and secondary seals to utilize in the improved igniter design. The trade study is presented in Table 2.6.4. The primary seals selected for use on the igniter adapter to SRM case and the S&A-to-igniter adapter are aerospace G-T rings. These rings are radial squeeze seals and are commonly used to seal hydraulic fluid up to 8,000 psi. These seals are very resistant to extrusion due built-in nonextrusion rings, provide a positive seal at zero or low pressures due to radial compression at installation, and are not subject to rolling or spiral failures. These G-T ring seals permit sealing with larger gaps than O-rings under

TABLE 2.6.3. IGNITER ASSEMBLY SEALS.

	PRESENT IGNITER			IMPROVED IGNITER		
	PRIMARY	SECONDARY	ENVIRONMENTAL	PRIMARY	SECONDARY	ENVIRONMENTAL
S&A						
• BARRIER-BOOSTER SHAFT	1	1	0	1	1	0
• NSIs	2	2	0	2	2	0
S&A TO IGNITER ADAPTER	1	1	11	1	1	11
IGNITER ADAPTER‡ TO IGNITER CASE	1	37•	37••	-	-	-
IGNITER ADAPTER TO SRM CASE	1	1	40	1	1	41
TOTALS	6	42	88	5	5	52

• 36 OF THESE 37 SEALS FUNCTION AS SECONDARY AND ENVIRONMENTAL SEAL

•• INCLUDES 36 SEALS LISTED AS SECONDARY

‡ DOES NOT INCLUDE PRESSURE TRANSDUCER SEALS

TABLE 2.6.4. SEAL TRADE STUDY.

	O-RING		C-RING, METAL	STATIC FACE SEAL	FLEX METAL GASKET	G-T RING	LATHE CUT SEAL RING	GASK-O-SEAL
	RUBBER	METAL						
RESILIENCE (SPRINGBACK)	7	8	10	8	9	8	7	7
COMPRESSION SET RESISTANCE	5	10	10	7	9	7	7	5
TOUGHNESS (DAMAGE TOLERANCE)	7	4	5	8	7	8	8	7
RELAXATION MODULES	5	8	8	5	7	5	5	5
HIGH TEMPERATURE TOLERANCE	4	10	10	4	8	4	4	4
GAP SEALING CAPABILITY	5	7	10	9	4	9	6	5
MATING SURFACE FINISH/MACHINING	8	6	6	8	2	8	8	8
EXTRUSION RESISTANCE	5	10	10	8	9	8	7	6
TOTALS	46	63	69	57	55	57	52	47

RATED 1 THROUGH 10, WITH 10 HIGHEST

expansion of a pressure vessel as it is pressurized. Aerospace G-T rings are also designed to fit any groove defined in specification MIL-G-5514F. Rubber compounds allow temperature coverage from -70°F to +450°F.

The secondary seals for the igniter adapter to SRM case and the S&A-to-igniter adapter are resilient metal C-rings. These rings will seal up to 9,800 psi in a gland with a 32 RMS finish and can handle temperatures from cryogenic to 2,200°F. A metal C-ring seals at low and no pressure due to compression from the flange joint. System pressure then supplements the sealing force by forcing the walls of the ring against its mating surfaces.

Both the G-T ring and metal C-ring seals are more compression set resistant than standard O-rings due to their basic designs. In dynamic loading situations where the gap between mating sealing surfaces tends to open, their resiliency assures that they will maintain contact with the sealing surfaces. By separating the seals into radial and face seals with different temperature capabilities for each, we are assured that no credible single event can cause a failure of both the primary and the secondary seal.

The aft closure will be sealed with a single static face seal that is similar in design to the G-T rings described above. It consists of an "L" shaped elastomeric sealing element and a mating nonextrusion ring. At low or zero pressure, the static face seal (SFS) seals like an O-ring. A pressure increase causes the elastomer to seal more tightly while the nonextrusion ring precludes extrusion. SFSs can seal with clearance gaps up to 0.015 inch and to pressures exceeding 10,000 psi. A single seal is utilized due to the fact that any leakage here would be into the SRM main chamber and should not compromise ignition (assuming leakage is not gross).

2.6.8 SUMMARY

The proposed igniter design utilizes a one-piece case/igniter adapter made from 200 maraging steel that is insulated internally and externally with Kevlar and silica-filled Hypalon. An aft closure bolts to the case and allows grain casting and mandrel pulling from the aft end of the igniter. An HTPB propellant, ARCADENE 360A, a variant on our well characterized MLRS propellant, will be utilized for the propellant grain. A combination of elastomeric and metal seal rings will be utilized to provide the minimum number of primary and secondary seals while providing superior sealing under all operating conditions of the SRMs.

3.0 PERFORMANCE

The selection of the heads-up trajectory as the baseline for the Block II SRM configuration results in an increase of the head-end maximum expected operating pressure (MEOP) to 1,085 psia from 1,015 psia. The increase in pressure was required to produce the higher thrust level dictated by the heads-up trajectory and is discussed in detail in Section 3.1. The higher MEOP requires increasing the basic case wall thickness, resulting in an increase of motor case weight. The 6.9 percent increase in MEOP requires an additional 0.032 inch of basic case wall.

The increase in case wall thickness is more than offset by the reduced insulation thickness of the Block II asbestos-free configuration. In fact, the average 0.054-inch reduction of insulation thickness allows an average net 0.022-inch increase of the propellant grains' outer diameter. Table 3.0.1 presents the change in propellant and inert weights for the heads-up Block II SRM compared to the current high performance motor (HPM) SRM.

The impact of changes in inert weight and propellant weight on payload capability are given by the following partials:

Inert Weight:	0.0182 lbm/lbm
Propellant Weight:	0.083 lbm/lbm

Therefore, the 2,727-lbm increase in SRM inert weight will cause a 496-lbm reduction in payload capability. Also, the propellant weight reduction of 1,669 lbm will cause a payload capability reduction of 139 lbm. Therefore, the total change in payload capability resulting from the Block II improvements is a reduction of 635 lbm.

It must be emphasized that the 635-lbm decrease does not include the basic advantage of flying the heads-up trajectory rather than the current one. While ARC has not been supplied with a value, it is likely that the payload increase associated with the heads-up trajectory will more than offset the 635-lbm reduction.

TABLE 3.0.1. HEADS-UP BLOCK II WEIGHT SUMMARY.

LOWER DENSITY ASBESTOS-FREE INSULATION	- 4,333
IMPROVED LARC FIELD JOINT (NO FACTORY JOINT)	+ 260
CASE THICKNESS INCREASE OF 0.032 INCH	+ 6,800
NET SRM INERT WEIGHT CHANGE	+ 2,727
PROPELLANT WEIGHT LOST TO IMPROVED JOINT CONFIGURATION	- 2,560
PROPELLANT WEIGHT GAINED ON SEGMENT ODS (+ 0.054 - 0.032 = + 0.022 INCH)	+ 891
NET SRM PROPELLANT WEIGHT CHANGE	- 1,669

3.1 MOTOR BALLISTIC PERFORMANCE

Included as one of the design study areas was an investigation into the SRM modifications necessary to produce the heads-up thrust history. The required nominal burning rate thrust history bandwidth at 60°F was presented in Enclosure 22 of a letter from Larry Wear, "Responses to Block II SRM Requests." Simply stated, the heads-up thrust history requires a 10-percent increase in thrust level with a reduction in burning time to produce the total impulse required by Specification No. CPW1-3300. Figure 3.1.1 presents the required thrust band presented in CPW1-3300, while Figure 3.1.2 presents the heads-up thrust requirement.

Before heads-up modifications were investigated, a simple ballistic prediction model was established for the current HPM. Figure 3.1.3 presents the baseline predicted thrust, which agrees well with the required bandwidth. Figure 3.1.4 compares the predicted pressure history with the nominal HPM curve. This simple prediction model does not include erosive burning behavior. This accounts for the low predicted pressure over the initial 15 seconds and the higher level during the 85- to 105-second time span. The predicted delivered vacuum specific impulse is 267.19 lbf-s/lbm.

Four different design parameters were investigated in an effort to produce the heads-up thrust history with minimum impact on the existing design. Combinations of propellant burning rate, propellant formulation, nozzle throat geometry, and propellant burning surface area versus web distance were studied. A number of different approaches were identified to produce the heads-up thrust history. Each approach also has a negative impact to some extent. For each approach, the impact of payload was calculated, and SRM components were identified that would be impacted by the approach. Table 3.1.1 summarizes the impact of the approaches that will be discussed.

The first approach investigated was to merely increase the burning rate of the current propellant. This can be accomplished by adjusting the amount of iron oxide (Fe_2O_3) and/or the ground-to-unground ratio of ammonium perchlorate (AP). The required base burning rate at 625 psia and 60°F was determined to be 0.386 in/s compared to the current 0.362 in/s baseline. Figure 3.1.5 presents the predicted thrust history based on a burning rate of 0.386 in/s.

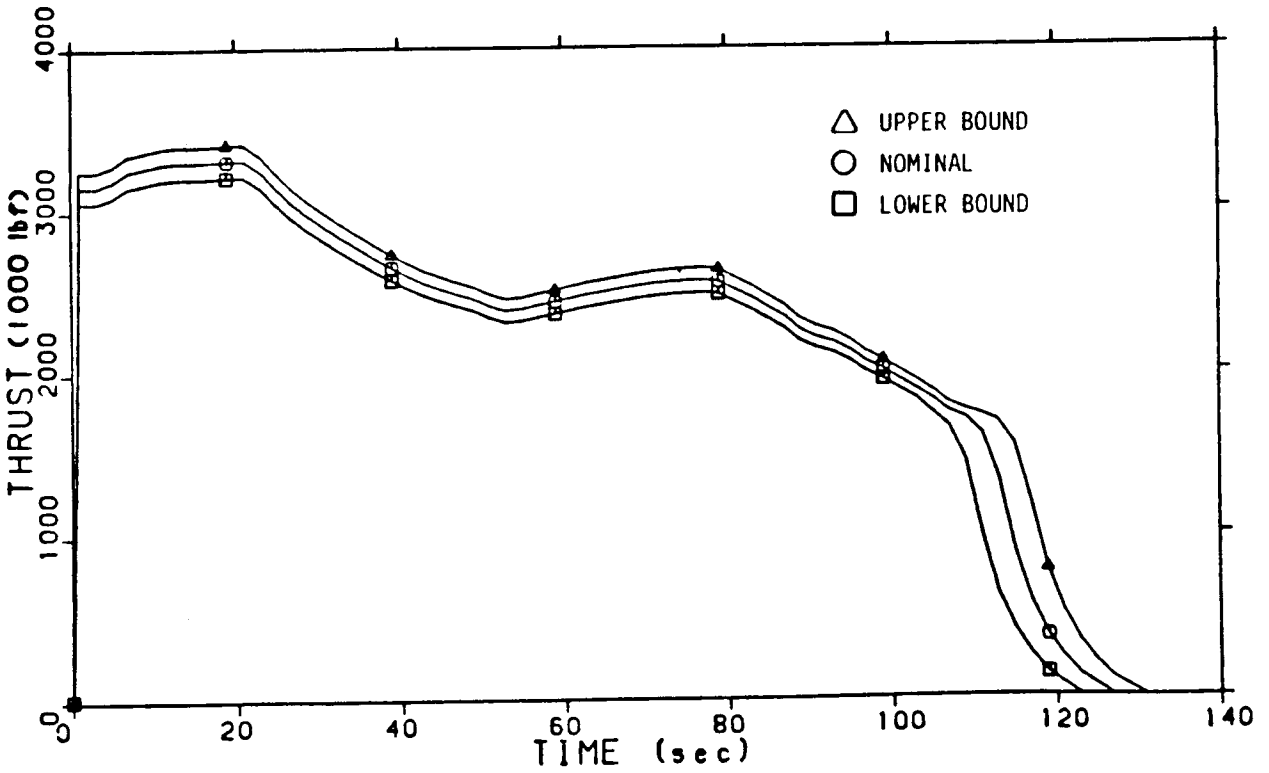

FIGURE 3.1.1. SPECIFICATION NO. CPW1-3300 REQUIRED THRUST BAND.

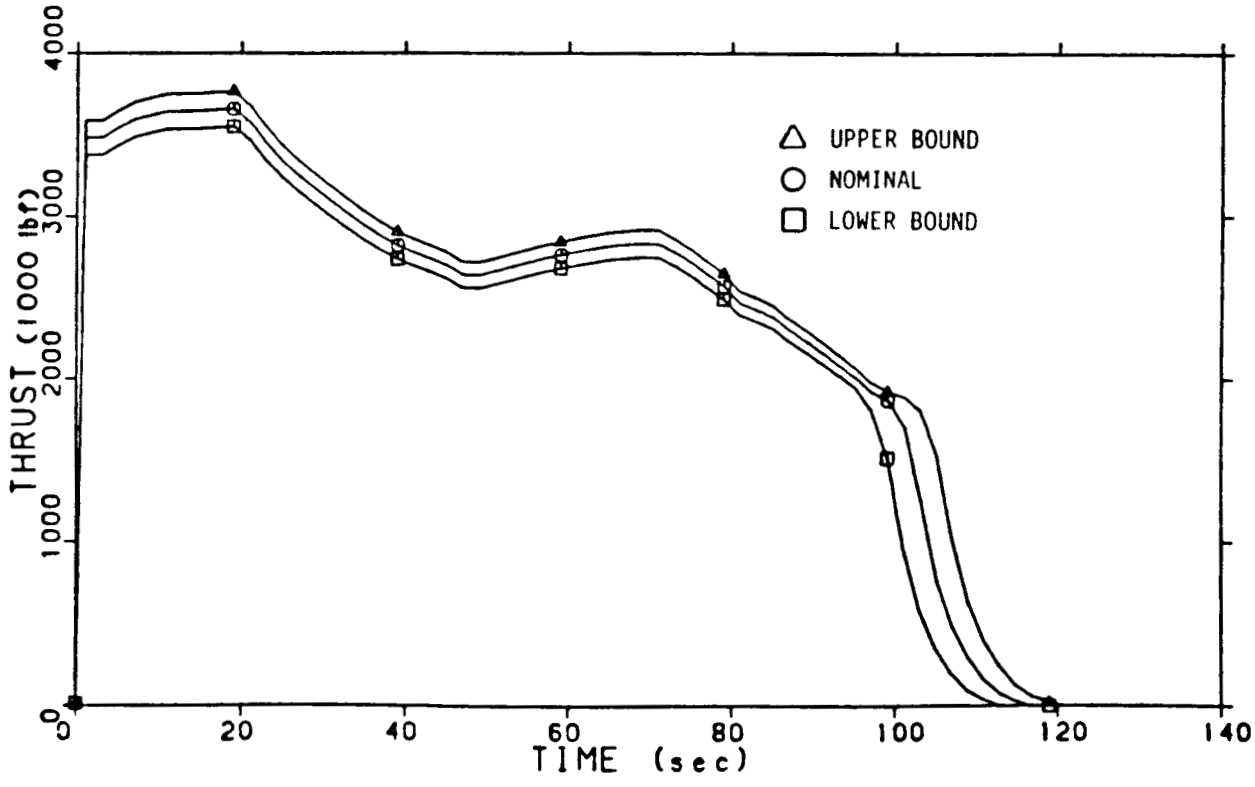

FIGURE 3.1.2. REQUIRED "HEADS-UP TRAJECTORY" THRUST BAND.

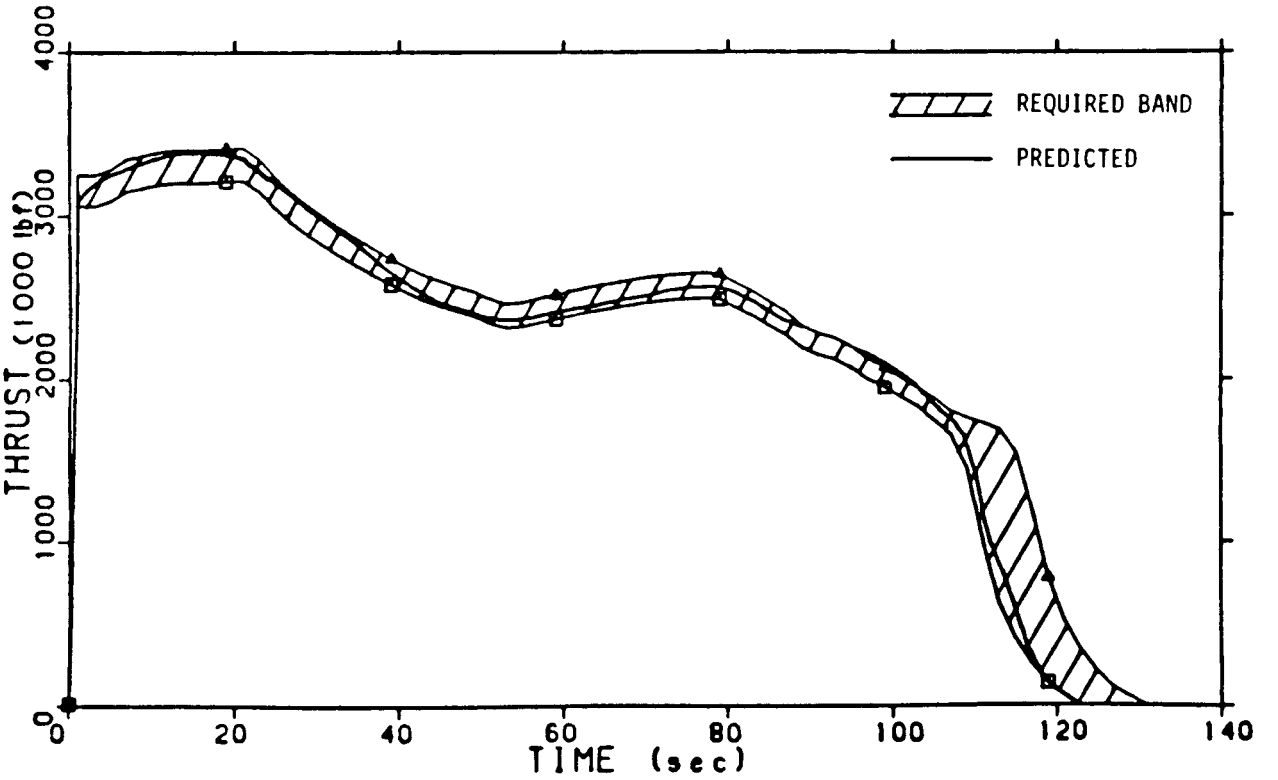

FIGURE 3.1.3. PREDICTED NOMINAL HPM THRUST HISTORY AT 60°F.

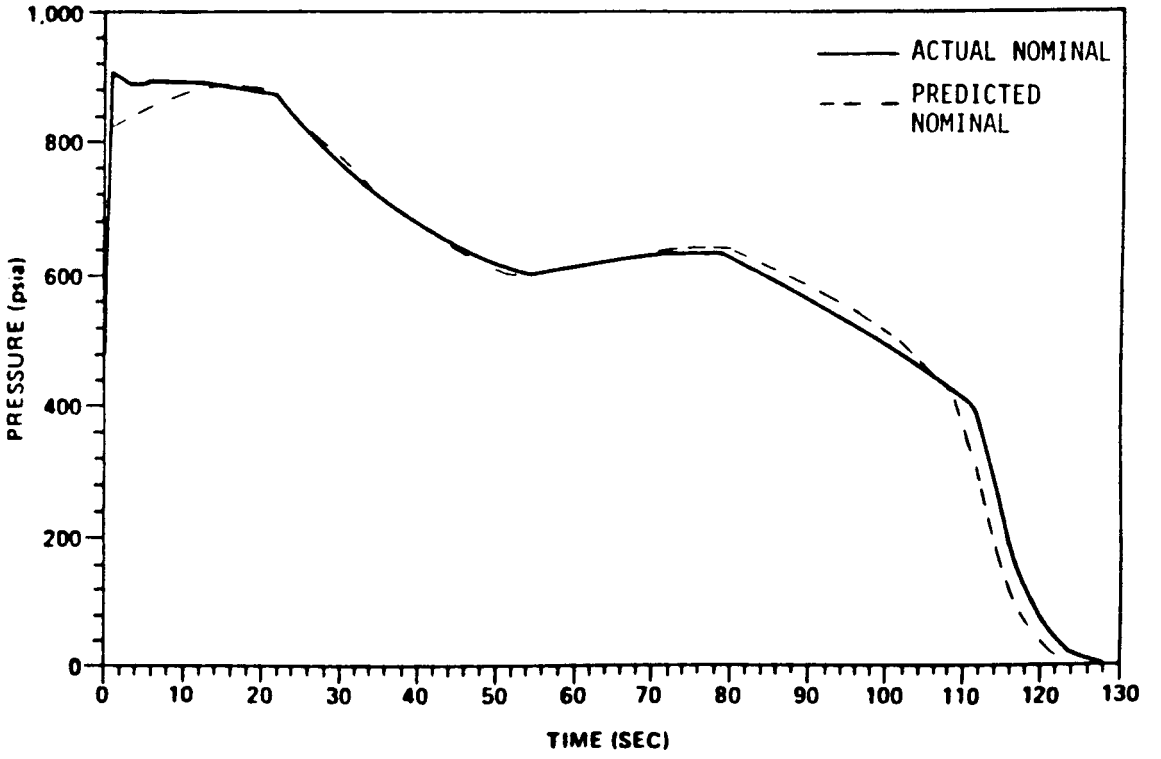

FIGURE 3.1.4. PREDICTED NOMINAL HPM THRUST PRESSURE HISTORY AT 60°F.

TABLE 3.1.1. SUMMARY OF HEADS-UP THRUST MODIFICATIONS.

	APPROACH			
	1	2	3	4
REQUIRED BURNING RATE, in/s	0.386	0.399	0.362	0.378
NOZZLE DIAMETER, in	53.86	56.49	51.00	53.86
MEOP, psia	1,120	1,015	1,215	1,120
PAYLOAD IMPACT W/D6AC CASE THICKNESS INCREASE, lbm	-1,800	-1,560	- 887	- 40
PAYLOAD IMPACT W/HIGHER STRENGTH STEEL @ CURRENT THICKNESS, lbm	0	-1,560	+2,576	+1,840
COMPONENT DEVELOPMENT/ REDESIGN REQUIRED*	NONE	NOZZLE STRUCTURE AND FLEX-BEARING	20% MEOP INCREASE LIKELY HIGH ENOUGH TO REQUIRE COMPLETE REDESIGN	HT PROPELLANT DEVELOPMENT

* ASSUMES CURRENT PBAN CAN BE TAILORED TO REQUIRED RATE.

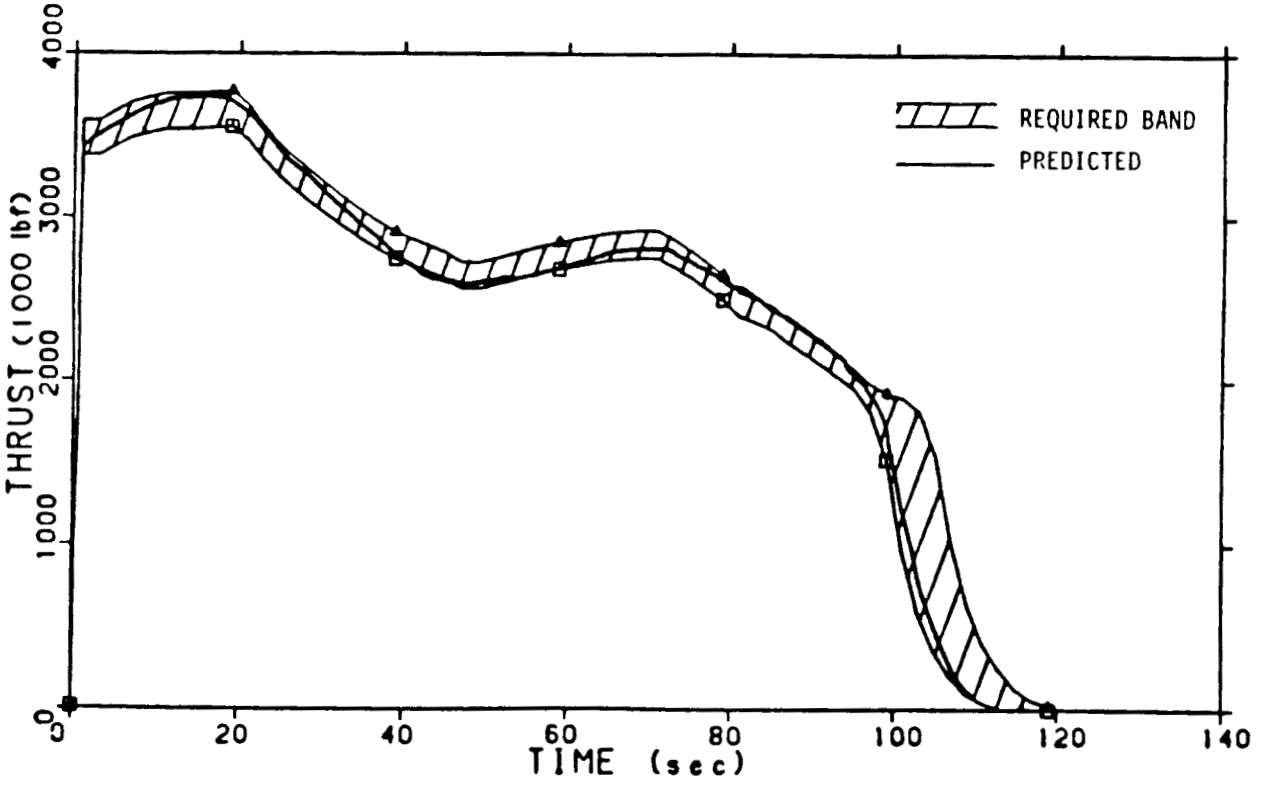

FIGURE 3.1.5. PREDICTED HEADS-UP THRUST HISTORY AT 60°F AND r_b = 0.386 IN/S.

While the required thrust band is achieved, this approach would increase maximum expected operating pressure (MEOP) to approximately 1,120 psia. The increase in MEOP would prohibit use of existing hardware. The required increase in case wall thickness using D6AC steel would result in an approximate 1,800-lbm payload capability loss. This approach will involve no additional redesign or development beyond the concept currently proposed for the Block II SRM.

The second approach also involved an increase in burning rate, but nozzle throat area was also increased to retain MEOP at its current level. The required burning rate and initial throat diameter were determined to be 0.399 in/s and 56.490 inches, respectively. Other minor nozzle modifications would include reoptimization of the nozzle exit cone contour and use of a carbon phenolic material with a 15 percent lower nozzle erosion rate.

While satisfying, in general, the required thrust band, the resulting delivered specific impulse is reduced to 265.24 lbf-s/lbm from the current 267.19. The loss of 1.95 lbf-s/lbm delivered specific impulse results in a payload reduction of 1,560 lbm. Also, the increase in nozzle throat diameter is sufficiently large to require the redesign of the metal backup structure of the nozzle.

The third approach investigated was a nozzle throat diameter reduction. Like the first approach, this method will increase MEOP. However, the nozzle diameter reduction will increase the delivered specific impulse. Also, the reduction will structurally allow the use of carbon/carbon as the nozzle throat material (lower erosion rate) within the envelope of the existing metal parts. The nozzle diameter required for this approach is 51.0 inches.

Again, the desired thrust band is achieved. MEOP is 1,215 psia, but the delivered specific impulse is increased to 270.41 lbf-s/lbm. The delivered I_{sp} and increased inert weight trade to yield a 887-lbm decrease in payload. It is likely that such a great increase in MEOP will cause other components besides the case wall to increase in weight. Therefore, the payload capability would likely decrease somewhat below the number just presented.

The fourth approach considered was the use of a higher energy and density HTPB propellant. The HTPB propellant will also likely have a pressure exponent that is

somewhat higher than that of the PBAN propellant. This approach will require tailoring of the burning surface area versus web history such that the maximum burning surface area and the minimum surface area are closer to the web averaged mean. The required burning rate for the HTPB propellant would be 0.378 in/s at 625 psia and 60°F.

Again, this option results in raising MEOP to approximately 1,120 psia. The increased case wall thickness would result in a net 40-lbm payload increase. The increased wall thickness is offset by a 0.6-lbf-s/lbm increase in theoretical specific impulse and 20,800 lbm of extra propellant due to the higher propellant density. Also included is a 2,000-lbm increase in the insulation required for HTPB propellant use.

In addition to the four specific options discussed, a great number of other specific combinations of the four parameters exist. It is clear, however, that the current nozzle flex-bearing support structure cannot accommodate the increase in nozzle throat diameter (56.49 inches) required to maintain MEOP at its current level. Therefore, if the Block II SRM is to produce the heads-up thrust history, some increase in MEOP will result.

Based on the Block II SRM design studies to date, the best way to achieve the heads-up trajectory is the first approach (raise burning rate and maintain nozzle throat diameter). This is largely based on the minimum amount of additional development or redesign associated with this approach. Also, several factors can reduce the projected MEOP (at 90°F) increase from 1,015 psia to 1,120 psia associated with the selected option.

The MEOP of the current HPM configuration is driven by the erosive burning pressure spike that occurs on ignition. The pressure overshoot decays exponentially over the first 10 seconds of burning. The observed maximum pressure of the current HPM SRM is 30 to 40 psia higher than the maximum pressure that would result if there were no erosive burning. Therefore, reducing the burning surface area over the initial 10 seconds to compensate for the erosive burning will allow an MEOP reduction of approximately 35 psia. Applying this reduction to the earlier stated MEOP of the selected heads-up design approach (increase burning rate) reduces the MEOP of the proposed heads-up trajectory configuration to 1,085 psia. This is a 6.9-percent increase over the 1,015 psia MEOP of the current HPM SRM.

The reduction of the initial burning surface area during the first 10 seconds is achieved by modifying the inhibitor pattern on the aft face of the two center segments. The amount of inhibited surface required to reduce initial pressure by 35 psia is approximately 10,000 in^2 of burning surface area. The modified inhibitor pattern is shown in Figure 3.1.6. The width of the inhibitor projections is 8 inches, which is equal to twice the web distance burned at 10 seconds. Over the burning period of 10 to 20 seconds, the burning surface area closely matches that of the current grain configuration. Figure 3.1.7 compares the total burning surface area produced by the original and modified grain face inhibitor configurations.

The predicted ballistic performance produced by the heads-up modifications (burning rate and grain inhibition) is presented in Table 3.1.2.

ORIGINAL PAGE IS
OF POOR QUALITY

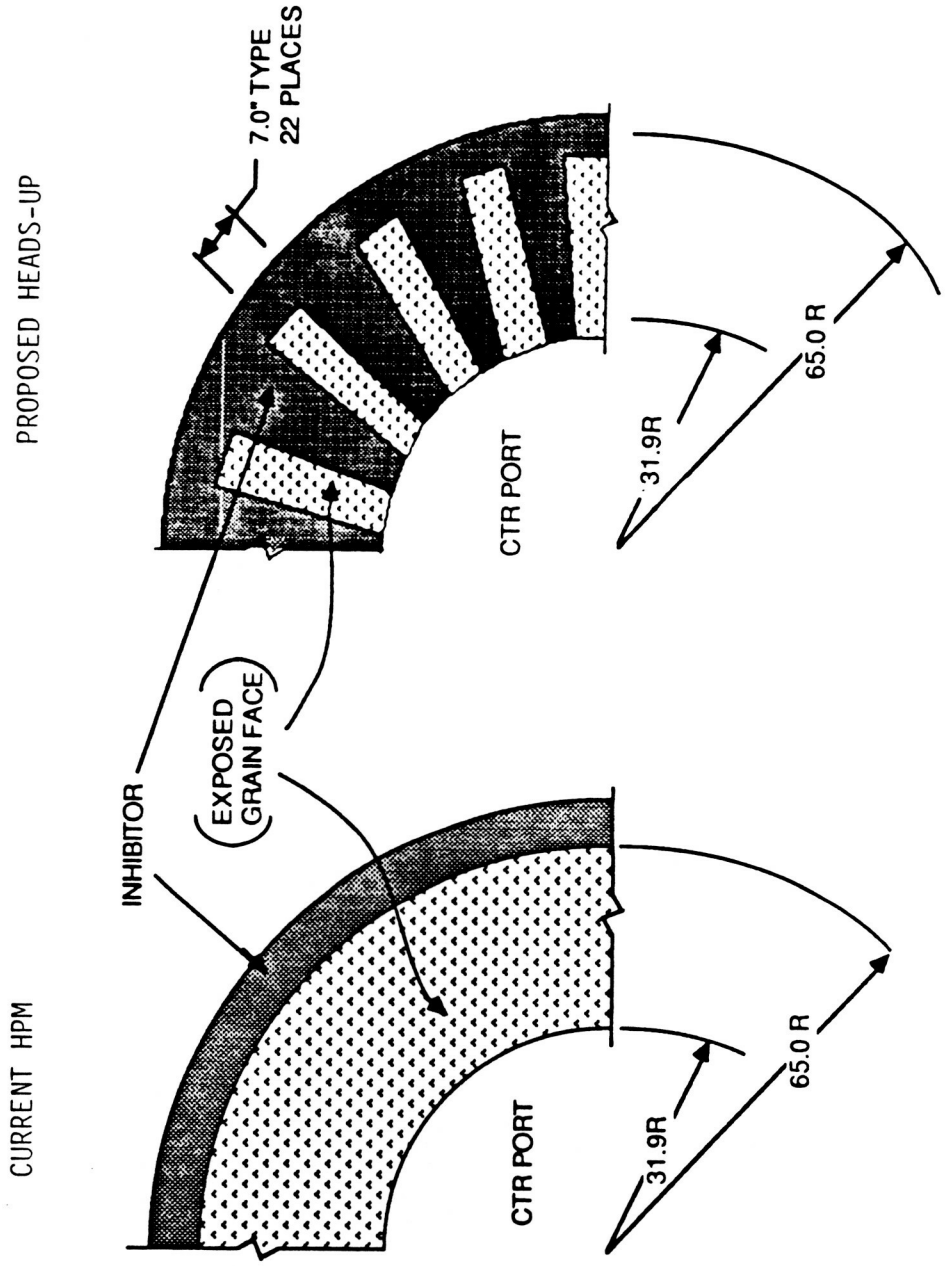

FIGURE 3.1.6. CENTER SEGMENT AFT INHIBITOR.

ORIGINAL PAGE IS
OF POOR QUALITY

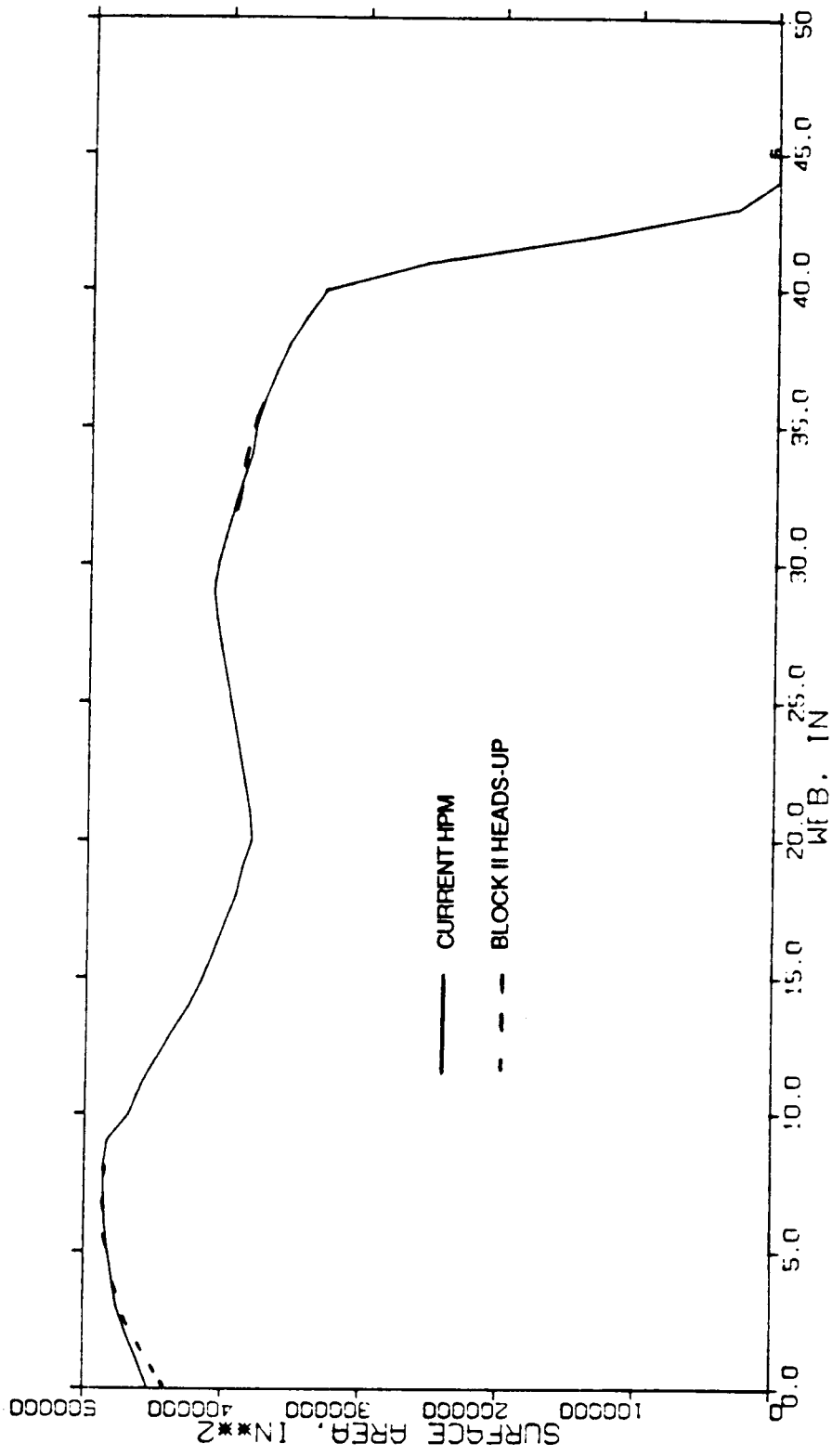

FIGURE 3.1.7. BASELINE SRM 3D GRAIN CONFIGURATION MODEL.

TABLE 3.1.2. PERFORMANCE TOLERANCES AND LIMITS.

Parameter	Individual Motor Performance *			Matched-Pair Performance
	Nominal	Tolerances (%)	Limits	Max. Difference (%)
Web time (sec)	98.5	±5.0	93.8 - 103.4	2.0
Action time (sec)	109.7	±6.5	103.0 - 116.8	3.0
Web time avg pressure (psia)	744.8	±5.3	707.3 - 784.3	2.0
Max. head end pressure (psia)	977.8	±6.5	918.1 - 1041.4	N/A
Max. sea level thrust (Mlbf)	3.75	±6.2	3.52 - 3.98	N/A
Web time avg vac thrust (Mlbf)	2.91	±5.3	2.76 - 3.06	2.0
Vacuum delivered specific impulse (lbf-sec/lbm)	267.2	±0.7	265.3 - 269.0	1.0
Web time vac total impulse (Mlbf-sec)	285.5	±1.0	282.7 - 288.4	1.4
Action time vac total impulse	295.3	±1.0	292.4 - 298.3	1.4

* Based on a PMBT of 60°F.

3.2 JOINTS AND SEALS

The heads up mission internal MEOP has been determined to be 1,073 psig at the forward end of the SRM. Following the calculations of Section 2.3.1.5, the minimum membrane wall will increase

$$t_{min} = 0.459 \left(\frac{1073}{1004}\right)$$

$$= 0.491 \text{ inch.}$$

The corresponding nominal membrane wall thickness will be 0.511 inch.

The impact of the higher operating pressure on the metal case joint is expected to be minimal. The critical safety factors per Section 2.3 were large enough to accommodate the 1.069 increase in loading. Therefore, no change in metal thickness or bolting is anticipated. Similarly, no change in the joint insulation arrangement or thickness will be required.

The primary impact on the nozzle-to-case joint for the heads-up trajectory is due to the revised loads caused by motor design changes made to meet the new performance requirements. Chamber pressure in the joint region increases by approximately 6.9 percent to 972 psig. The nozzle blow-off load actually decreases slightly to 1.14 x 10^6 pounds. The reduction is due to a 10-percent increase in thrust, which offsets the pressure load. Joint deflections and stresses are a function of both the reduced blow-off load, which is reacted by the bolted interface, and the increased pressure acting on the motor aft dome and nozzle fixed housing. A comprehensive analysis is required to evaluate accurately the impact of this combination. However, since a complete reanalysis of the structure was not possible, a conservative approach was used that assumed all loads increased by 6.9 percent. A review of the margins of safety previously shown in Figures 2.3.31 and 2.3.38 for the joint hardware and insulation, respectively, shows that all critical margins exceed 0.069 and, therefore, the current design has adequate strength to carry the increased load. The revised minimum margins would be +0.09 for the hardware and +0.46 for the insulation. To evaluate the seal function, the gap versus pressure data reported in Section 2.3 was extended to 972 psig. This is included as Figure 3.2.1, which shows the maximum gap at the primary seal would be 0.0063. When multiplied by two and compared to the conservative "springback" of 0.012 inch recommended by the seal manufacturer, a negative margin of safety results, indicating that some redesign is

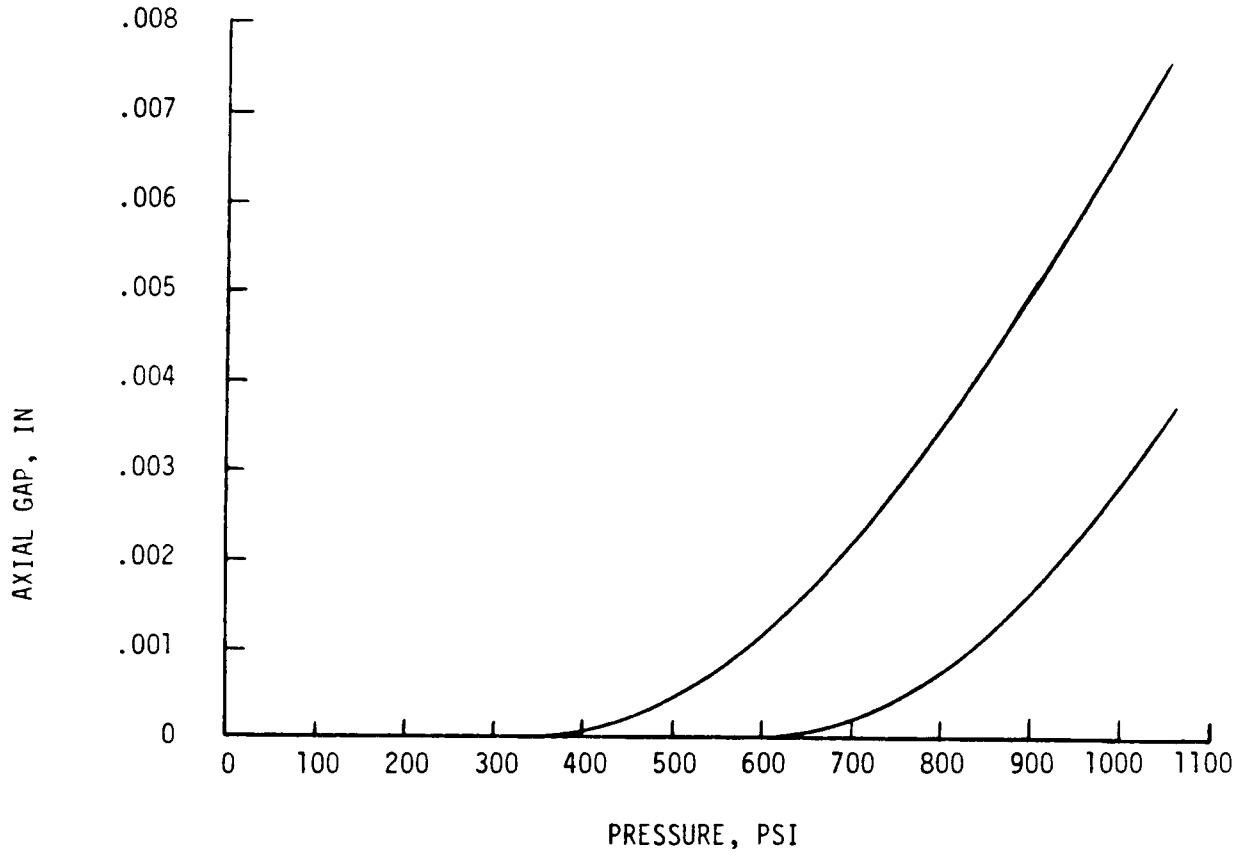

FIGURE 3.2.1. SEAL GAPS VERSUS EXTENDED MOTOR PRESSURE.

required. The design changes that could be investigated would include increasing the bolt pre-load or size, increasing the primary seal size, and increasing the nozzle flange thickness. It is not possible to determine which of these approaches would provide the optimum design; however, we believe the weight impact would certainly be less than that incurred in going from the 51-L design to the current design for the HPM.

3.3 ASBESTOS-FREE INSULATION

The thermal analyses described in Section 2.4 used the current HPM ballistics in determining boundary conditions and burn times. This approach was necessary so that a direct comparison to the available data and predictions for the HPM design with asbestos insulation could be made. To assess the impact of the heads-up trajectory on the nonasbestos insulation, select analyses were rerun using the appropriate ballistics. The higher operating pressure for this heads-up design will increase the amount of insulation degradation while the shortened burn time will decrease insulation degradation. The shortened burntime dominates and the net result is analytically predicted to be a 4.3-percent decrease in degraded insulation thickness.

An assessment of the thermal impact of the heads-up trajectory was also performed on the nozzle throat. Ablation analyses were performed at the throat location to predict the erosion, char, and resulting safety factors for both the current HPM and the heads-up ballistics. The results show that the heads-up trajectory will have a 14.4-percent decrease in throat erosion and a 3.8-percent increase in char thickness. These predictions combine to yield a 10-percent increase in the safety factor at the throat for the heads-up design when compared to the HPM design.

3.4 NOZZLE DESIGN

The motor design changes required to meet the heads-up trajectory performance requirements impact the nozzle design in terms of both thermal response and structural integrity. The effects of increased mass flow and revised burntime on liner erosion and insulation requirements are discussed in Section 3.3 of this report. Similarly, the nozzle-to-case joint region is considered in Section 3.2. The remaining nozzle structural impacts resulting from motor changes are discussed below.

The increases in MEOP and thrust required to meet the heads-up requirements result in revised loading on the nozzle shell structure and on the flex bearing. Since the basic nozzle concept was retained in the Block II SRM design, no significant stress analysis was conducted as part of this program. Attempts to obtain the documented stress analysis for the current design were unsuccessful. Therefore, only a qualitative evaluation of design impacts due to this load increase was possible. In those places in the nozzle shell that are critical for internal pressure, either motor pressure or the correspondingly increased nozzle internal pressure profile, the stresses will be increased by approximately 6.9 percent. Discussions with NASA personnel indicate that some areas of the nozzle are not adequate for this increase; therefore, increases in material thicknesses would be required. The weight impact of this increase is expected to be less than 6.9 percent of the nozzle structural weight, since not all areas require increases.

In those areas of the nozzle assembly critical for blow-off loads, including the flex bearing, loads will vary somewhat less than 6.9 percent. This is because the thrust increases more than MEOP; thus, blow-off loads that are pressure loads minus thrust load increase less than pressure loading by itself. In addition to reviewing structural adequacy for this load, a clearance check for deformed structure should be conducted. In summary, the changes in nozzle structure are expected to include only local thickness increases with the resulting weight increase.

3.5 IGNITER

The improved Block II SRM igniter performance was discussed in Section 2.6.5. The igniter was designed to duplicate the performance of the current production igniter, thereby having no impact on the overall motor performance. The igniter propellant, discussed in Section 2.6.4, is a well characterized version of ARCADENE 360A, an HTPB, 88 percent solids-loaded composite propellant. This propellant is a variant of the MLRS propellant of which ARC has loaded over 28 million pounds into MLRS motors.

Based on the above, the ballistic performance of the igniter represents very low risk to the SRM Block II Program.

4.0 PRELIMINARY DEVELOPMENT AND VERIFICATION PLAN

4.1 DESCRIPTION

The Space Shuttle Block II SRM is used as a major subsystem of the solid rocket booster (SRB) for the shuttle vehicle. The shuttle vehicle booster will consist of two SRBs, each of which will use a solid rocket motor. The two SRMs will operate in parallel with the main engines, provide impulse, and enable thrust vector control to propel and control the space shuttle vehicle from lift-off to SRB staging. The SRM will consist of a lined, insulated, segmented rocket motor case loaded with solid propellant; an ignition system complete with an electromechanical safe and arm device, initiators, and igniter assembly; a moveable nozzle; an exit cone with a linear-shaped charge for severance and a nozzle plug; instrumentation; and integration hardware including electrical brackets, systems tunnel base, grounding provisions, stiffener rings, and attachment provisions to the forward and aft SRB skirts and the SRB/external tank (ET) attachment ring.

The four SRM casting segments are comprised of six case segments. The bolted joint configuration will be integrated into all case segment field joints. The forward and aft closure and SRM skirt attachment joints will retain the existing tang and clevis joint concept. Closures will be assembled to case segments with factory joints. The Block II case segments, roll formed from D6AC steel into case lengths equal to casting segments, will retain the weld-free concept of the Block I motors. The same TPH-1148 propellant will be used. However, design improvements to the insulation/inhibitor system at the field case joints will be incorporated. All materials will be asbestos-free.

The ARC Block II SRM will be a highly reliable motor that permits expeditious assembly and maximum visibility of joint integrity during SRM stacking at the launch facility.

4.2 OBJECTIVE AND SUMMARY

This Program Plan describes how ARC proposes to develop and verify the Block II SRM using the NASALaRC/ARC-designed bolted joint protected by an unvented

insulation joint. The program milestone schedule shown in Figure 4.2.1 highlights major events that will be accomplished and documented.

This Program Plan describes ARC's understanding of the effort required to develop and verify the Block II SRM. ARC has the nucleus of the management and technical disciplines to perform the Block II SRM Development and Verification (D&V) Program successfully. An aggressive staffing plan will be developed and initiated in advance of Block II SRM Program initiation.

Block II SRM requirements will be verified by analysis, inspection, and testing from the component to the subscale to the system level. ARC understands SRM D&V requirements and offers the program flow logic diagrammed in Figure 4.2.2 to accomplish NASA's objectives in a timely manner. The D&V matrix shown in Figure 4.2.3 displays the analysis and tests planned to verify each component.

4.3 MANAGEMENT

Overall responsibility for the Block II SRM rests with the SRM Project Director, who reports directly to the Senior Vice President and General Manager of the ARC Propulsion Division. The SRM Project Office at our Camden, Arkansas facility will direct all D&V tasks, including the detailed motor and facilities design effort. Initial propellant/liner/insulation laboratory testing will be accomplished at our Gainesville, Virginia facility, and the technology and/or personnel will be transferred to Camden to assure transition from the laboratory to full-scale operations. Figure 4.3.1 shows the SRM project organization structure and responsibilities.

4.4 SRM DESIGN AND ANALYSIS

The ARC Block II Conceptual Design Motor eliminates all deficiencies identified in the Shuttle 51-L SRM. The integrity and high reliability of the ARC Block II SRM will be verified during the planned program. This design offers marked advantages with regard to ease of assembly and inherent reliability as compared with the SRM presently being designed and tested under the SRM Recovery Program. The design trades conducted in reaching the SRM design recommended by ARC were heavily weighted toward flight safety and reliability and resulted in the selection of materials, components, and designs having an existing database. The two novel concepts proposed by ARC -- bolted

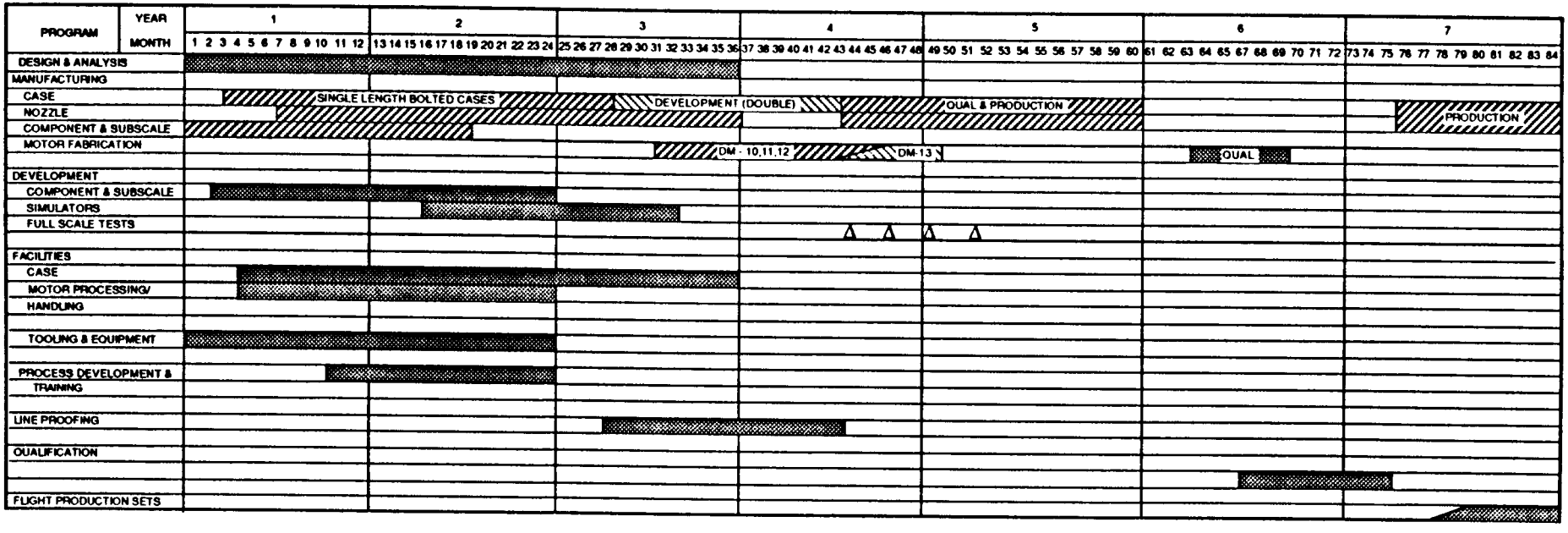

FIGURE 4.2.1. BLOCK II SRM PROGRAM MILESTONE SCHEDULE.

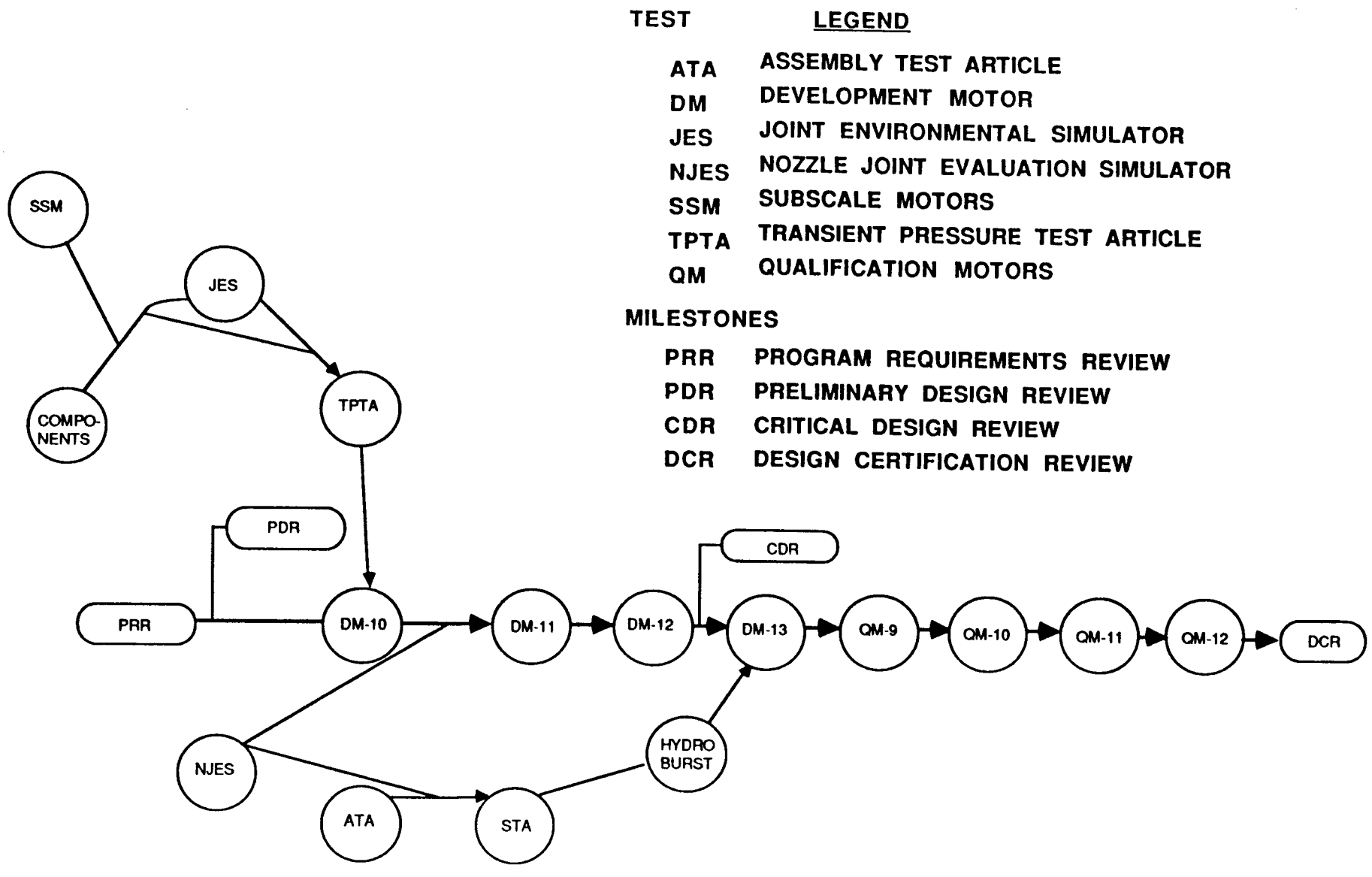

FIGURE 4.2.2. VERIFICATION TEST FLOW LOGIC.

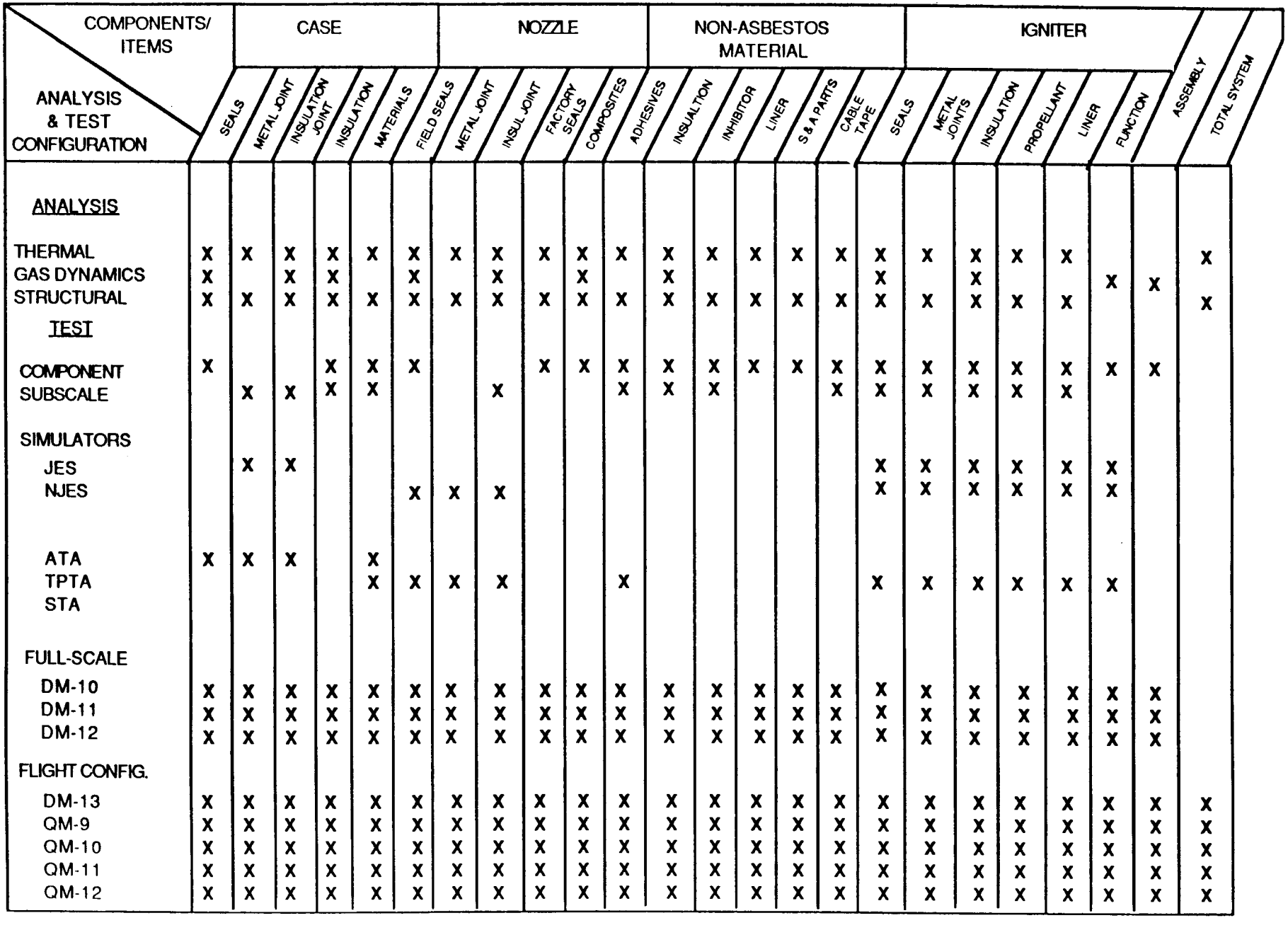

FIGURE 4.2.3. DEVELOPMENT AND VERIFICATION MATRIX.

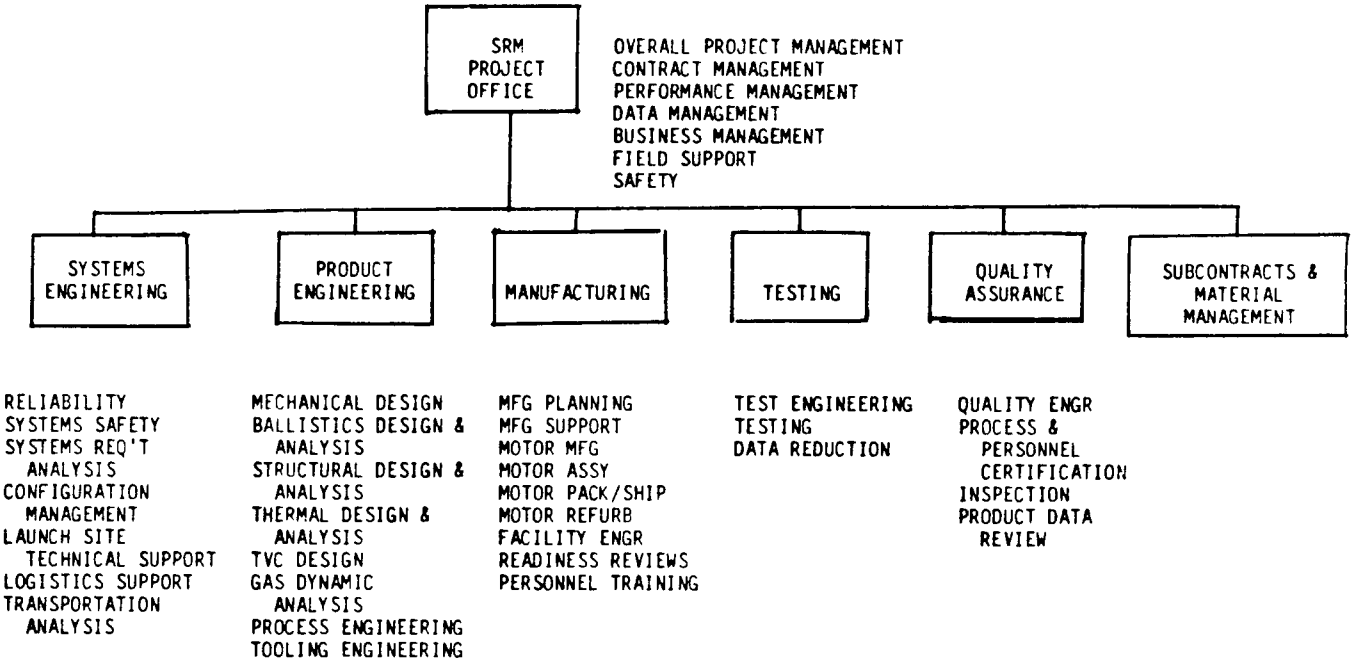

FIGURE 4.3.1. SRM PROJECT ORGANIZATION.

case field joint and double-length case segments -- are based on sound engineering technology and will be thoroughly verified during the D&V Program. The bolted case field joint is based on extensive work done by the NASA Langley Research Center and confirmed by ARC analysis. Bolted, face-sealed joints are typically used for large diameter nozzle-to-case joints. The double-length case segment concept has been studied by Ladish Co., Inc. and rated feasible with additional foundry, forging, and heat treatment facilitization. ARC has extensive experience in developing asbestos-free insulation; several rocket systems are in production using this improved material. These concepts have been analyzed to define their structural, thermal, and gas dynamic characteristics. ARC plans to work closely with the MSFC Aeroballistic Lab trajectory group to assure that ARC's SRM design satisfactorily interfaces with the shuttle vehicle's flight performance.

The Block II Engineering Task will start with the review and design impact analysis of all SRM system and performance requirements. The preliminary Contract End Item (CEI) Specification (Part I) submitted with this report will be compared to overall SRM and mission requirements following ATP to establish a baseline. We anticipate no problem in meeting the SRM requirements; however, our program planning is so structured that any problem that arises will receive immediate attention and action.

4.5 COMPONENT AND SUBSCALE TESTS

Component tests were selected to provide empirical data for analysis, to validate analytical models, and to demonstrate the feasibility of ARC Block II SRM design concepts. Table 4.5.1 summarizes the component tests proposed. Parallel with the early case subcontractor effort, ARC will conduct component development of asbestos-free insulation, insulation joints, seals, bond characterizations, and the igniter. ARC plans aeroheat testing exposure of systems tunnel sections at ARC. ARC offers its free jet testing facility, which will duplicate SRM flight conditions to provide early empirical data to verify the systems tunnel design. Some special tests, such as the case material properties evaluation, have previously been performed by MTI yielding a comprehensive database.

4.6 COMPONENT AND MOTOR MANUFACTURING

Full-size motor manufacturing will begin with cases fabricated from current length forgings and will use bolted joints. ARC has selected this approach for

TABLE 4.5.1. COMPONENT TESTS.

COMPONENT	TEST	OBJECTIVE	TEST QTY	TEST CONDITIONS
CASE	MATERIAL PROPERTIES	CHARACTERIZE MATERIAL AT FORCED EXTREMES OF SPECIFICATION	TBD	STANDARD ASTM TEST SPECIMENS, HOT/COLD TEMP, SALT IMMERSION, SURFACE TREATMENT VARIED FOR STRESS CORROSION
	FABRICATION RING	DEVELOP MACHINING TECHNIQUES	6	AMBIENT
	MANUFACTURING TOLERANCE	VALIDATE MFG TOLERANCES	10	END RINGS 146-INCH END RINGS
	HEAT TREAT	DEVELOP & CHARACTERIZE HEAT TREAT PROCESS	TBD	SUBSCALE & FULL SCALE RINGS
	HYDROTEST	EVALUATE JOINT, VERIFY CASE INTEGRITY	1 FWD, 1 CENTER, 1 AFT SECTIONS WITH FWD & AFT CLOSURES	INSTRUMENT FOR Pc, DEFLECTION, STRAIN
	HYDROBURST	VERIFY CASE DESIGN MARGIN	2 FWD, 1 AFT	INSTRUMENT FOR Pc, DEFLECTION, STRAIN

TABLE 4.5.1. (CONTINUED).

COMPONENT	TEST	OBJECTIVE	TEST QTY	TEST CONDITIONS
CASE & NOZZLE FIELD JOINT	FIELD HANDLING (1/3 SCALE MOTOR)	EXAMINE ASSEMBLY & DISASSEMBLY	2	STEEL/INSULATION JOINT SEGMENT; AMBIENT ENVIRONMENTS
	SEAL ENVIRONMENTS (INCLUDE ALL SEALS)	VERIFY INTEGRITY AT ENVIRONMENTAL AND TOLERANCE EXTREMES	10 EA	METAL SECTIONS, BASELINE & ALTERNATE SEALS, TEMPERATURE & HUMIDITY EXTREMES, MAXIMUM GAPS
	SEAL HANDING	VERIFY SEAL INTEGRITY UNDER ADVERSE HANDLING	6	CLEAN & CONTAMINATED SURFACES, IMPOSED DAMAGE, TEMPERATURE & HUMIDITY EXTREMES
	BOLT STRESS CORROSION	VERIFY INTEGRITY UNDER LONG TERM EXPOSURE TO STRESS	6	METAL JOINT SECTION; SALT WATER IMMERSION, 70% ULT PRELOAD
	BOLT PRELOAD	VERIFY BOLT PRELOAD NDT METHOD	6	3 SETS OF ULTRASONIC EQUIPMENT; IMPOSED MAX RANGE OF CALIBRATION; MATCH ACTUAL VERSUS NDT BOLT EXTENSION

TABLE 4.5.1. (CONTINUED).

COMPONENT	TEST	OBJECTIVE	TEST QTY	TEST CONDITIONS
CASE INSULATION LINER, & INHIBITOR, NOZZLE ABLATIVES	MATERIAL PROPERTIES	CHARACTERIZE STRUCTURAL, THERMAL, & BOND PROPERTIES AT PROCESS & ENVIRONMENT EXTREMES	6 EACH MATERIAL, TEST	UNIAXIAL, BIAXIAL, ZERO TIME, ACCELERATED, & REAL TIME AGING
	EROSION	CHARACTERIZE MOTOR ABLATIVES	6 EACH MATERIAL, TEST CONDITION	SUBSCALE EROSION TEST MOTORS
	FLOW VISUALIZATION	EVALUATE MOTOR COMPONENTS UNDER IMPOSED ADVERSE FLOW; VALIDATE FLOW MODEL	3 EACH CONDITION	INDUCED VORTEX & CIRCUMFERENTIAL FLOW

TABLE 4.5.1. (CONTINUED).

COMPONENT	TEST	OBJECTIVE	TEST QTY	TEST CONDITIONS
IGNITER	SEAL ENVIRONMENTS	VERIFY INTEGRITY AT ENVIRONMENT & TOLERANCE EXTREMES	10 EA	IGNITER HARDWARE & MOTOR INTERFACE SECTION; BASELINE/ ALTERNATE SEALS, TEMP/ HUMIDITY/TOLERANCE EXTREMES
	PROPELLANT, LINER, INSULATION BOND CHARACTERI-ZATION	CHARACTERIZE BOND	6 EA CONDITION	
	HARDWARE HYDROTEST	VERIFY HARDWARE INTEGRITY	2	AMBIENT ENVIRONMENTS PREDICT/MEASURE DEFLECTION, STRAIN
	HARDWARE HYDROBURST	VERIFY DESIGN MARGIN	2	AMBIENT, MEASURE STRAIN
	DEVELOPMENT STATIC TESTS	EVALUATE IGNITER BALLISTICS, STRUCTURE	6	OPEN AIR, 2 AMBIENT, 2 HOT, 2 COLD, WITNESS PANELS, HIGH FREQ Pc TRANSDUCERS
	DEVELOPMENT ENVIRONMENT TEST	EVALUATE IGNITER PERFORMANCE	2	FULL SEQUENTIAL EXPOSURE TO ENVIRONMENTS, STATIC TEST 1 HOT, 1 COLD OPEN AIR, HIGH FREQ Pc
	MAIN GRAIN IMPINGEMENT TEST	EVALUATE IGNITER FLOW FOR POTENTIAL GRAIN DAMAGE	2	INERT FORWARD SEGMENT, 1 HOT, 1 COLD

Development Motor tests DM-10, 11, and 12 to allow early full-scale testing. DM-13 and Qualification Test motors would use longer, weld-free case segments incorporating the bolted joint design. Table 4.6.1 shows the configuration, quantity, and schedule of case segments. Tables 4.6.2 and 4.6.3 add the planned fabrication schedule for nozzle assemblies and igniter hardware. For the total D&V Program, motor preparation, insulation, and lining and casting schedules are shown in Table 4.6.4.

4.7 SYSTEM LEVEL TESTS

System-level tests are chosen to represent the SRM as it will function under space shuttle mission conditions. System level D&V tests are summarized in Table 4.7.1.

Figure 4.7.1 shows the SRM Joint Evaluation Simulators (JES) test series. JES will be fabricated from existing SRM standard weight hardware with the new bolted joints welded in place of the clevis and tang joints. Standard weight segments from the existing inventory will be used to provide the required case safety factor with the higher projected MEOP for the heads-up trajectory. The JES hardware will be loaded with inert propellant overlaid at the joints with a thin layer of live propellant as in the current Recovery Program tests. Nozzle Joint Evaluation Simulators (NJES) similar to the current NJES test series will be fabricated and tested at our Camden facility. Figure 4.7.2 defines the NJES test series.

Transient Pressure Test Articles (TPTA) similar to JES units will be fabricated and tested at NASA/MSFC with applied structural launch flight loads. An Assembly Test Article consisting of 160-inch-long bolted joint hardware will be shipped to NASA/Kennedy Space Center. Eight tests of assembly and disassembly methods will be conducted with the baseline and alternate seals. Seal verification tests of each joint will be conducted at 50, 100, and 200 psia. Video camera coverage will be provided from exterior and interior views during assembly, leak test, and disassembly. The test quantity was selected to individually test the variables shown in Figure 4.7.3.

One set of SRM hardware including forward closure, center segments, ET attachment ring, aft stiffener segments, aft closure, and aft skirt will be shipped to NASA/MSFC for assembly and test as a Structural Test Article (STA). A full series of SRM launch and flight structural loads will be conducted on the STA both at nominal load and nominal loads multiplied by full design margins. This test will verify SRM structural integrity.

TABLE 4.6.1. CASE SEGMENT CONFIGURATION.

	FWD CLOSURE	160" CASE	160" CASE	160" CASE	160" CASE	160" CASE	160" CASE	86" ET	120" STIFF	120" STIFF	AFT CLOSURE	NEW OR REFURB	1ST SHIP SCHEDULE MO/ARO
JES	T*		C B	B B						B T	C B	3N + 6R	14
NJES	T*										C B	2N + 8R	14
ATA	T*		C B	B C							C B	N + 7R	18
TPTA	T*		C B	B B						B T	C B	4R	-
DM-10	T*	C T*	C B	B T	C B	B T	C B	B C	C T*	C T*	C B	R	-
-11	T*	C T*	C B	B T	C B	B T	C B	B C	C T*	C T*	C B	R	-
-12	T*	C T*	C B	B T	C B	B T	C B	F C	C T*	C T*	C B	R	-
-13	T*	C B		B B		B B		B T			C B	N	40
QM-9	T*	C B		B B		B B		B T			C B	N	60
-10	T*	C B		B B		B B		B T			C B	N	60
-11	T*	C B		B B		B B		B T			C B	N	60
-12	T*	C B		B B		B B		B T			C B	R	-

T - TANG, C - CLEVIS, B - BOLT, N - NEW, R - REFURBISHED, * EXISTING HARDWARE

TABLE 4.6.2. NOZZLE FABRICATION SCHEDULE.
(NUMBER = MONTHS ARO)

	HARDWARE	DELIVER TO ARC
DM-10	22N	32N
DM-11	24N	34N
DM-12	25N	36N
DM-13	25N	36N
QM-9	51N	60N
QM-10	51N	60N
QM-11	51N	60N
QM-12	51N	60N

TABLE 4.6.3. IGNITER MANUFACTURING SCHEDULE.
(NUMBER = MONTHS ARO)

	HARDWARE	INSULATED	LINED/LOADED
HYDROBURST	8N	-	-
IGN-1	8N	10	10
IGN-2	9N	10	10
IGN-3	10N	11	11
IGN-4	10N	11	11
IGN-5	10N	11	11
IGN-6	10N	11	11
IGN-7	11N	12	13
IGN-8	11N	12	13
IGN-9	11N	12	13
IGN-10	11N	12	13
JES 1	15R (IGN-1)	16	18
JES 2	15R (IGN-2)	16	18
JES 3	15R (IGN-3)	16	18
JES 4	15R (IGN-4)	16	18
JES 5	15R (IGN-5)	16	18
JES 6	15R (IGN-6)	16	18
JES 7	15R (IGN-7)	16	18
JES 8	15R (IGN-8)	16	18
JES 9	15R (IGN-9)	16	18
JES 10	15R (IGN-10)	16	18
NJES-1	20R (IGN-1)	21	23
NJES-2	20R (IGN-2)	21	23
NJES-3	20R (IGN-3)	21	23
NJES-4	20R (IGN-4)	21	23
NJES-5	20R (IGN-5)	21	23
NJES-6	20R (IGN-6)	21	23
NJES-7	20R (IGN-7)	21	23
NJES-8	20R (IGN-8)	21	23
TPTA-1	25R (IGN-1)	26	28
TPTA-2	25R (IGN-2)	26	28
TPTA-3	25R (IGN-3)	26	28
TPTA-4	25R (IGN-4)	26	28
TPTA-5	25R (IGN-5)	26	28
TPTA-6	25R (IGN-6)	26	28
TPTA-7	25R (IGN-7)	26	28
TPTA-8	25R (IGN-8)	26	28
TPTA-9	25R (IGN-9)	26	28
TPTA-10	25R (IGN-10)	26	28
DM-10	31R (IGN-1)	32	34
DM-11	31R (IGN-2)	32	34
DM-12	31R (IGN-3)	32	34
DM-13	31R (IGN-4)	32	34
QM-9	36R (IGN-5)	37	38
QM-10	36R (IGN-6)	37	38
QM-11	36R (IGN-7)	37	38
QM-12	36R (IGN-8)	37	38

TABLE 4.6.4. MOTOR MANUFACTURING OPERATIONS.

	REFURB	INSULATION	LINING	CASTING	SEG ASSY
JES-1 THRU 10	17	19	21	21	22
NJES 1 THRU 10	24	26	28	28	29
TPTA 1 THRU 4	22/23	24	25	25	26
DM-10	31	34	36	36	30
DM-11	31	34	36	36	39
DM-12	31	34	36	36	39
DM-13	N	44	46	46	47
QM-9	N	63	64	64	65
QM-10	N	63	64	64	65
QM-11	N	63	64	64	65
QM-12	52	63	64	64	65

LEGEND: 1st NUMBER = MONTH OPERATION BEGINS

TABLE 4.7.1. SYSTEM LEVEL D&V TESTS.

	OBJECTIVE	RATIONALE
JES-1 & 2	COMPARE ARC VERSUS MTI JOINT, INSULATION, SEAL	USE COMPARATIVE DESIGNS IN SAME MOTOR FOR DIRECT CORRELATION; TWO FIRINGS PROVIDE REPLICATE DATA, ALLOW EARLY LOOK AT METAL O-RING/ C-RING, AND STRESS RELIEF OPTIONS
JES-3 & 4	EVALUATE PERFORMANCE OF JOINT, BASELINE/ALTERNATE SEALS	ESTABLISH PERFORMANCE OF ALTERNATES TO SUPPORT DESIGN SELECTION
JES-5 THROUGH 10	EVALUATE PERFORMANCE UNDER POTENTIAL FAILURE MODES AND EFFECTS (FMEA)	(6) FIRINGS ARE PROVIDED TO ALLOW A RANGE OF FMEA TO SUPPORT DESIGN SELECTION; PRELIMINARY FMEA CANDIDATES SHOWN
NJES-H1 & H2	DEMONSTRATE STRUCTURAL INTEGRITY	PISTON SUPPORTED NOZZLE CLOSURE ALLOWS REPRESENTATIVE JOINT STRUCTURAL RESPONSE; TWO TESTS PROVIDE REPLICATE DATA
NJES-H3	DEMONSTRATE STRUCTURAL MARGIN	HYDROBURST VERIFIES DESIGN AND ANALYSIS; QUANTIFIES DESIGN MARGIN; CONDUCT TEST AFTER REFURBISHMENT THROUGH SEVERAL TESTS TO CONSERVE HARDWARE, REDUCE RISK
NJES-1 & 2	COMPARE ARC VERSUS MTI JOINT, INSULATION, SEAL	COMPARE DESIGNS UNDER THE SAME TEST CONDITIONS/EQUIPMENT; ALLOWS EARLY LOOK AT ALTERNATE SEALS
NJES-3 & 4	EVALUATE PERFORMANCE OF JOINT, BASELINE/ALTERNATE SEALS	ESTABLISH PERFORMANCE OF ALTERNATES TO SUPPORT DESIGN SELECTION
NJES-5 THROUGH 10	EVALUATE PERFORMANCE UNDER POTENTIAL FMEA	(6) FIRINGS ARE PROVIDED TO ALLOW A RANGE OF FMEA TO SUPPORT DESIGN SELECTION; PRELIMINARY FMEA CANDIDATES SHOWN

TABLE 4.7.1. (CONTINUED)

TPTA-1 THROUGH 4	EVALUATE PERFORMANCE OF JOINT, BASELINE/ALTERNATE SEALS WITH EXTERNAL LOADS	REPEAT JES 1 THROUGH 4 SEQUENCE IN NASA/ MSFC HOT FIRING/LOAD TEST FACILITY; SUPPORT DESIGN SELECTION
ATA-1 & 2	EVALUATE ASSEMBLY TECHNIQUES	PROVIDES EARLY EVALUATION OF ASSEMBLY TECHNIQUES WITH BASELINE/ALTERNATE SEALS
STA-1	VERIFY CASE DESIGN INTEGRITY	STRUCTURAL LOAD TEST PROVIDES VERIFICATION OF DESIGN INTEGRITY EARLY IN PROGRAM
HYDROBURST	VERIFY CASE DESIGN MARGIN	HYDROBURST VERIFIES DESIGN AND ANALYSIS; QUANTIFIES DESIGN MARGIN
DM-10	EVALUATE DESIGN PERFORMANCE AT 60°F MBPT	INITIAL FIRING CONFIRMS BALLISTIC, STRUCTURAL, THERMAL, GAS DYNAMIC ANALYSIS; DEFINES BASELINE TO ALLOW DESIGN TO ADJUSTMENTS
DM-11	EVALUATE DESIGN PERFORMANCE AT 20°F	CONFIRMS PREDICTIONS OF ADJUSTED DESIGN
DM-12	EVALUATE DESIGN PERFORMANCE AT 90°F	CONFIRMS DESIGN PREDICTIONS, ESTABLISHES BASELINE AT 90°F
DM-13	EVALUATE DESIGN PERFORMANCE AFTER EXPOSURE TO SEQUENTIAL ENVIRONMENTS	CONFIRMS DESIGN CAPABILITY TO WITHSTAND ENVIRONMENTS
QM-9 THROUGH 12	VERIFY DESIGN INTEGRITY AFTER EXPOSURE TO ALL SIGNIFICANT SRM ENVIRONMENTAL CONDITIONS	(4) MOTORS WERE SELECTED TO PROVIDE DUPLICATE DATA AT ENVIRONMENTAL EXTREMES

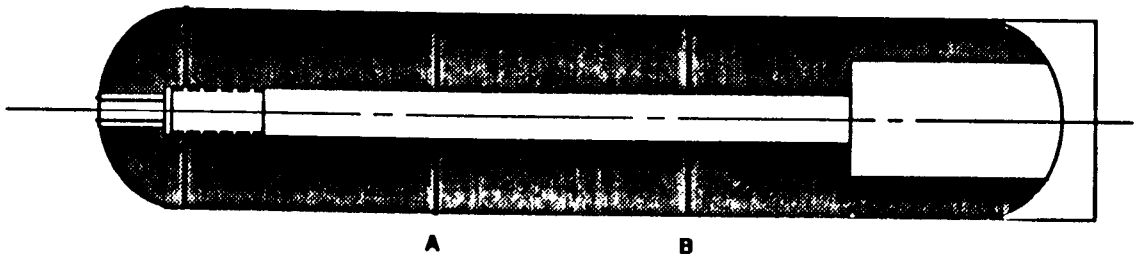

CONFIG.	JES 1		JES 2		JES 3		JES 4		JES 5		JES 6		JES 7		JES 8		JES 9		JES 10	
JOINT	A	B	A	B	A	B	A	B	A	B	A	B	A	B	A	B	A	B	A	B
SEAL MATERIAL																				
● METAL O-RINGS		X			X	X	X	X	X	X	X	X	X	X	X	X	X	X	X	X
● METAL C-RING		X		X	X		X		X	X	X	X	X	X	X	X	X			X
● ARCTIC NITRILE O-RING	X		X	X		X		X												
MTI INSULATION DESIGN	X		X																	
ARC INSULATION DESIGN																				
● MOD 1 STRESS RELIEF		X			X	X			X	X	X	X	X	X	X	X	X	X	X	X
● MOD 2 STRESS RELIEF				X			X	X												
● FULL BOND		X		X	X	X	X	X		X	X			X	X					
● PARTIAL BOND									X			X	X			X	X	X	X	X
SEAL DAMAGE																				
● PRIMARY												X		X						
● SECONDARY																X				
● INSULATION																		X		
PRIMARY SEAL OMITTED																				
TEST JOINT TEMPERATURE																				
● 20°F	X	X	X	X	X	X	X	X	X	X	X	X	X	X	X	X	X	X	X	X
CAPTURE FEATURE JOINT	X		X																	
BOLTED JOINT		X		X	X	X	X	X	X	X	X	X	X	X	X	X	X	X	X	X

FIGURE 4.7.1. SRM JOINT EVALUATION SIMULATOR TEST SERIES.

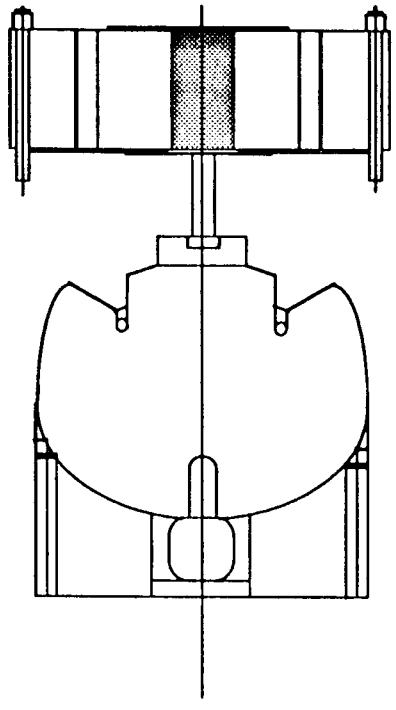

	NJES H-1	NJES H-2	NJES 1	NJES 2	NJES 3	NJES 4	NJES 5	NJES 6	NJES 7	NJES 8	NJES H3	NJES 9	NJES 10
INSULATION DESIGN													
● STRESS RELIEF #1			X		X	X	X	X	X	X	X	X	X
● STRESS RELIEF #2				X									
● PARTIALLY BONDED			X	X									
● FULLY BONDED					X	X	X	X		X		X	X
JOINT													
● ARC	X	X		X	X	X	X	X	X	X	X	X	X
● MTI			X										
SEAL													
● C-RING	X	X		X	X	X	X	X	X	X	X		
● ARCTIC NITRILE/SILICONE	X	X	X	X	X	X	X	X	X	X	X		
SEAL DAMAGED													
● PRIMARY							X						
● SECONDARY								X					
● INSULATION									X			X	X
PRIMARY SEAL													
● OMITTED										X			
TEST CONDITIONS,20°F													
● HYDROTEST	X	X											
● HYDROBURST											X		
● HOT FIRING			X	X	X	X	X	X	X	X		X	X

FIGURE 4.7.2. SRM NOZZLE JOINT EVALUATION SIMULATOR TEST SERIES.

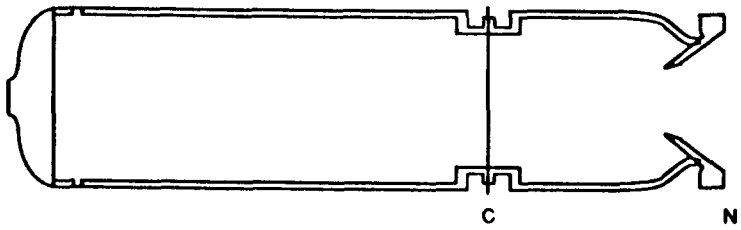

CONFIG.	ATA-1		ATA-2		ATA-3		ATA-4		ATA-5		ATA-6		ATA-7		ATA-8	
JOINT	C	N	C	N	C	N	C	N	C	N	C	N	C	N	C	N
PRIMARY SEAL																
● METAL O-RING	X	X			X	X	X	X	X	X			X	X	X	X
METAL C-RING			X	X							X	X				
SECONDARY SEAL																
● METAL O-RING	X	X			X	X	X	X	X	X			X	X	X	X
● ARCTIC NITRILE O-RING			X	X							X	X				
TEMPERATURE																
● -7°C (20°F)	X	X	X	X			X	X	X	X	X	X	X	X		
● 32°C (90°F)					X	X									X	X
FAILURE MODES & EFFECTS																
● SCORED/BENT SEAL							X	X								
● SHIMMED OPEN JOINT									X	X	X	X			X	X
● METAL SLIVER													X	X		

FIGURE 4.7.3. ASSEMBLY TEST ARTICLE.

Four Development Test Motors were selected to allow for the following:

- Design evaluation at 20°F, 60°F, and 90°F;
- Design iteration;
- Design evaluation after sequential exposure to SRM environments.

Four Qualification Motors were selected to provide duplicate data at environmental extremes.

4.8 FACILITIES, EQUIPMENT, AND TRANSPORTATION

The Development and Verification Plan for facilities, equipment, and transportation will be accomplished in two phases. Phase I will include construction of those facilities that are absolutely necessary for the production of a single-test SRM. Some of the production processes can be achieved by rescheduling production of other programs. In addition, temporary facilities can be used. Partial completion of certain facilities will also aid in the implementation of a "bare bones" operation during Phase I. Phase II construction will include completion of the remaining, less essential facilities.

By rescheduling the MLRS Program so that production is completed prior to the required delivery dates, the mixers, grinders, storage facilities, conditioning facilities, and labor force from the MLRS Program can be used in the production of SRM propellant until a full-up production line is operational. This accelerated schedule can be achieved by working extra days and shifts.

Temporary equipment can be used in several areas to meet the D&V production schedule. Mobile boiler plants will provide heating for comfort, curing, and processing until the completion of Phase II. Lift house and rail loading functions will be handled by mobile cranes until a permanent structure is built.

Partial completion of the road network, steam system, and power will allow for early production. Sewage will be collected in collection tanks and hauled to the existing sewage treatment plant until the sewage system is complete.

Phase I construction will permit production of the D&V SRM within 18 months of contract award. Phase I facilities will include

- Case preparation,
- Casting tooling assembly,
- Casting tooling clean-up,
- Casting pits (3),
- Casting control room,
- X-ray,
- Cast house,
- "Lift house" (temporary mobile crane),

- Segment assembly,
- Equipment/tooling storage,
- Steam plant (mobile),
- Roads (partial network),
- Site clearing (partial),
- Sewage system (collection tasks),
- Rail loading/unloading crane (temporary mobile crane).

Phase II construction will parallel the construction in Phase I. It would, however, have lower priority until Phase I portions are complete. Phase II construction is expected to be complete about 2 years after contract award (see Figure 4.8.1).

Transportation of the SRM will pose no special problem. Table 4.8.1 is provided as a routing schedule.

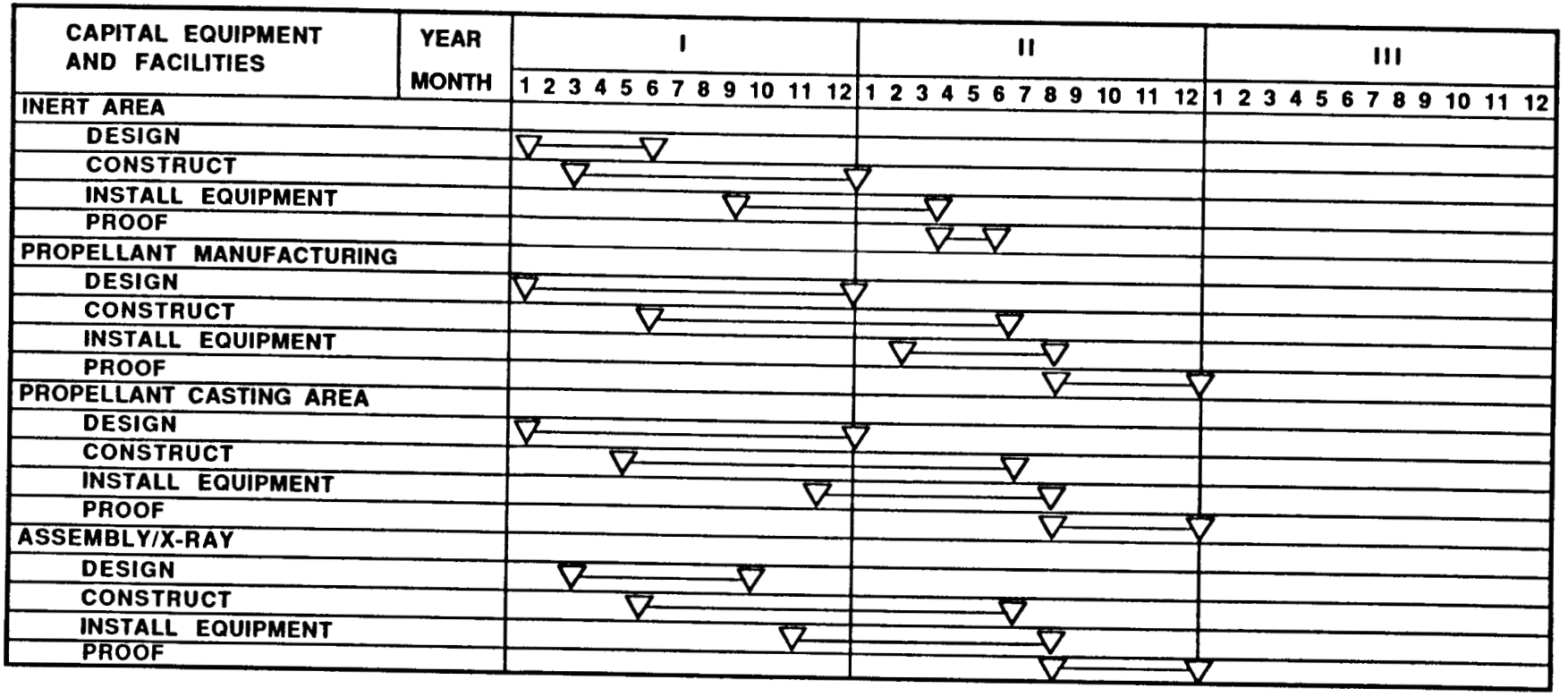

FIGURE 4.8.1. CAPITAL EQUIPMENT AND FACILITIES.

TABLE 4.8.1. PROPOSED RAIL ROUTING OF SRM HARDWARE.

CAMDEN, ARKANSAS TO KENNEDY SPACE CENTER

LOAD ON EAST CAMDEN AND HIGHLAND RAILROAD AND SWITCH TO SOUTHERN PACIFIC AT CAMDEN

SOUTHERN PACIFIC TO NEW ORLEANS VIA SHREVEPORT

SEABOARD RAILROAD TO JACKSONVILLE, FLORIDA

FLORIDA EAST COAST RAILROAD TO VANDENBERG AIR FORCE BASE/KENNEDY SPACE CENTER

CAMDEN, ARKANSAS TO WESTERN TEST RANGE

LOAD ON EAST CAMDEN AND HIGHLAND RAILROAD AND SWITCH TO SOUTHERN PACIFIC AT CAMDEN

SOUTHERN PACIFIC DIRECT INTO WESTERN TEST RESEARCH FACILITY VIA LAS VEGAS, NEVADA

CAMDEN, ARKANSAS TO MORTON THIOKOL INC., CORINNE, UTAH

LOAD ON EAST CAMDEN AND HIGHLAND RAILROAD AND SWITCH TO SOUTHERN PACIFIC AT CAMDEN

SOUTHERN PACIFIC TO KANSAS CITY SOUTHERN AT SHREVEPORT, LOUISIANA

KANSAS CITY SOUTHERN TO NORTH PLATTE, NEBRASKA VIA KANSAS CITY

UNION PACIFIC FROM NORTH PLATTE TO CORINNE, UTAH

MORTON THIOKOL INC., CORINNE, UTAH TO CAMDEN, ARKANSAS

THE REVERSE OF THE ROUTING FROM CAMDEN TO MORTON THIOKOL INC. AS DESCRIBED ABOVE WILL BE UTILIZED.